OCTG Premium Threaded Connection 3D Parametric Finite Element Model

Nabeel Ahsan

Thesis submitted to the faculty of the Virginia Polytechnic Institute and State University in partial fulfillment of the requirements for the degree of

Master of Science
In
Mechanical Engineering

Robert L. West, Chair
David H. Coe
Norman E. Dowling

June 2, 2016
Blacksburg, Virginia

Keywords: Oil Country Tubular Goods, Finite Element Analysis, Digital Image Correlation, 3D, Helical Threads

OCTG Premium Threaded Connection 3D Parametric Finite Element Model

Nabeel Ahsan

ABSTRACT

Full 360 degree 3D finite element models are the most complete representation of Oil Country Tubular Goods (OCTG) premium threaded connections. Full 3D models can represent helical threads and boundary conditions required to simulate make-up and service loading. A methodology is developed to create a 360 degree full 3D parametric finite element model with helical threads as an effective design and analysis tool. The approach is demonstrated with the creation of a metal-to-metal seal integral joint full 3D model with manufacturer supplied geometry. The premium connection is decomposed into smaller parts to generate parametric geometric features. A controlled parametric meshing scheme is developed to manage mesh density in contact regions to effectively represent the mechanics in regions of interest while minimizing total element count. The scripted parametric approach allows for efficient geometric and mesh updates. Several methods to reduce and manage model runtimes are presented. An elastic-plastic material model is created with material coupon tensile tests results. Digital Image Correlation (DIC) is used to measure full-field displacement and strain data on the surface of the box. Experimental set up and data processing procedures are discussed. Error metrics are developed to correlate the finite element model results with the DIC experimental data. The DIC make-up experimental results are used to reconcile the finite element model to develop a minimum error make-up model relative to the pin rotation. The friction coefficient is estimated and the make-up torque-turn behavior is verified. The calibrated 3D finite element model is validated with ISO_13769 load series B axial and internal pressure loading experimental DIC data. Metal-to-metal seal metrics of contact pressure and seal length are evaluated.

OCTG Premium Threaded Connection 3D Parametric Finite Element Model

Nabeel Ahsan

General Audience Abstract

Oil Country Tubular Goods (OCTG) refers to a class of specialized steel pipe manufactured according to American Petroleum Institute (API) specifications used in the oil and gas industry. OCTG consist of oil and gas well consumables such as well casing, production tubing, and drill pipe. The production tubes are joined together in the well casing by threaded connections which are API standard or proprietary "premium connections". Premium connections are subjected to strict design guidelines and qualification tests to prevent any failure that may result in environmental and economic losses. Qualification of each connection variant via physical testing takes time and costs over $900,000. Full 360 degree 3D finite element models are the most complete representation of premium threaded connections. A methodology is developed to create a 360 degree full 3D parametric finite element model with helical threads as an effective design and analysis tool for premium connections. Digital Image Correlation (DIC) experimental results from connection make-up and service loading tests are used to reconcile and validate the full 3D finite element model. The 3D finite element model validated with experimental results can be used to predict connection performance and behavior for design selection. This research effort can be used to develop virtual connection qualification tests to significantly reduce physical testing costs and time.

Acknowledgements

I would like to thank my advisor, Dr. Robert L. West for his time and guidance throughout this research effort. The accomplishments of this work would not be possible without his direction and assistance. I would like to thank Dr. David H. Coe and Dr. Norman E. Dowling for their knowledge and support throughout this work.

Special thanks to Nick Angelini for his work on developing and coding the scripts and Yi Li for all his work on DIC system and data processing.

I am very grateful for my parents Arshad and Shaheen Ahsan for their unconditional love and support throughout all of my life adventures. Thanks to all of my family, Adeel, Umair, Bouchra, Akeem, and Samar for their love and support.

Many thanks to all of my colleagues on the VT Motorsports team for becoming my family in Blacksburg over the last few years.

NABEEL AHSAN

Virginia Polytechnic Institute and State University

June 2016

"The art of living is neither careless drifting on the one hand nor fearful clinging to the past on the other. It consists in being sensitive to each moment in regarding it as utterly new and unique, in having the mind open and wholly receptive." – Alan W Watts

Table of Contents

List of Figures

List of Tables

Nomenclature

English Symbols

Box	Female component of the premium threaded connection
CAD	Computer aided drawing
E	Young's modulus
eTT	Tangential strain
eZZ	Longitudinal strain
FE	Finite elements
FEA	Finite element analysis
HPHT	High-pressure High-Temperature
MIJ	Metal-to-metal seal integral joint
MTC	Metal-to-metal seal threaded and coupled joint
Pin	Male component of the premium threaded connection
p	Pressure
R_i	Inside radius of the cylinder
R_o	Outside radius of the cylinder
R-T-Z	Cylindrical coordinate system. R, radial direction. T, tangential direction. Z, axial direction
SSE	Sum squared error
uT	Tangential displacement
uZ	Longitudinal displacement

Greek Symbols

ϵ	Nominal strain
$\tilde{\epsilon}$	True strain
μ	Coefficient of friction
σ	Nominal stress
$\tilde{\sigma}$	True stress
σ_Z	Normal stress in longitudinal direction
σ_θ	Normal stress in tangential direction
ν	Poisson's ratio

Other Symbols

2D	Two dimensions or two dimensional
3D	Three dimensions or three dimensional

Chapter 1 Introduction

1.1 Research Motivation

Oil Country Tubular Goods (OCTG) refers to a class of specialized steel pipe manufactured according to American Petroleum Institute (API) specifications used in the oil and gas industry. OCTG consist of oil and gas well consumables such as well casing, production tubing, and drill pipe. Drill pipes are used for drilling; well casing lines the well bore. Production tubing transports the oil and gas to the surface. The production tubes are joined together in the well casing by threaded connections which are API standard or proprietary "premium connections". The chief differences between the API and premium designs are that the premium designs include radial, metal-to-metal pressure seals, have torque shoulders to limit axial advancement of the pin into the coupling or box during make-up, and use modified buttress-type or hooked threads. Generally, the thread form design for a premium connection is not intended to seal pressure, as are API round threads [1].

Modern oil wells are reaching depths of over 25000 ft. resulting in high-pressure high-temperature (HPHT) operating conditions. API regulations consider pressure greater than 15000 psig or temperature higher than 350˚F as HPHT well operation [2]. Premium connections are specifically designed to be used in HPHT well conditions. Premium connections are subjected to strict design guidelines and qualification tests to prevent any failure that may result in environmental and economic losses.

The design and size of each well differs from one drilling site to the next. Premium connections have intricate proprietary designs produced in various configurations to meet the requirements of the well design. OCTG manufacturers produce several families of connections made available in various sizes, weights, and material grades. A family of connections can be sub-divided into groups based on the connection features. Generally, a sub-group is those connections with similar design elements. For example, a "group" of metal seal connections would have the same thread pitch, seal profile, and general design characteristics [3]. It is critical to understand the performance limits of all variants of a connection in the family to avoid any structural or functional failures.

Qualification of each connection variant via physical testing takes time and costs over $900,000. The time and costs of connection qualification process can be significantly reduced with product-line evaluation. The product-line evaluation approach develops a connection performance envelope where only the critical and common commercial sizes are subjected to physical testing to verify and validate the finite element (FE) models. Performance of remaining connections in the group is verified by an FEA based interpolation. In addition to structural and sealability performance envelopes, an operational envelope for the connection including assembly torque range and durability under multiple make and break cycles may be defined for the connection and confirmed by the evaluation program [4]. Figure 1.1 illustrates an example of a connection performance envelope developed with product-line evaluation.

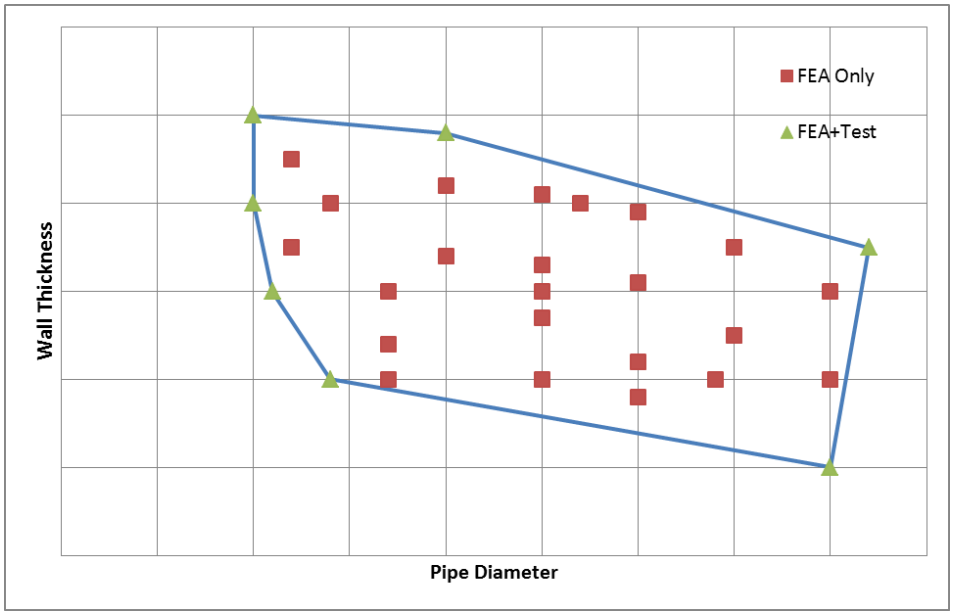

Figure 1.1: Product-line evaluation premium connection performance envelope sample.

The current best practice utilizes axisymmetric FE models calibrated with strain-gage data from the connection outer surface. Axisymmetric models do not account for the spiral of the helical thread geometry and cannot represent torque vs turn behavior of the physical make-up conditions. A full 3D FE model can represent the helical threads and proper boundary conditions required to match the physical make-up of the connection. Following are some benefits of developing full 3D FE models for premium connections:

1. Full 3D FE models are the most complete representation of OCTG premium threaded connections.
2. 3D FE models provide the best technical estimate of connection make-up and boundary conditions before service loading is applied.
3. Verified and validated 3D FE model represents an analytical model closely coupled with experimental data. Provides confidence is connection performance, better comprehension of sealing mechanisms, frictions factors, and other features of the connection.
4. 3D FE models enable better modeling of extreme events such as overpull, high temperature performance, casing wear impact on the connection, and sour environment performance.
5. Verified and validated 3D FE models combined with product-line evaluation approach can reduce connection qualification time and costs considerably.
6. 3D FE model can be used as a design tool to analyze connection performance. Design trade-offs can be implemented on connection configurations with virtual tests for any loading scenario requiring less physical tests throughout the design process.

The objective of this research is to develop a methodology for creating a full 3D FE model for premium threaded connection which can be used as a design and analysis tool to reduce physical testing and optimize connection performance. Figure 1.2 provides an illustration of the collaboration of this research effort in OCTG premium threaded connection design, testing, and qualification process.

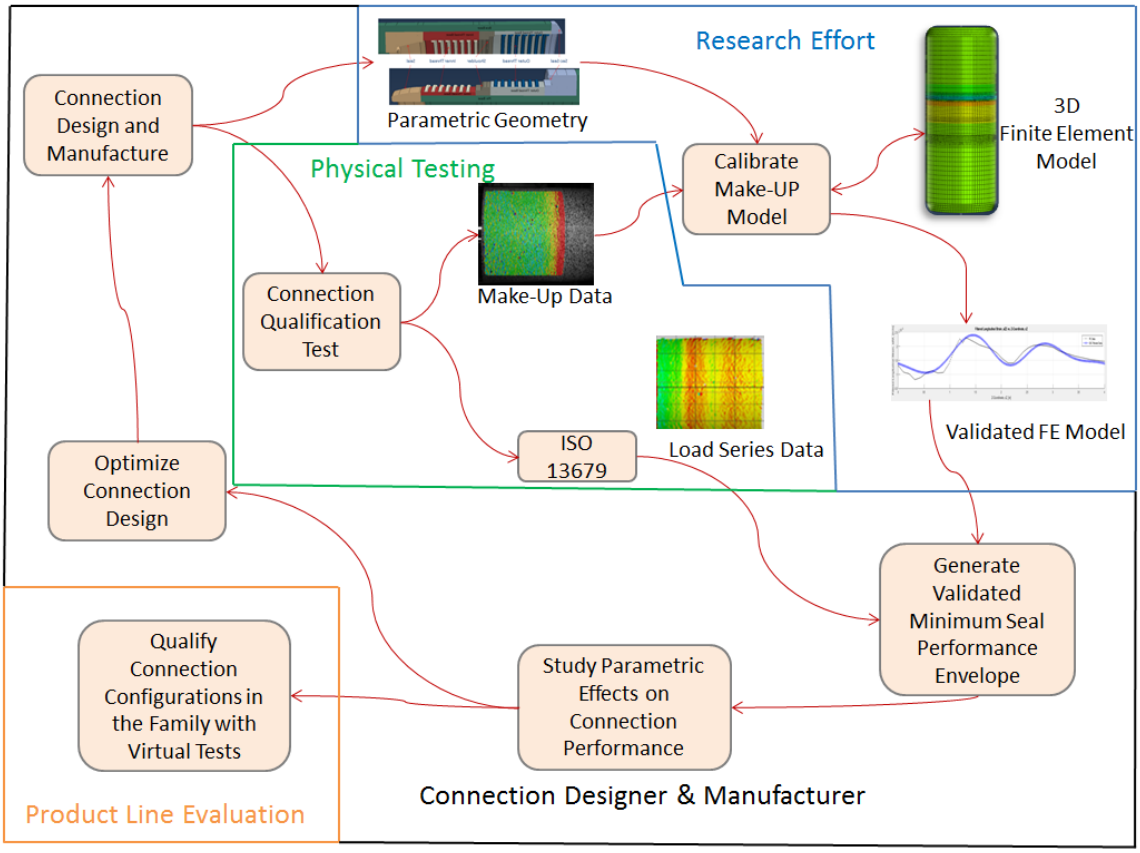

Figure 1.2: OCTG premium threaded connection design and qualification work flow collaboration with the research effort.

1.2 Research Hypothesis

Full 3D FE models of premium connections can be developed with connection geometry and material test data provided by the manufacturer. Connection geometric features and meshing scheme can be parametrized and scripted to update connection configuration and mesh density. The 3D FE model can be reconciled with digital image correlation (DIC) displacement and strain data under make-up conditions. After achieving the proper make-up condition, the 3D FE model is validated with ISO or API service loading testing. The validated model is used to predict connection performance and behavior for design selection. Parametric studies can be implemented to understand effects of the geometric features and their configurations to optimize connection performance. Once the FE model is validated, it can be used to develop virtual qualification tests for product-line evaluation.

1.3 Research Goals

Axisymmetric FE models are preferred over 3D FE models due to the effort and computing resources required to develop effective 3D models. The complex geometric features of the premium connections, multiple contact regions along with the high mesh density required to acquire accurate seal performance results pose a difficult problem. There is no evidence of a successful approach for a full 3D FE model of premium threaded connections in the public domain. To meet the research objectives, the 3D FE modeling approach must achieve the following goals:

1. The full 3D FE model must be parametric for user defined geometry and mesh updates.
2. The full 3D FE model should provide an efficient way to update the parameters.
3. The full 3D FE model must be manageable for the user and tractable for available computing resources.

Incorporating DIC to acquire testing data along with conventional strain gages provides full-field displacement and strain results. These DIC experimental results are critical for verification and validation of the FE models and force the analytical results to be developed at higher standards.

The goal of this research effort is to develop a methodology to create a full 3D with helical threads FE model with geometry supplied form the manufacturer and Abaqus finite element software. Credibility of the 3D FE model is evaluated with how well the FE results correlate with DIC experimental data for make-up and service loading. Required modeling effort and computing resources assess the manageability of the FE model. It is feasible for a manageable and tractable 3D FE modeling approach to be integrated into industry practice.

1.4 Research Scope

The focus of this research is to:

1. Develop a parametric modeling approach to create full 3D with helical threads finite element models for OCTG premium connections to accurately represent the make-up conditions.
2. Develop a controlled parametric meshing scheme to keep the FE model tractable for available computing resources.
3. Calibrate the 3D FE make-up model with DIC displacement and strain experimental data.
4. Validate the 3D FE model against DIC experimental data from ISO 13679 Series B service loading [5] and evaluating metal-to-metal seal performance.

The optimization of connection configurations, geometric parameters, and seal performance is beyond the scope of this research. The ISO 13679 Series B service loading test is limited to axial loading and internal pressure only for this study. The validity of the DIC technology is also beyond the scope of this work. However, general details of DIC data acquisition and processing are presented.

1.5 Thesis Organization and Discussion

The thesis write up follows the order stated below:

1. Parametric 3D FE Model Development
2. DIC Measurements and Data Processing
3. 3D FE Make-Up Model Reconciliation
4. 3D FE Model Service Loading Validation Results
5. Conclusions and Recommendations

Chapter 2 Literature Review

The focus of this research is to develop a full 3D parametric FE model of an OCTG premium connection to reduce testing time and costs and optimize connection design and performance. Current industry practice of FEA modeling for premium connections only consists of axisymmetric models. There is no literature available in the public domain of a successful 3D FE modeling approach of OCTG premium connections. The validation of the FE models in this research relies on proper use of optical metrology technology for acquiring displacement and strain data from physical testing. The following sections provide a brief background on benefits of FEA for premium connection design and testing and why further development of FE models is essential.

2.1 OCTG Testing

The detailed process for OCTG connection performance testing is presented in ISO 13679 [5]. Together, finite element models and full-scale physical tests provide an effective set of tools for assessing the integrity and performance of complex structures such as the OCTG premium connections. As stated in the ExxonMobil connection evaluation program [6], "FEA can be used to evaluate quantitatively the seal quality, whereas the physical test results are binary (i.e., "leak" or "no leak")". The qualification testing of premium connections is designed to reproduce the worst combination of loading scenarios expected during service. Assaneli [7] explains that the testing has to be performed for every combination of tube dimensions and material properties that are to be qualified. He recognizes that it is extremely important to ensure the reliability of FE models as certain parts of the OCTG tests are allowed to be replaced by these models to ensure the safety of oil-well operations. The performance analysis of OCTG premium connections using FE models is progressively replacing the use of full-scale tests in the design phase of new connections and has been incorporated, in proper combination with full-scale tests, in the qualification procedure of existing connections.

2.2 OCTG Finite Element Analysis

Weiner [8] developed early work on API threaded connection analysis and seal performance. He simplifies the problem with linear elastic assumptions and established that "the end of the pin needs to be on the verge of yielding" for maximum sealability. Heijnsbroek's [9] research with metal-to-metal seals determines that contact stress at the sealing surface is the most important seal performance parameter and "yielding of the material at contact is needed for sealing". Assaneli [7] confirms "material-nonlinear-only analysis" on API threaded connections without presenting other details about their FE modeling techniques. Hilbert and Kalil [1] provide good insights into axisymmetric modeling of premium threaded connections. They emphasize three major nonlinearities; "surface interactions, material behavior, and deformation geometry" must be modeled to analyze the performance of premium threaded connections. They state that the axisymmetric assumption results in accurate stress and strain results but also acknowledge that "there is currently no verified, reliable, and general correlation between make-up torque and torque shoulder interference". Dvorkin [10] reinforces that realistic elasto-plastic material models, and contact algorithm able to represent large sliding situations between surfaces has to be included in finite element analysis of threaded connections.

Axisymmetric FE models are currently used for design and testing of the OCTG premium connections. Axisymmetric analysis assumes symmetry of the deformation field about the axis of rotation, this symmetry results in no dependence of displacement field in the circumferential direction. Axisymmetric models cannot account for the spiral of the helical threads and cannot simulate the physical torque-turn behavior of the connection make-up properly. Galle [11] recognizes that "despite the commonly accepted approach of using axisymmetric models to simulate the behavior of threaded connections, the make-up stage is not yet fully validated in literature". Sugino [12] explains that the axisymmetric models are assembled with threads and seal geometrically overlapped by a specific interference. An analytical finite element function of introducing a pretension is used at a "specific" part between the threads and the torque shoulder is axially extended to simulate the make-up condition.

Ostergaard [13] acknowledges that "the best applicable model of the premium connection is a full 360-degree representation of the box and pin". The 3D FE model has no associated modeling assumptions. The geometry, boundary conditions, loads, and stiffness distributions can be represented exactly. However, the complex geometry of premium connections along with required level of mesh density proposes an intricate and challenging problem. Hence, there is no literature associated with 3D FE models of OCTG connections in the public domain of any successful or failed attempts. A full 3D FE model can properly simulate the connection make-up and progress the goals towards theoretically predicting sealing capabilities and performance of a premium connection.

2.3 Product Line Evaluation

Hilbert and Kalil [1] recognize that the ability to see "inside" of a connection is the fundamentally most important contribution of FEA. Full-scale tests only provide "macroscopic" observations of the surfaces of a connection. Finite element analysis combined with full-scale testing can be an effective and efficient tool to investigate the effects of changes in dimensions, dimensional tolerances, or material properties on load limits and failure modes or threaded connections. Dvorkin [10] acknowledges that FE models are an ideal design tool for making parametric analysis in which the influence of different design parameters on the connection performance can be identified.

Bradley [3] distinguishes that FEA is valuable for the user to compare various connection designs under defined loading conditions to reduce the total number of designs to be considered for physical testing. Modeling the connection, applying material properties, and loading scenarios can be used to select the fewer designs for testing to reduce testing costs and time. He also states that is possible to use FEA to extrapolate or interpolate around variants of connections that have completed physical testing. Powers [4] defines that approach as product-line evaluation for a family of connections. Product-line evaluation approach includes finite element analysis of all of the family members within a range of size/weight/grade combinations, and rigorous physical testing of connections representing the boundaries of the range or worst cases within the range. Product-line evaluation approach significantly reduces time and costs associated with connection qualification. Khemakhem [14] constructs on Power's work to describe characteristic performance factors of sealability, structural integrity, galling resistance, environmental resistance, and fatigue resistance to predict performance of a group of connections bases on physical tests of a few connections.

2.4 Parametric FEA Modeling

Parametric modeling is used widely for design problems and FEA in many industries. Fan [15] provides an example of parametric FEA on an automotive braking system where the model geometry parameters updates are automated. Jiapeng [16] acknowledges the time consuming characteristics of FEA pre-processing especially for complex structures and provides insights for developing a parametric FE model of an aircraft wing structures with automated updates for geometry and mesh. Generating full 3D FE models is a time consuming process particularly for complex geometries of premium threaded connections. Creating a "one off" 3D FE model is a very inefficient way for it to be used as a design tool especially for the product-line approach where numerous FE models are required. Generating parametric full 3D FE models that allow automated geometric and mesh updates is the main objective of this research.

2.5 OCTG DIC Testing

The conventional make-up and service loading tests for premium connections utilize strain gages placed axially and circumferentially on the connection to acquire data at select points. Sparse strain gage placement does not capture the complex strain field produced by the geometrical features of the premium connection appropriately. Hilbert and Kalil [1] admit that the strain gage placement frequently misses the locations of high strain from the peaks detected by the FEA results. Dvorkin [10] acknowledges that it is usually difficult to identify the causes behind structural or functional failures in full-scale tests even if

extensive strain gaging instrumentation is used; many times unidentified connection manufacturing errors mask the test results.

DIC systems are capable of providing high spatial density full-field displacement and strain measurements. Ostergaard's [13] research verifies that DIC measurements can provide full-field validation data for FE models of OCTG premium connections make-up with appropriate correlation techniques. Galle [17] acknowledges the DIC testing provides measurements over a large surface which provides more information about the strain behavior beneficial to observe abnormalities such as material defects. Galle [11] demonstrates that DIC measurements show similar results as strain gages and it is the preferred method for numerical validation purposes. DIC experimental process requires special attention for specimen preparation, test set up, and system calibrations to ensure appropriate deformation results. However, the high spatial resolution results are more beneficial than conventional strain-gage data.

Chapter 3 3D Parametric Finite Element Model

In today's commercial workflow, 3D FE models are typically generated by importing 3D solid parts or assemblies into finite element software from CAD software. This process results in a one off 3D model which does not allow few geometric updates to the parts. Meshing of the complex geometry and helical threads prove to be problematic with 3D solid parts and assemblies. It was quickly realized that importing solid parts will end up with an intractable FE model since a proper mesh would require over 1 million 3D brick elements, also acknowledged by Ostergaard [13]. This approach also contradicts the objective of this research of using the FE model as an effective design tool since it does not allow parametric updates within the model.

Creating a full 3D FE model geometry and then partitioning and meshing the model are the two most time consuming tasks. Importing of CAD models for the geometry makes sense only if the model needs to be created once. To utilize the model in the design process, it must allow for parametric updates to perform design trade-offs and test different configurations. The analyst will have to build and run multiple models, starting from the beginning every time is not a productive approach. Creating effective parametric 3D models in FE software must be manageable for the analyst. It is important for the element count to be minimized and mesh schemes to be controlled throughout the parts to keep the FE models tractable for computing resources. A methodology developed to build manageable and tractable full 3D FE models for OCTG premium connections is presented in this chapter.

3.1 3D Parametric FE Model Approach

To meet the objectives of this research, development goals are set for an effective 3D FE model listed below in Table 3.1.

Table 3.1: 3D FE model development goals.

1	The full 3D FE model must be parametric for user defined geometry and mesh updates
2	The full 3D FE model should provide an efficient way to update the parameters
3	The full 3D FE model must be manageable for the user and tractable for available computing resources

There are two main types of premium connections, metal-to-metal seal threaded and coupled joint (MTC) and metal-to-metal seal integral joint (MIJ) [18]. MTC connections utilize a coupled box where a pin is threaded into each end. MIJ connections incorporate the box with the pipe and there is only one threaded connection. There are several variations of both coupled and integral joints. Figure 3.1 provides a visual representation of MTC and MIJ connection set up.

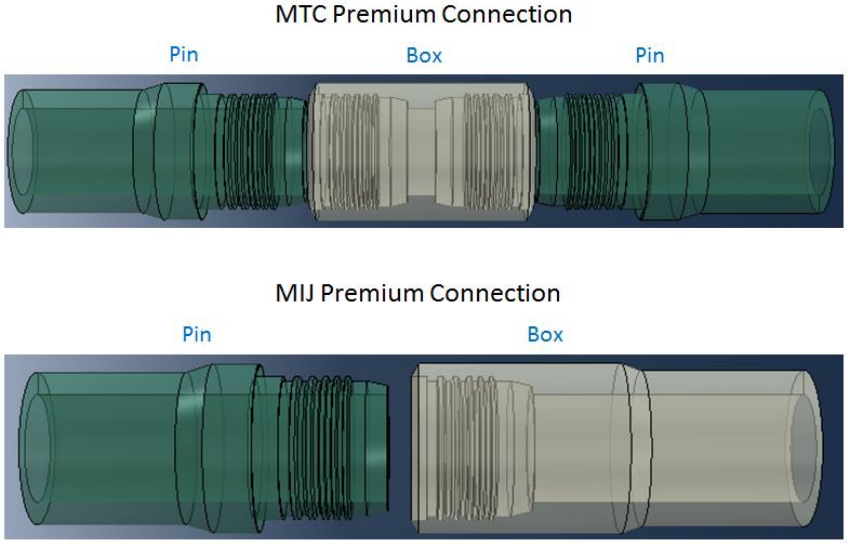

Figure 3.1: Box and pin set up for two main types of OCTG threaded premium connections.

A methodology is developed to create a full 3D parametric finite element model with helical threads for a MIJ premium connection to achieve the modeling goals in Table 3.1. The MIJ connection is selected for this research because connection geometry and DIC testing data is provided by a manufacturer for demonstration. A scripted parametric approach is developed for updating the geometry of the connection and to control the meshing of the components. Scripting allows an efficient way of exploration of design configurations and features of the joint that define the mechanics of the connection such as seals and the torque shoulder. Python scripts are developed that update the model geometry and mesh as defined by the user and generate the new FE model within seconds. The same process performed manually can take hours to complete. The scripting process needs extra time and effort to develop a base model, but it pays off when the model requires geometry or mesh updates. For example, if the user needs to update the seal interference parameter, a new model can be created in seconds by updating seal geometry parameters with the scripts. 3D models imported as solid parts would require the user to create a completely new model which could take hours.

The scripted parametric approach allows the user to perform parametric trade-off studies to refine and optimize the design of the connection productively. This approach also provides an efficient way to generate FE models of different connections within a family, or product-line, for connection qualification. There are two main aspects of the modeling where parameterization is required:

1. Parameters associated with connection geometry.
2. Parameters associated with the meshing scheme.

Parameterization associated with both geometry and meshing is presented in the following sections.

3.2 Parametric Geometry Model

Importing CAD models of a connection into finite element modeling environments such as the Abaqus CAE (Complete Abaqus Environment) software is not feasible for the proposed modeling approach. The connection geometry is built inside Abaqus CAE from technical part drawings provided by the manufacturer. A premium connection assembly has two parts, the box and the pin. Both parts have intricate designs with complex geometric features. It is very difficult to model each part as one component especially with the considerations for finite element modeling. A critical step for the success of this approach is to decompose the geometry into smaller parametric components. The breakdown of the geometry allows the model to be created in small 90˚ sectors which is also valuable for the meshing scheme explained in section 3.3. In addition, the decomposition of the parts permits the model to be manageable and tractable. Creating a full 3D parametric model as one part would prove to be a problematic task.

3.2.1 Parametric Geometry Decomposition

The decomposition of the connection geometry is possible in multiple ways. The MIJ connection is decomposed systematically by splitting the geometric and mechanical features of the connection into separate components with the interface between connection feature regions well defined. The connection breakdown can be modified and customized to fit the needs of the designer and the analyst. Table 3.2 lists some general guidelines to breakdown the MIJ connection into parametric components.

Table 3.2: General guidelines to decompose premium threaded connection into parametric components.

Regions that can be well defined parametrically with available technical drawings
Regions that represent mechanical features of the box and pin parts
Interface regions between features of the connection
Contact regions that require variations in mesh density
Regions that may require different material models

3.2.1.1 MIJ Connection Breakdown

The MIJ connection geometry is decomposed into parametric components created in 90˚ sectors which are later merged into full 360˚ 3-D parts. MIJ connection pin and box parametric components created in this study are listed in Table 3.5 and displayed in Figure 3.2 and Figure 3.4.

Table 3.3: MIJ premium connection parametric components.

Pin and Box Base
Primary Seal
Secondary Seal
Shoulder
Inner Thread Base
Outer Thread Base
Inner Thread
Outer Thread

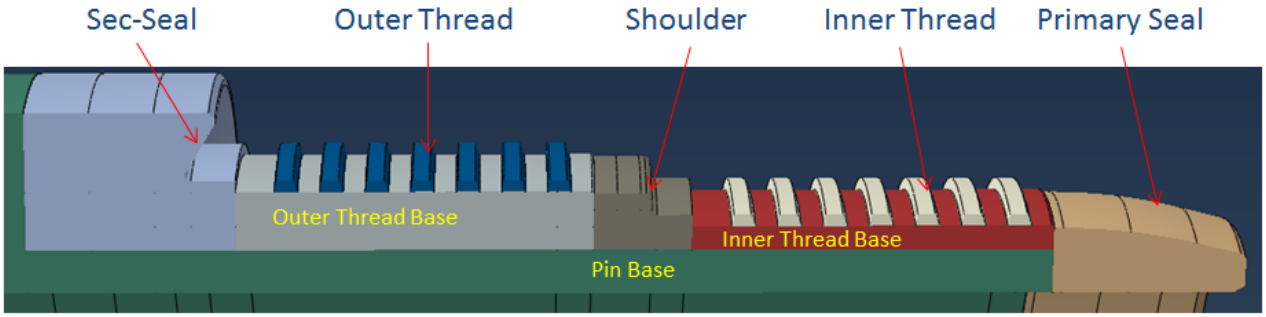

Figure 3.2: Component breakdown of the MIJ premium connection pin.

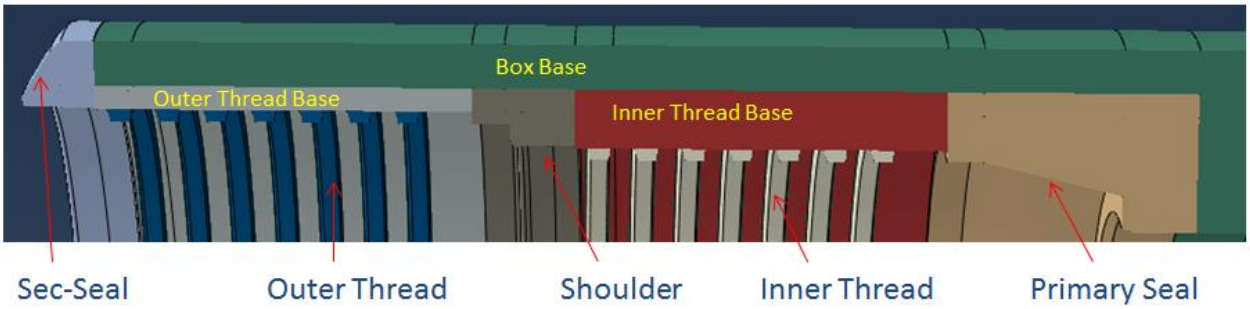

Figure 3.3: Component breakdown of the MIJ premium connection box.

The pin and box base serve as the inner and outer shells that govern the overall connection wall thickness and diameter. The rest of the connection features are decomposed systematically following the guidelines listed in Table 3.2. Primary and secondary seals combined with the shoulder region and threads represent the main mechanical features of the connection which define the primary seal performance and the torque-turn behavior. Overall geometric dimensions required to breakdown the connection features are extracted from manufacturer supplied technical drawings. Primary and secondary seals along with the shoulder have specific contact regions that require geometric and meshing parameters to control connection configurations and mesh density. The inner and outer thread bases provide the interface between all of the components and produce effective assembly points for locating the threads. Helical threads are created as separate components presented later in section 3.2.2. There is no single solution for a proper decomposition of a premium connection. The breakdown of connection features is subjective to the connection and parameters of interest to the designer or the analyst.

3.2.1.2 Geometric Parameters

Generating 3D finite element models can be a very time consuming process. The models are parametrized and scripted for an efficient way of updating the parametric geometry and creating new models of different connection configurations. The modification of geometry parameters and assembly of the box and pin is automated using Python scripts. All the components shown in Figure 3.2 and 3.3 are sketched in the Abaqus CAE environment using dimensions from technical part drawings. The dimensions are named accordingly under the Abaqus CAE parameter manager and copied into a .csv file. Python scripts are developed to generate the 3D models using the defined parameters. All sketches must be fully constrained to execute the Python scripts. The fully constrained sketch allows part parameters to be updated while keeping the geometry accurate. A brief explanation of fully constrained sketch behavior is provided in Appendix A.

Relationships are developed between geometric constraints, dimensions, and parameters that control the geometry in the Abaqus sketch module. Developing fully constrained sketches of the components may require extra dimensions than the ones available in the manufacturer drawings. The "expression builder" feature in Abaqus CAE parameter manger is used to generate the required dimensions. Mathematical expressions are produced to create the extra dimensions as needed. Generating dimensional relationships streamlines the parameterization of the connection by only utilizing dimensions available in the technical drawings for .csv files. There is no need for the user to calculate any dimensions that are not readily available from the part drawings. Figure 3.4 displays a fully constrained sketch illustrating parameterized dimensions.

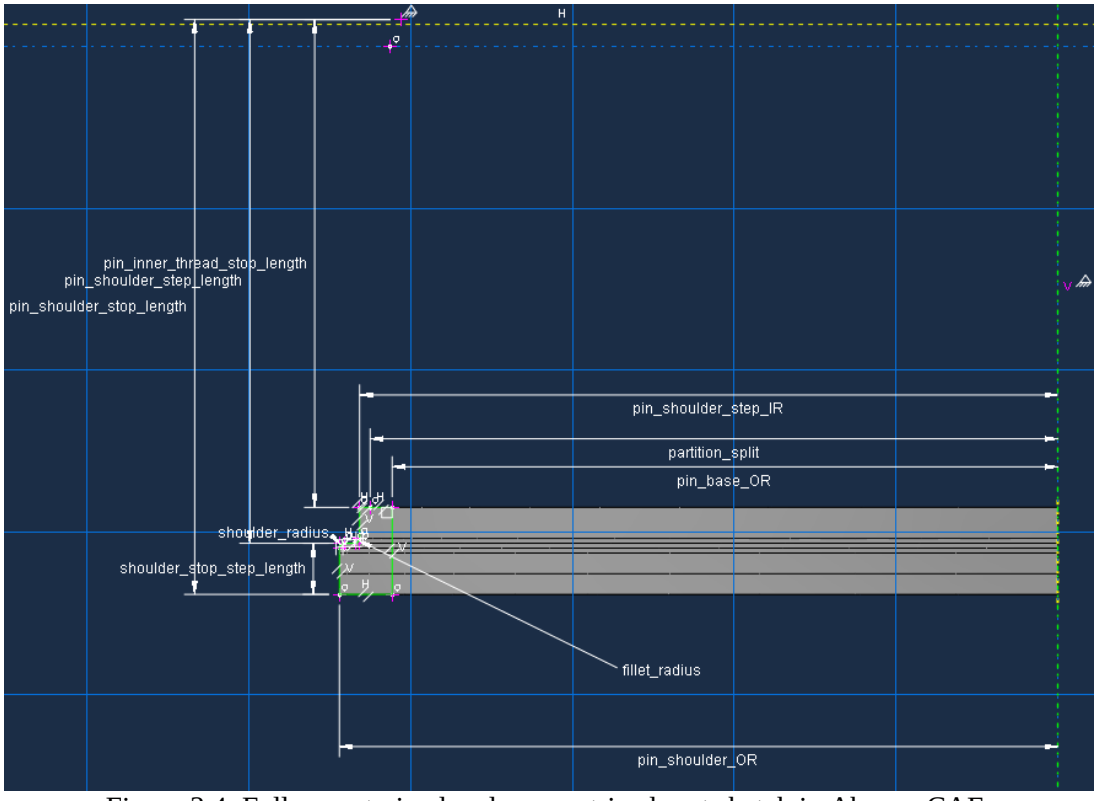

Figure 3.4: Fully constrained and parametrized part sketch in Abaqus CAE.

As stated before, each component is created as a 90˚ sector. This is a critical stage in keeping the models manageable. Developing the component models as subcomponents that can take advantage of symmetries allows for an easier process of creating sets, partitions, and defining surfaces. Mistakes made at this stage of the modeling process require a lot of time to troubleshoot. The 90˚ sector models reduce the chances of error significantly compared to full 360˚ components. The sets and surfaces defined here are used later in the modeling process to define contact, loads, and boundary conditions.

Systematic partitioning is a key aspect for a controlled parametric meshing scheme. Smaller sector models permit an easier partitioning and meshing process before it is applied to the fully revolved components. More on meshing schemes is explained later in section 3.3. Smaller sector models require less effort and time for all the manual processes. The user defines parameters on the minimal set of features requiring the least manual operations. The scripting process performs the tedious aspects of building and instantiating the full 360˚ section and parts. The scripted parametric approach reduces the complexity and error prone operations associated building FE models. It allows for scaling the model to a full premium connection product-line as well as manufacturing variations such as high and low seal and thread interference. The approach also facilitates design trade-off studies for connection design and model-test correlation.

3.2.2 Helical Thread Generation

The helical threads are generated by applying a parametric approach similar to the rest of the premium connection components. The main modification is defeaturing the thread geometry. Full geometry of the helical threads details small geometric features which are typically not required for the analysis. The thread small geometric features complicate the meshing process requiring high mesh densities in the thread regions to represent the small features. The thread regions in the model require a lot of computing resources for solving the contact problem. Defeatured threads significantly cut down the number of elements while maintaining the representative stiffness of the thread region in the connection. Lower element count in the thread contact region reduces the model runtimes considerably. Thread geometry is defeatured by removing the radii on all the edges. No other modifications are made on the thread form and geometry. Defeaturing the threads is a necessary step to keep the 3D model tractable for computing resources. Figure 3.5 displays an example of the defeatured thread for the MIJ connection used for this research. The advantages of defeatured threads on the model runtimes are discussed in section 3.8.1

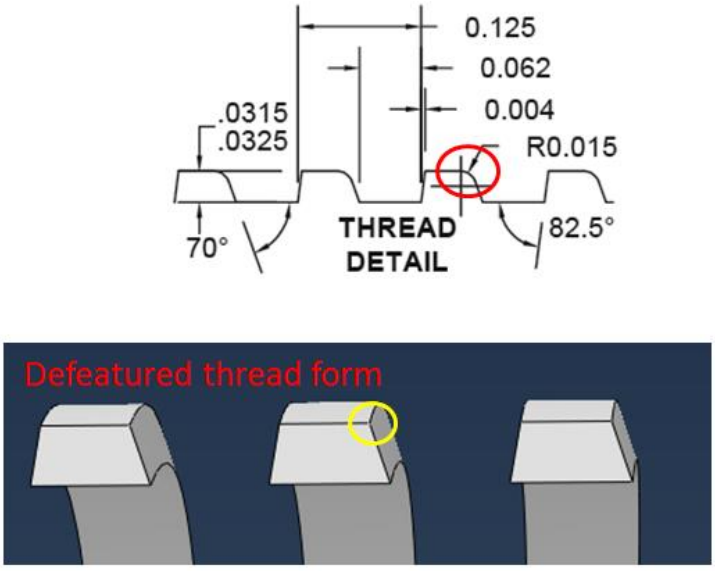

Figure 3.5: Helical threads are defeatured by removing edge radius (top). Cut view of the modeled defeatured helical thread form (bottom).

The helical thread form and geometry is also parametrized using the technical drawings. One way to generate the helical thread revolutions is by prescribing the pitch and sweep angle in the revolve function of the Abaqus CAE Sketch module. However, revolving the threads 360˚ or higher creates multiple surface divisions in the thread faces. These divisions produce distorted elements during the meshing process. Figure 3.6 illustrates the geometry splits in the thread face from a 360˚ revolution. After additional investigation of the process, generating a 180˚ revolved sector of a thread is found to be the best solution. Assembling threads into a full helical thread section requires multiple revolutions compared

to all the other components that only need one 360˚ revolved part. Creating the original sector into 180˚ saves time and effort during assembly from a 90˚ sector. The simplified thread geometry requires fewer partitions and sets when compared to other components. Therefore, creating other components into 180˚ sectors is a disadvantage. An illustration of an 180˚ single thread sector is presented in Figure 3.7.

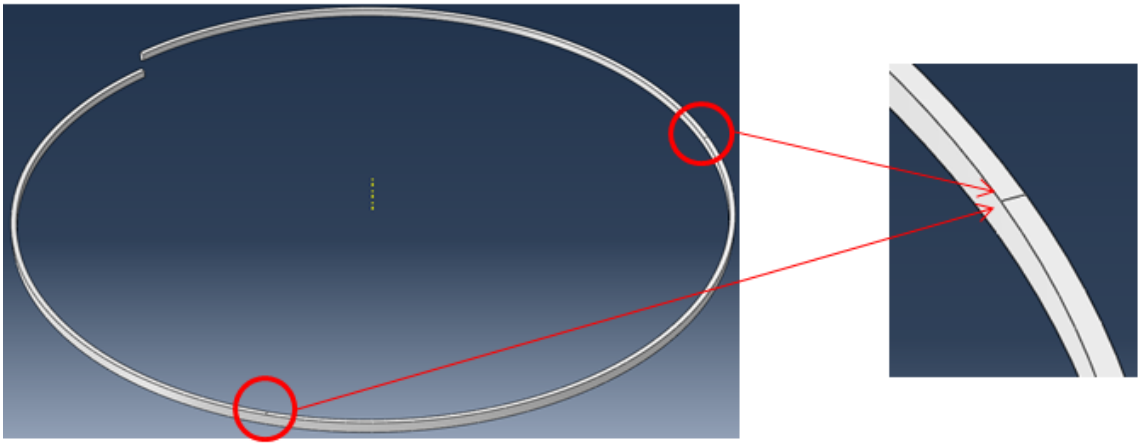

Figure 3.6: 360˚ revolved single thread displaying surface divisions in the thread face.

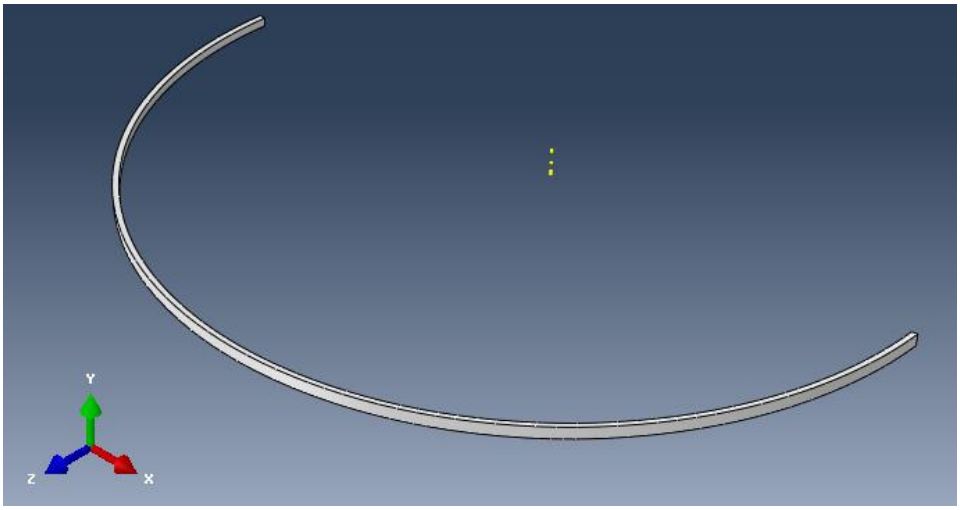

Figure 3.7: 180˚ revolved single thread used for creating helical thread parts.

3.2.3 Connection Pipe Section

Modeling the full length of the pipe section of the test specimens is necessary to apply boundary conditions accurately. The length of the pipe on the connection of the test specimens can be anywhere from a few inches to a few feet long. Therefore, 3D beams are used with pipe section profile to create the pipe and adjust the specimen length. The use of beam elements for the pipe can reduce the element count of the connection model by thousands of elements. The beam section profile and length is prescribed parametrically from the technical drawing similar to rest of the connection geometry. Figure 3.8 displays a rendered beam section compared with 3D structured mesh of the same size section. These modeling decisions are made in order to keep the 3D FE model manageable by controlling and minimizing element count. The results of a make-up model are compared using beam and 3D brick elements to justify this decision in section 3.8.2.

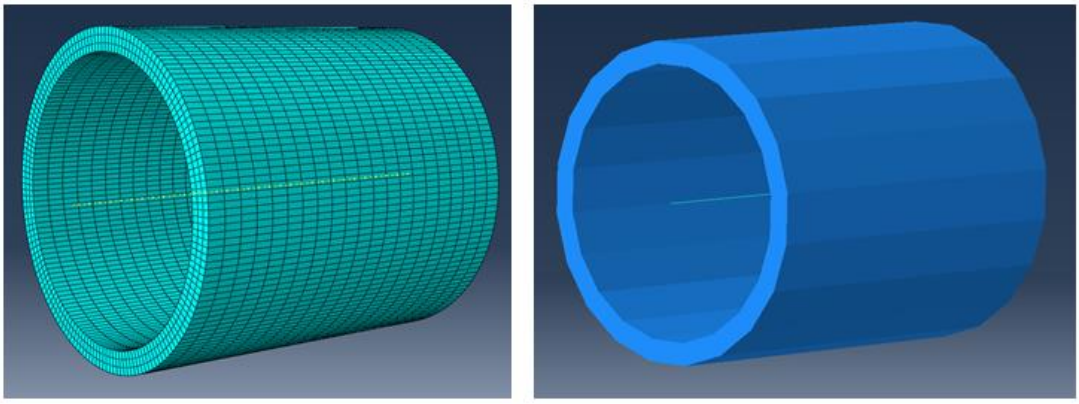

Figure 3.8: A 5” pipe section ~ 15k 3D elements (left) compared to 1 beam element (right).

3.2.4 3D Model Assembly

The assembly of the components into full 360˚ parts is automated by a Python script. This method is developed to update parameters and generate new models easily and efficiently and allows the FE models to be used as a design tool. Model parameters for geometry and mesh seeding are stored in .csv files. The user can update any parameter as needed and generate a new model within seconds. Figure 3.9 illustrates a data flow diagram of the Python script operation.

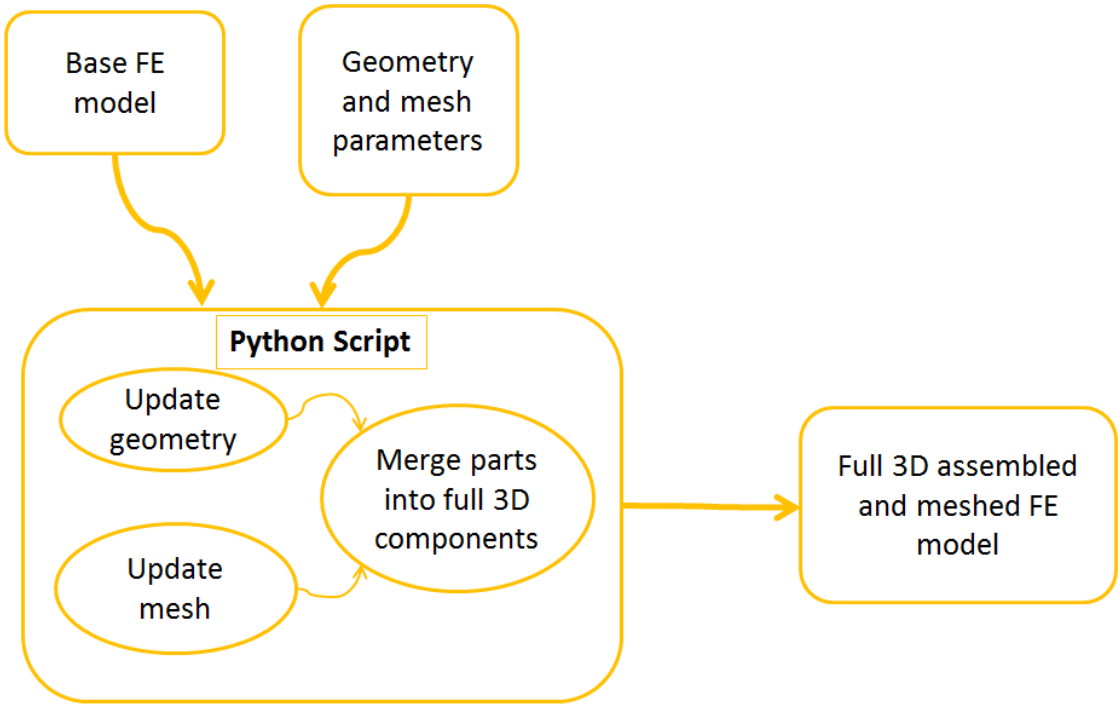

Figure 3.9: 3D FE model generation Python script data flow diagram.

The Python scripts update all of the geometry and mesh seed parameters on the sector components. Each component is meshed and merged into a 90˚ sector of the complete pin and box parts displayed in Figure 3.10. The radial pattern feature is used to copy the merged sectors four times around the central axis which are then merged into a full 360˚ pin and box. The “mesh merge” option is used to merge the 90˚ sector components into a single 360˚ part. This allows the part to be meshed at the component level and does not require re-meshing of the part as it would if a “geometry merge” was performed. Details of the meshing scheme are discussed in section 3.3.

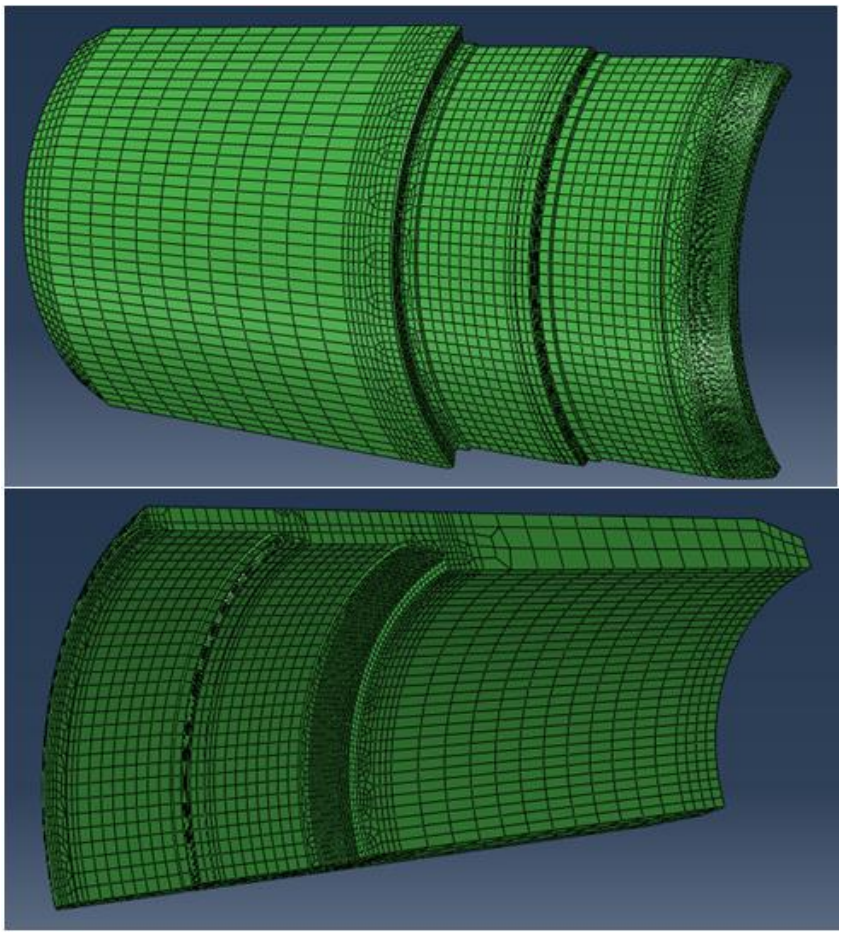

Figure 3.10: MIJ premium connection pin (top) and box (bottom) 90˚ sector merge assemblies.

Thread generation is also automated within the same Python script. However, the process is slightly different since the original components are created as a single 180˚ thread, and more than one revolution is required. The linear pattern feature is used to create the required number of thread revolutions, and then the radial pattern feature is used to produce a full 360˚ helical thread part. The helical threads are assembled onto the pin and box with a surface to surface "Tie" constraint. The part merge function is not feasible in this situation due to the helix angle of the threads. Merging two components requires the mesh elements on the merged surfaces to be aligned. In this case, it is not possible to match the elements representing the threads with the elements representing the pin or box thread base surfaces due to the helix angle. The surface based "Tie" constraint ties all active degrees of freedom for the defined surfaces. Multi-point constraints between the slave node degrees of freedom and master element nodal degrees of freedom are defined at the intersection of the slave node with the master surface element. For this case, box and pin surfaces are set as master and threads are set as slaves.

Surface-to-Surface "Tie" constraints allow for mesh transitions between the surfaces which is critical for mesh refinement purposes [19]. Mesh transition through the tie constraint is essential in this case since the box and pin surfaces have a finer mesh than the threads. With the surface to surface "Tie", the thread and the thread base surface behave as a single combined part and the user has the flexibility of mesh mismatch between the two surfaces. Section 3.3.1 presents the details on the necessity of mesh alignment when merging two components. Figure 3.11 displays the pin and box parts completely assembled into full 360˚ 3D parts with helical threads.

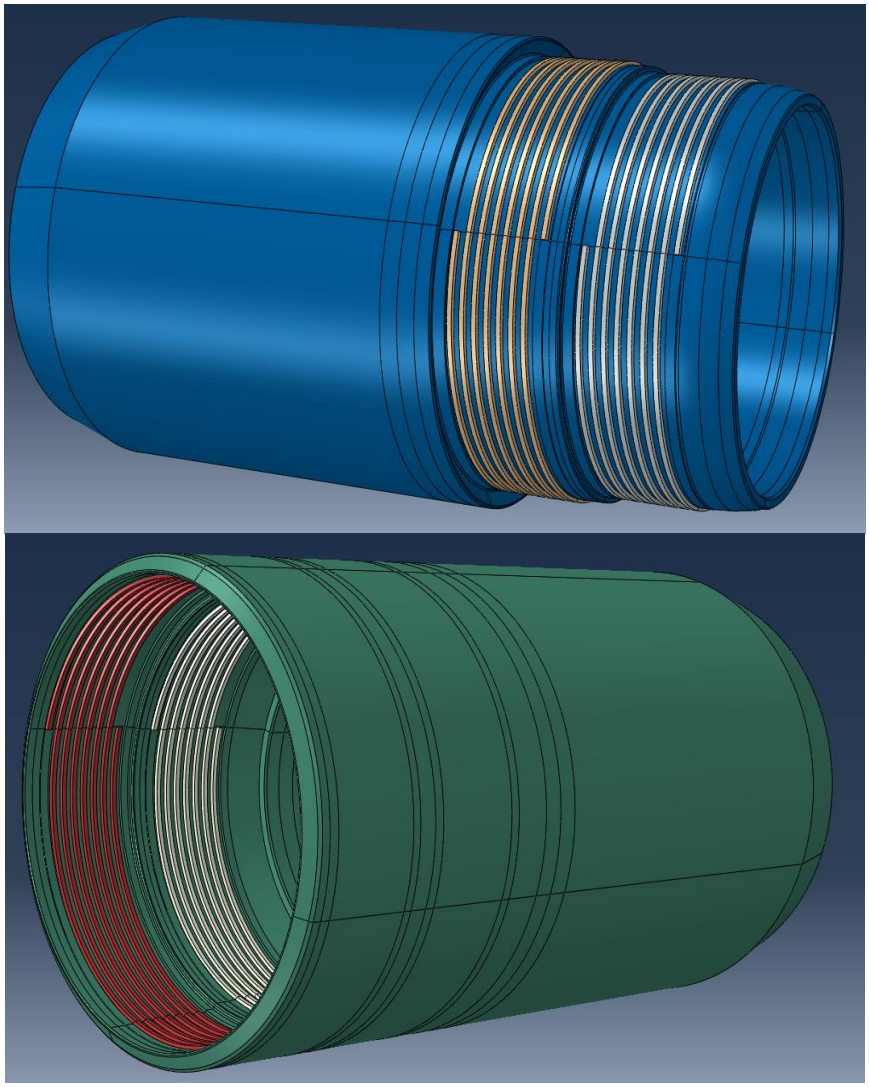

Figure 3.11: MIJ premium connection full 360˚ 3D with helical thread pin (top) and box (bottom).

The pin and the box are assembled together to an estimated "hand-tight" position which is typically connection design dependent. The "hand-tight" position for the MIJ premium connection demonstrated here is estimated as the point where the primary seal on the pin makes physical contact with the box. The location of the box and pin is selected from reference points available in the manufacturer's technical drawings defining assembly at the hand-tight position. The assembled location of the box and pin depends on the data available from the drawings or the CAD models and can be modified by the user accordingly. The pipe section beams are then added to the assembly to adjust the overall length of the connection. The beams are attached to the pin and box with a surface based structural coupling constraint. The coupling constraint couples the motion of the nodes on a surface to the motion of a reference node allowing boundary conditions to be applied on the beams. Figure 3.12 displays the pin coupled to the beam element pipe section. The box end of the connection assembly has a similar coupling interaction. Figure 3.13 displays the complete assembly of the full 3D MIJ premium connection finite element model.

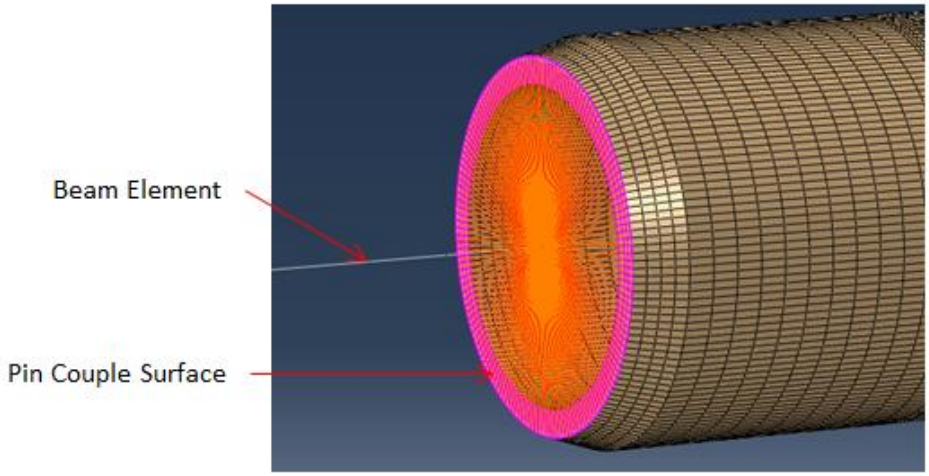

Figure 3.12: Beam element pipe extensions coupling interaction on the pin end.

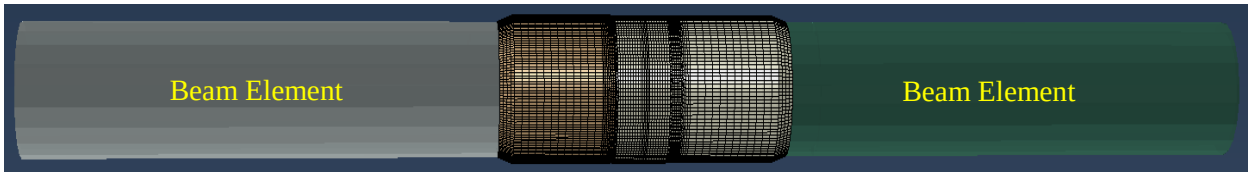

Figure 3.13: Full 3D MIJ premium connection finite element model assembly.

3.3 Parametric Mesh Scheme

Mesh generation is the second most time consuming task after the model geometry is built. The goals for the parametric modeling approach restated in Table 3.4 apply here as well.

Table 3.4: 3D FE model development goals.

1	The full 3D FE model must be parametric for user defined geometry and mesh updates
2	The full 3D FE model should provide an efficient way to update the parameters
3	The full 3D FE model must be manageable for the user and tractable for available computing resources

Improper mesh scheme can make the model intractable for computing resources or provide inaccurate results. The meshing of every component must be performed systematically for a successful 3D FE model. The conventional approach of meshing 3D components as one part is not practical for the geometry of a typical premium connection. The primary goal for a controlled meshing scheme is to develop an effective mesh that generates a converged solution with minimal number of elements. An effective mesh scheme is achieved by partitioning and meshing the parts parametrically. A fine mesh is used in the regions of interest only and a coarse mesh is used in the rest of the model. The parametrization permits the mesh density to be controlled in every region of the model by the user.

Premium connection geometries are always difficult to mesh effectively. The metal-to-metal seals are the focus for the model, while they are less than ~0.1% of the total mesh area. Development of a proper meshing scheme is critical in keeping the full 3D model tractable. Although the parameterization of seed sets is a lengthy process in itself, extra time spent creating seed sets and mesh parameters pays off during the analysis phase. Creating new models with updated geometry and mesh schemes takes seconds instead of hours or possibly days. Efficiency of this approach keeps the 3D FE model manageable for the user. The scripted/parametric meshing process allows the operator to increase or decrease the mesh density as desired. If the mechanics and the results for the metal-to-metal seal is the area of interest, the operator can allocate a finer mesh in the seal contact region only. An effective mesh scheme permits the model to stay

tractable with minimal element count which translates to lower runtimes allowing the 3D FE model to be used as an efficient design tool.

3.3.1 Mesh Seed Parameters

Systematic partitioning of the parts is a critical step for creating mesh seed parameters. It is essential that the partitions in the components align with each other during the assembly in order for the mesh to merge correctly. The partitions must be created methodically so they can be updated along with the geometry requiring the formation of additional expressions in the geometry parameter manager. Smaller 90˚ sectors of each component make the partitioning process efficient by reducing the manual operations. The edges formed from these partitions are created into sets to generate seed parameters. The "seed edge by number" of elements option is specified instead of "seed edge by size" of elements to control the mesh properly. The seed parameters and seed number data is stored in a .csv file and read into the Python script similar to the geometry parameters.

In order for the mesh to merge correctly during the component assembly process, the number of elements on two merged edges must be equal. Experience and care are necessary when assigning seeds since troubleshooting these issues can require a lot of time. An illustration of aligning partitions and mesh seed numbers is shown in Figure 3.14. A mismatch in partitions, or seed numbers, will not merge the nodes on that certain edge. The outcome for mismatches in the mesh is poor results, as the edge(s) will split in two under loading because the elements are not connected through nodes on a common edge. Due to some geometric features of the connection, some partitions produce small edges which can easily hide these errors. Experience and care must be engaged throughout the partitioning and seeding process to ensure accurate results.

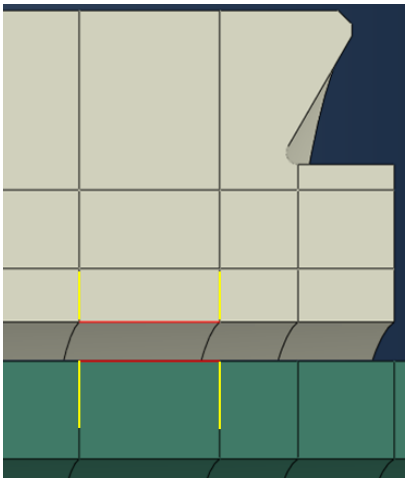

Figure 3.14: Partitions within the components must align with each other (yellow); Number of seeds for merging edges must be the same (red).

Figure 3.15 illustrates an example of node misalignment through a partition mismatch and the effect of this misalignment under loading. A mistake made during defining geometric parameters caused the node misalignment displayed in Figure 3.15. There was a typing error between the parameter .csv file and Abaqus CAE base model which caused a partition to not update correctly. Equal number of elements on two edges and length mismatch produced nodes that did not align properly. Developing geometric and seed parameters require special attention to small details. Simple mistakes can provide inaccurate results and take a lot of time to troubleshoot. The effects of node misalignment also provide another reason why the threads cannot be merged into the pin or the box to create one part. The helix angle on the threads makes it almost impossible to align the mesh at each node. Therefore, a surface "Tie" constraint serves the best in that region.

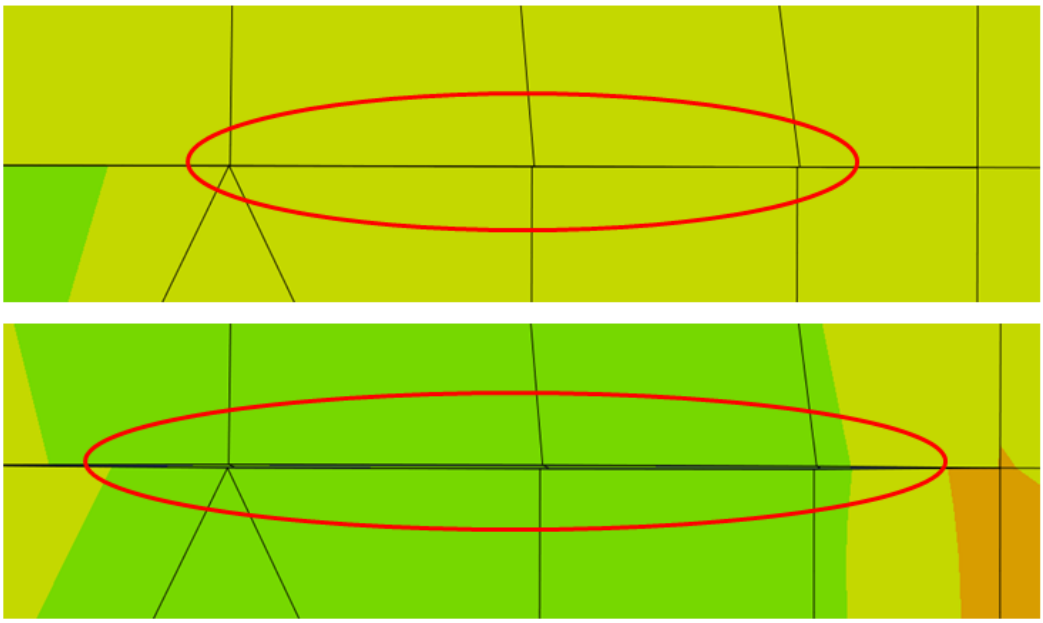

Figure 3.15: Node misalignment due to element size mismatch (top). Non-merged nodes split the edge in two when loaded (bottom).

The analyst must also pay attention to the aspect ratio of geometric features of the parts when assigning mesh seeds to ensure a sufficient aspect ratio of the elements. The cylindrical geometry of the connections requires mesh refinement in longitudinal and circumferential direction simultaneously for proper aspect ratio of the elements. Some regions may require further partitions or extra elements to avoid poorly shaped elements. There is a major trade-off between element count and aspect ratio especially in the seal regions where a fine mesh is required. Mesh refinement in the circumferential direction rapidly increases the total element count. A lot of mesh design and effort goes in to making sure the aspect ratio of the elements is not skewed when setting seed parameters. In the seal regions, the average aspect ratio is kept less than 2.5:1 and less than 5:1 for the less critical areas of the connection. Figure 3.16 displays cut view of the fully partitioned pin and box MIJ connection used in this study.

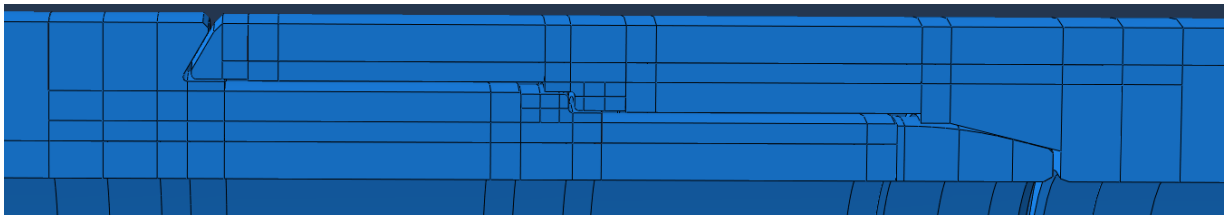

Figure 3.16: Cut view of fully partitioned MIJ connection pin and box.

Seed parameters are also generated for all threads in a similar process. In order to minimize the element count, threads are meshed with only one element through the thickness. The stiffness of the threads is represented well and it saves thousands on the element count allowing the mesh to be denser in the regions of interest. Figure 3.17 displays a set of helical threads assembled and meshed.

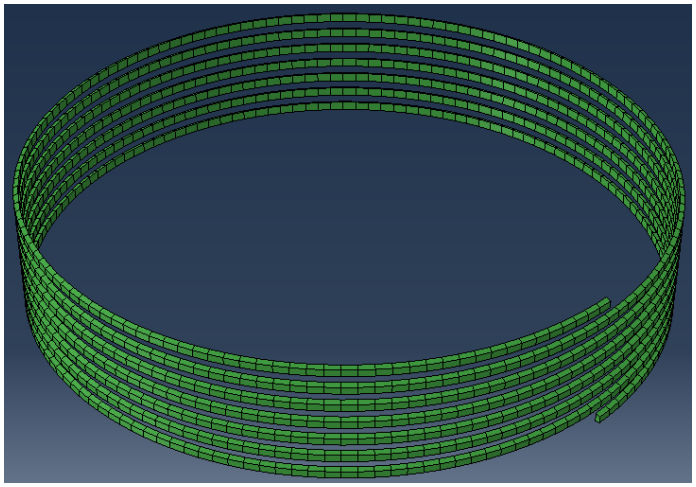

Figure 3.17: Assembled and meshed MIJ connection helical threads.

3.3.2 Mesh Transition Regions

Mesh transition regions are created in order to control the mesh density in the desired areas of the components. The methodical partitioning of the components discussed in the previous section assists in creating mesh transition regions. Due to the cylindrical geometry, mesh transition is required in the hoop direction as well as the longitudinal direction. Since the scope of this project is focused on the metal-to-metal seals, the transition regions on the box and pin are implemented in the primary and secondary seal regions only. Mesh transition regions can be utilized in any region where a change in mesh density is desired. The "sweep" meshing strategy is used throughout the model which allows the operator to have control over the sweep path direction. Mesh transition regions are formed by defining the sweep path perpendicular to the desired transition path. Figure 3.18 displays two mesh transition zones with their respective sweep paths on the pin seal.

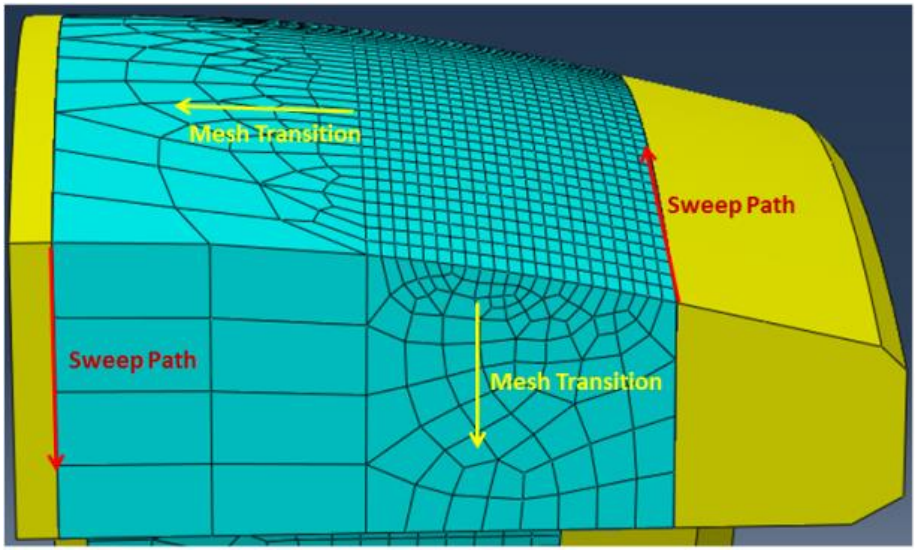

Figure 3.18: MIJ connection pin seal mesh transition regions illustrating corresponding "sweep paths".

The analyst must pay attention to maintaining proper element aspect ratio and shape when defining the mesh transition region. Transitioning from a very fine to a very coarse mesh can result in distorted elements. If needed, the user can define multiple transition regions for a gradual mesh density change. Working with small sectors instead of a complete assembly makes the process easier. The analyst can quickly try various mesh transition rates and chose the best possible mesh.

3.3.3 Mesh Strategy for Contact Regions

There are several contact regions in the MIJ connection which require different mesh strategies. The hoop direction mesh causes the largest increase in element count and has the most effect on the element aspect ratio. The most effective mesh strategy requires several iterations to minimize the high mesh density regions. The analyst must start with an overall coarse mesh and observe the contact regions. Partitions and transition regions are updated to enforce high mesh density regions to the specific contact areas only. The primary seal requires a higher mesh density for converging seal metrics results of contact pressure and seal length. Multiple mesh transition regions are built in the primary seal regions for both pin and the box for high mesh density in the seal contact region. The secondary seal and shoulder are meshed densely requiring only one transition region due to a small contact area. Defeatured threads and other regions of the connection are meshed coarsely in the first iteration. The mesh scheme for the MIJ connection is refined through several iterations. Figure 3.19 illustrates an example of contact region development through mesh refinement in the MIJ connection shoulder. Mesh iteration 2 properly simulates the contact area closer to the physical contact in the connection.

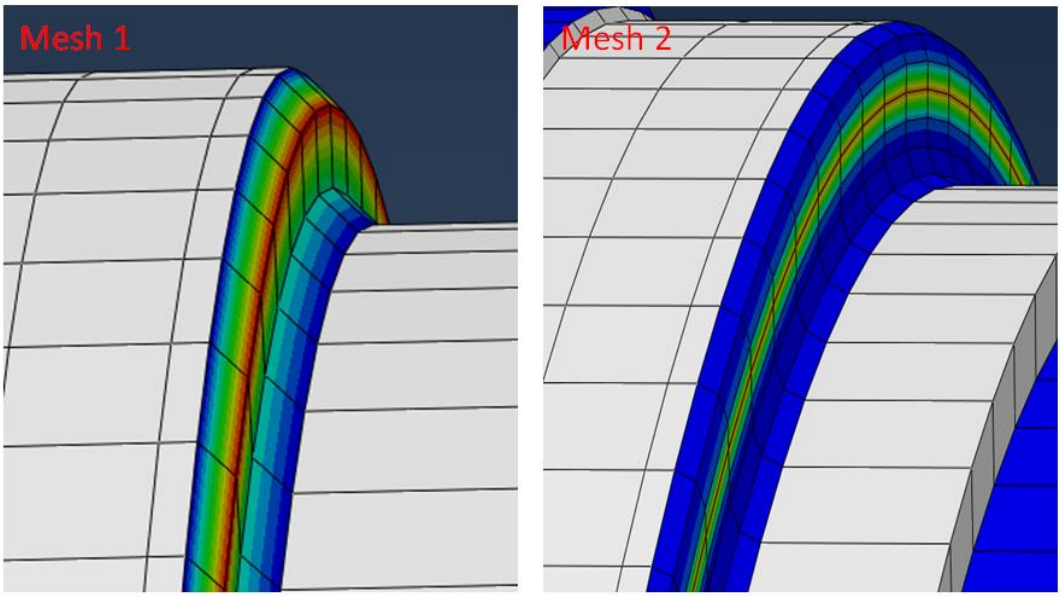

Figure 3.19: Developed of shoulder contact region through mesh refinement.

Contact regions are meshed with a finer mesh on slave surfaces than master surfaces. The pin contact surfaces are set as the slave and box contact surfaces are set as the master. The master/slave contact interaction is explained in section 3.5. Figure 3.20 displays a cut view of the box and pin illustrating the coarse mesh throughout the parts except the seals and shoulder regions. The controlled meshing scheme allows the analyst to maintain an effective mesh for the type of analysis while minimizing the element count. Figure 3.21 shows the full 360˚ components of the fully meshed MIJ connection developed in this study.

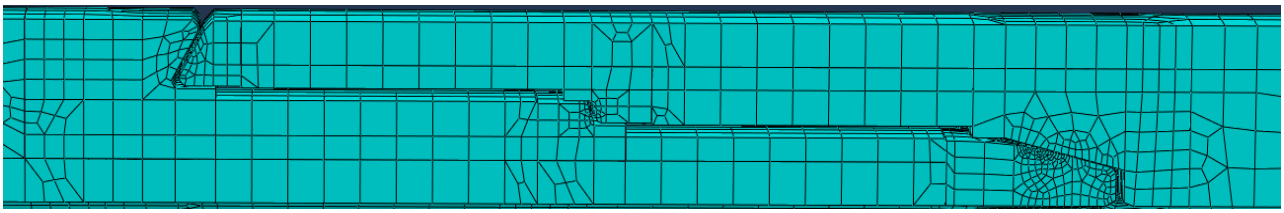

Figure 3.20: Cut view of fully meshed MIJ connection box and pin. Mesh is kept coarse throughout the model except seals and shoulder contact regions.

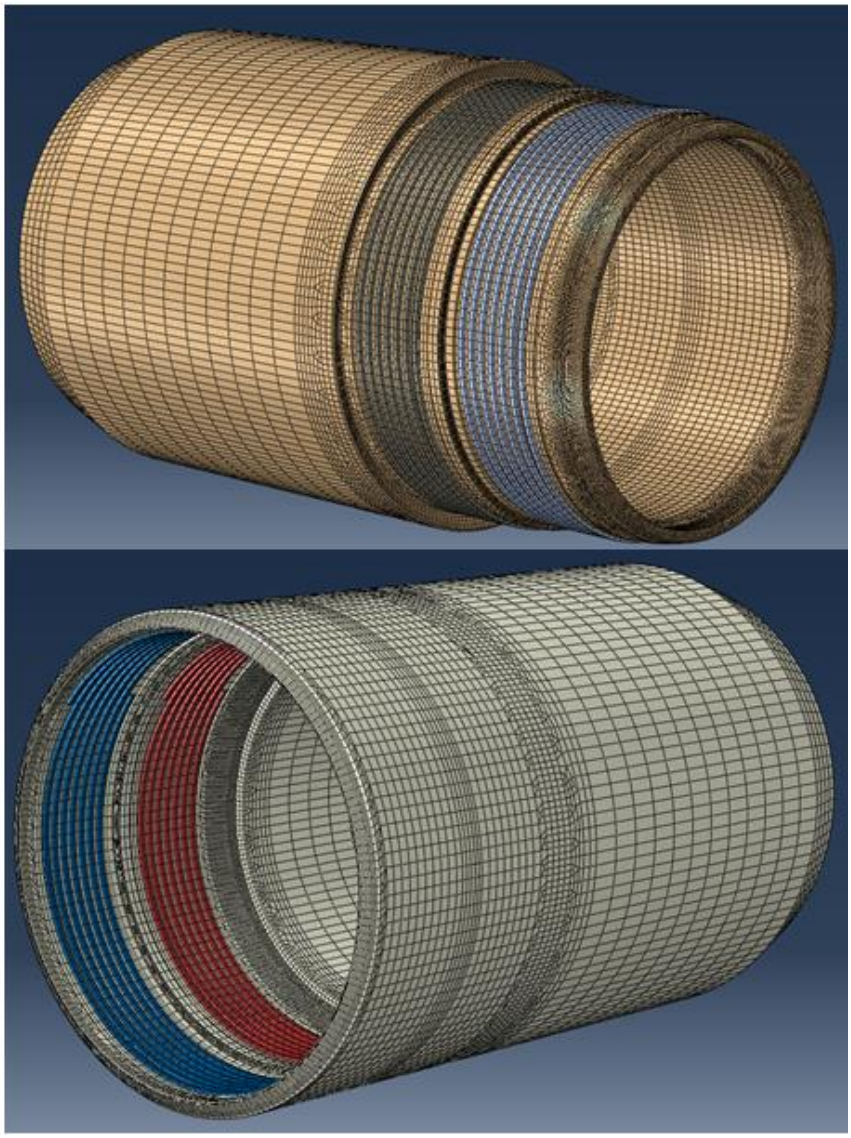

Figure 3.21: Fully meshed and assembled MIJ connection pin (top) and box (bottom).

3.3.4 Mesh Elements and Model Run Time

The mesh element selection and level of integration have a significant influence on the accuracy of results and model run times. Linear 3D brick elements (Abaqus C3D8 family of elements) are preferred in the pipe connection due to use of the elastic-plastic material model and beam elements (B31 shear flexible elements) are used for the pipe extensions. Second order elements are not recommended due to limitations that arise from volumetric locking by plastic deformation which causes their response to be too stiff. Model run times are lower when using reduced integration C3D8R elements, but full integration C3D8 elements provide more accurate results. Linear 3D, reduced integration elements (C3D8R) use only 1 integration point compared to 8 integration points for the full integration linear element (C3D8). This requires less computing resources and lowers the model runtime. C3D8R elements can be used to get quick estimates of the results and study contact regions to develop the mesh scheme in the early phases of model development. However, final model validation is performed using full integration elements. Since the thread regions are meshed coarsely with only one element through the thread thickness, incompatible mode C3D8I elements are used for all thread components. The loaded thread sections display some bending in the region, and the incompatible mode elements improve the bending behavior in the linear brick elements. Elements selection for the MIJ 3D FE model is displayed in the Table 3.5.

Table 3.5: Abaqus element types used in the 3D FE model.

Part	Element Type
Box	C3D8
Box threads	C3D8I
Pin	C3D8
Pin threads	C3D8I
Beam extensions	B31

Minimizing element count is critical to keep the 3D models tractable. However, the mesh density must be high enough in regions of interest to provide accurate results. The parametric approach using controlled meshing of components is very effective for this case. It is possible to develop full 3D models with less than 200,000 elements that provide credible results with reasonable run times using this modeling/meshing approach. Table 3.6 illustrates the element distribution within the components and run times through 4 versions of model/mesh refinement. The total model run times displayed in Table 3.6 include connection make-up and ISO 13679 load series B sequence. Run times for just the make-up condition only are approximately 4 times lower. A desktop workstation is used to run the first 3 model versions. Even though model version 4 is capable of running on the desktop computer, the model is run on a Linux compute server [21] to save time. Model version 4 is only used for converging seal metrics. All of the FE model validation and error analysis is performed with model version 3.

Table 3.6: Element distribution and run times from model refinement

	Version 1	Version 2	Version 3	Version 4
Total Model Run Time (hrs)	7	5.7	12	N/A
Total Elements	109000	112700	171100	558300
Components	**% of Total Elements**			
Pin	68.6	69.7	71.6	74.2
Box	28.0	27.1	26.3	25.2
Pin Threads	1.8	1.7	1.1	0.4
Box Threads	1.5	1.5	1.0	0.3
Pin Seals	46.0	44.8	47.5	65.9
Box Seals	9.9	9.6	9.2	14.9
All other Pin sections	20.8	23.1	23.0	7.9
All other Box sections	16.6	16.0	16.1	9.9

The element distribution values listed in Table 3.6 show the effectiveness of the parametric approach. Mesh density is controlled with consistently high percentage in the seal regions throughout all versions of refinement. Element count is kept minimal in the thread regions. The element count from version 1 to version 2 is pretty similar. The model refinements from version 1 to version 2 are made to adjust mesh transition regions to improve the mesh in the seal contact regions. These refinements are explained later in section 5.4. The mesh is converged in the seal contact region and outside surface of the box. The locations of the defined data sets are presented in Section 3.7. The convergence results from mesh revisions are listed below in Table 3.7.

Table 3.7: Mesh convergence results for the 3D FE model

% Converged	
Seal Contact Pressure	Surface Longitudinal Strain
1.6	3

3.4 Material Model

It is vital to have accurate material data to perform validation of the 3D FE models. An isotropic elasto-plasticity material model is generated from the provided ASTM A370 tensile test data. The tests are performed on material coupons created from the MIJ connection tubing prior to machining of the connections. Tensile tests are performed on four coupons cut from the test specimen every 90˚ around the circumference of the tubing. Material coupons are tested every 90˚ to sample for variations in the material throughout the tube. Figure 3.22 shows a representation of the locations of material coupons around the steel tube.

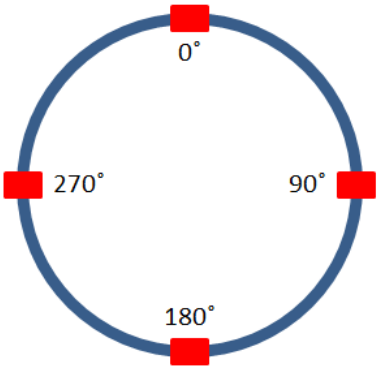

Figure 3.22: 4 material coupons are tested every 90˚ for each specimen prior to machining of the connection.

The average of the 4 tensile results is used to create the material model in Abaqus since it is not possible to know the locations the coupons are cut from after the machining of the connection. The data for Young's modulus, E, is provided from the tensile test along with nominal stress,σ, and nominal strain,ϵ plots. Figure 3.23 displays the nominal stress vs nominal strain plot from one of the test samples.

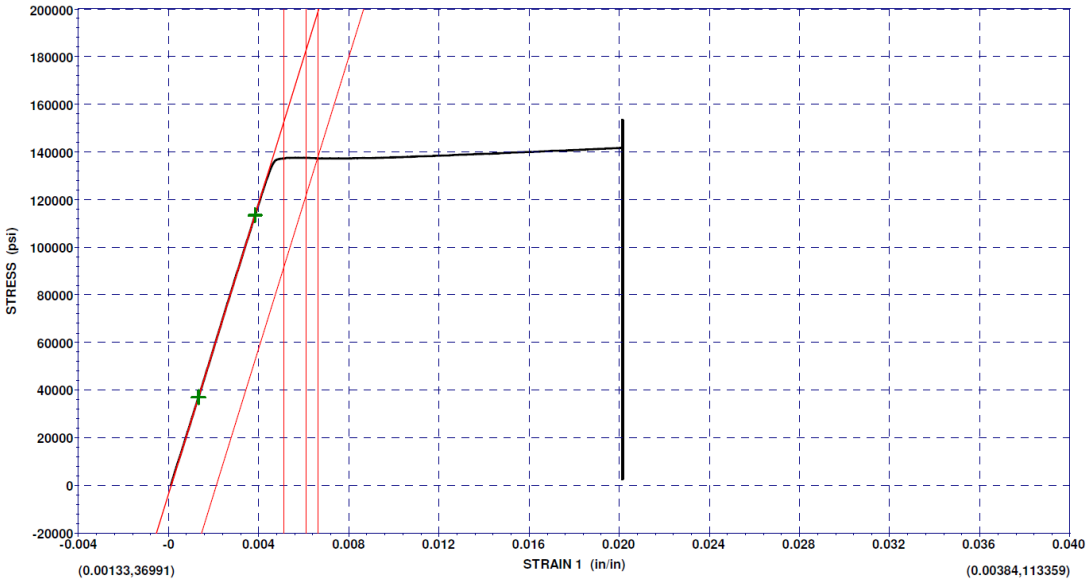

Figure 3.23. Material coupon tensile test nominal stress vs nominal strain plot.

The nominal strain data collected during the tensile tests is partial. The extensometer is pulled off the sample prior to reaching peak stress. The peak load and peak stress results are provided but there is not enough data to calculate strain values at peak stress. The test results only provide a few useful data points after the material yield point. The isotropic elasto-plasticity material model is generated in Abaqus which is very commonly used for metal plasticity models. The material model employs classical metal plasticity with using the von Mises yield surface, associated plastic flow, and isotropic hardening. Abaqus software

requires nominal stress and strain data converted to true stress and strain values and separation of elastic and plastic strain components from total strain when defining the plasticity material model. True stress and true strain allows a ductile metal subjected to finite deformations to have the same stress-strain behavior in tension and compression prior to the necking region [19]. Equations 3.1, 3.2, and 3.3 below are used to calculate true stress, true total strain, and true plastic strain from nominal stress and nominal strain respectively,

$$\tilde{\sigma} = \sigma(1 + \epsilon) \tag{3.1}$$

$$\tilde{\epsilon} = \ln(1 + \epsilon) \tag{3.2}$$

$$\tilde{\epsilon}_p = \tilde{\epsilon} - \frac{\tilde{\sigma}}{E} \tag{3.3}$$

where $\tilde{\sigma}$ is the true stress, $\tilde{\epsilon}$ is the true total strain, and $\tilde{\epsilon}_p$ is the true plastic strain. These values are input into a table format in the material editor within the Abaqus CAE Property module. A main disadvantage of using this model is that Abaqus software considers the material perfectly plastic after it exceeds the last data point entered by the user. The analyst must keep a close eye on the results during the analysis to make sure the strain values remain within the provided material data. Plastic strain values did not exceed the material model for the MIJ connection in this study. A plot of the calculated true stress and true stain data is shown in Figure 3.24. Average calculated values of material properties for the MIJ box and pin are listed in Table 3.8.

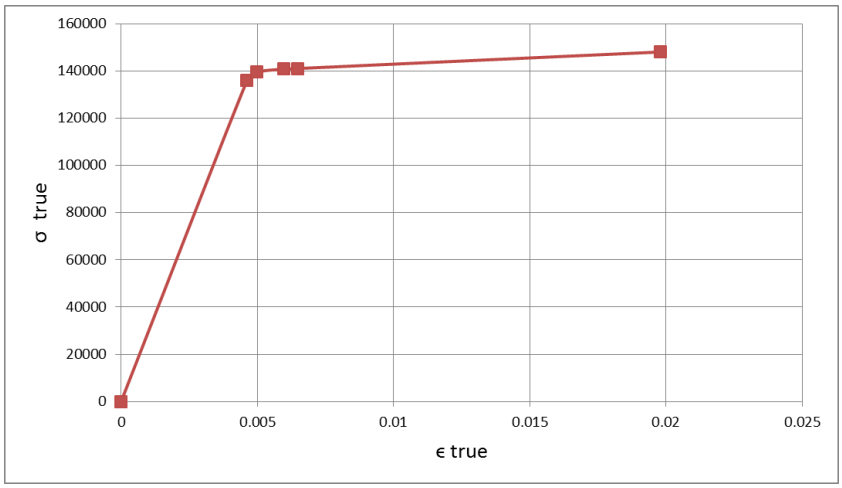

Figure 3.24: True stress vs true strain material model.

Table 3.8: Elastic-plastic material model used for the MIJ connection 3DFE model.

MIJ Box Material Properties			**MIJ Pin Material Properties**		
Elastic Properties	Young's Modulus (psi)	Poisson's Ratio (v)	**Elastic Properties**	Young's Modulus (psi)	Poisson's Ratio (v)
	3.05E+07	0.292		3.02E+07	0.292
Plastic Properties	σ true (psi)	ϵ plastic (in/in)	**Plastic Properties**	σ true (psi)	ϵ plastic (in/in)
	133215	0.00E+00		136053	0.00E+00
	138455	4.45E-04		139525	3.59E-04
	139434	1.41E-03		140797	1.31E-03
	139511	1.90E-03		141044	1.80E-03
	146192	1.50E-02		148053	1.49E-02

3.5 Contact Solution

Surface contact between metal-to-metal seals, shoulder and threads represents large regions of boundary nonlinearities for the analysis of premium threaded connections. Solving the contact problem is a critical and challenging task in modeling premium connections. The contact problem is discontinuous and highly disruptive to the solution of the system of equations. The most common discontinuities involve abrupt "open-close" changes in contact and "stick-slip" changes in friction. One of the methods available in Abaqus Standard utilized for this model is the Newton-Raphson method with combination of incremental and iterative procedures for solving nonlinear problems such as contact. Contact surfaces should be defined carefully especially with defeatured geometry. Point or an edge contact between two surfaces can result in infinite stress often resulting in divergence of the solution.

Contact interaction must be defined for all the surfaces within the connection assembly that interact with each other at any time during the analysis. The *General contact* and *contact pairs* contact interaction share many underlying algorithms in Abaqus Standard. The *contact pairs* definition is the best practice for the premium connection application because it allows the user more control over contact surface selection, master and slave assignments, and for the initial overclosure treatment. *General contact* eliminates initial overclosure with strain-free adjustments by default while contact pairs treat initial overclosures as interference fits to be resolved in the first increment of the analysis [19]. The seals and thread interaction in some premium connections perform as interference fits depending on the initial assembly arrangement. The initial overclosures are not a concern for the MIJ model in this study since the threads are free running and the pin and box are assembled in a hand-tight position. However, selecting *contact pairs* over *general contact* is the proper approach that can be used with any type of thread and connection configuration.

The surfaces defined in the part module when 90˚ sectors are created for the components are assigned contact properties in the Abaqus Interaction module. The contact interactions are defined between the box and the pin after they are completely assembled with the helical threads. Normal and tangential mechanical contact properties for the contact model are defined with "Hard" contact using the penalty method. The hard contact property allows separation of two surfaces after contact is made. The tangential friction coefficient, which is linearly proportional to the make-up torque of the connection, is set at a value of 0.08. The friction coefficient value is estimated from a range provided in ISO 13678 [20]. The friction coefficient is used as a model validation parameter to match the torque turn plots from the make-up tests. Table 3.9 lists the contact surface interaction parameters for MIJ connection analysis.

Table 3.9: Contact surface interaction parameters.

Discretization method	Surface to surface
Sliding formulation	Finite Sliding
Slave adjustment	Adjust to remove overclosures
Surface smoothing	Automatic

The surface to surface discretization method is preferred to increase accuracy in stress and pressure results compared with the node to surface discretization method. The *finite sliding* tracking algorithm should be used because of the large displacements during the make-up step as it allows for sliding and rotation of contact surfaces. The *surface smoothing* option is also applied since all the contact surfaces are curved and a coarse mesh is used in some areas.

Contact pairs require a selection of master and slave surface. The Abaqus contact algorithm requires the following conditions to be met:

1. Master surface is always defined to be the stiffer member as it is used as the less deformable reference surface.
2. The slave surface to have a finer mesh than the master surface to enforce the contact rule that the slave node cannot penetrate the master surface.

Since the box and the pin are made of same material and exhibit comparable structural stiffness, either of the box or the pin could be defined as the master surface. The box is selected as the master as it usually has a slightly thicker wall. The pin is selected as the slave and meshed finer than the box in this case. Attention to geometric details must be given when creating contact surfaces especially with defeatured geometry.

3.5.1 Contact Regions

There are four main regions of the MIJ premium connection that require contact properties to be defined. Primary seal contact, secondary seal contact, mid shoulder contact, and contact in the threads. All of the box contact regions including the threads are defined as the master surface and the pin as the slave surface. Therefore, all of the pin components must have a finer mesh than the box components. Contact surfaces in the threads must be defined separately for flank contact and crest/root contact. Selecting the defeatured thread flank and crest as one contact surface results in point or line contact at the edges. The solver is unable to resolve the contact in the thread regions and aborts the simulation. The analyst should be careful with defeatured geometry in contact regions. Appropriate surface definition is critical for a proper contact solution. Figure 3.25 and Figure 3.26 display the defined contact surfaces of the MIJ connection developed for this study.

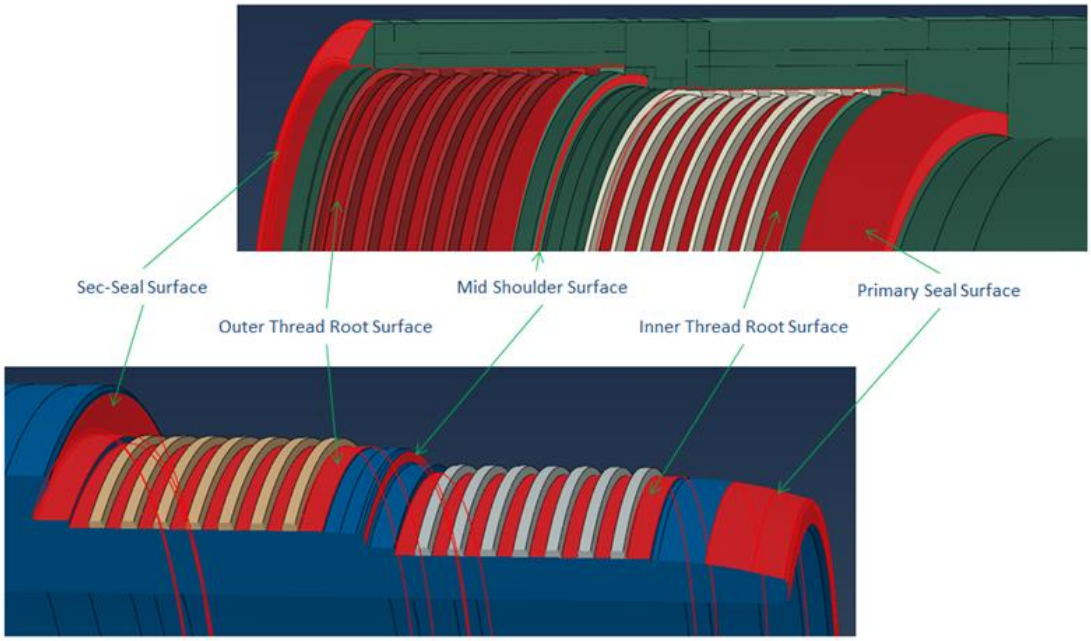

Figure 3.25: Cut-view of box and pin contact surfaces highlighted in red.

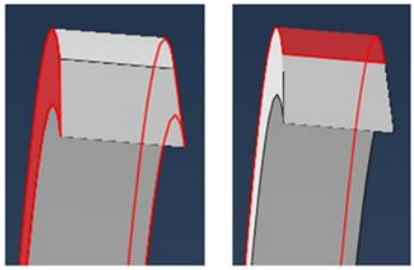

Figure 3.26: Thread flank contact surface (left) and crest contact surface (right) highlighted in red.

3.6 Boundary Conditions and Loading

The full 3D FE model with helical threads has a great advantage over axisymmetric models when it comes to applying boundary conditions and the representation of loading. Unlike the axisymmetric models, the make-up conditions can be applied exactly how the actual connection is tested. A datum axis for the cylindrical coordinate system, R-T-Z, is created to match the FE model consistent with the formulations for the physical mechanics of a cylinder with Z-axis in the longitudinal direction. Boundary conditions, prescribed pin rotation, and loads are applied in the cylindrical coordinate system.

The sequence of one or more analysis steps is defined in the Abaqus CAE Step module. Abaqus CAE creates an "initial step" at the beginning of model's analysis step sequence. The initial step allows the analyst to define boundary conditions, predefined fields, and interactions that are applicable at the very beginning of the analysis [19]. The initial step is followed by one or more user defined analysis steps. Analysis steps are associated with specific procedures performed during the test procedure. Results are stored in the output database file, .odb file, for each analysis step. The analyst can define as many analysis steps are necessary. Boundary conditions and interactions can be defined separately for each analysis step. *Static-General* analysis steps are created for nonlinear incremental analysis for the MIJ connection. The state of the model at the end of each general step provides the initial state for the start of the next general step. *NLGEOM* option in the step module accounts for geometric nonlinearities that develop from large displacement and large strains. The MIJ connection analysis includes large displacements from pin rotation and small strain. The *NLGEOM* option is selected in general steps to account for large displacement nonlinearity. Figure 3.27 illustrates and example of Abaqus CAE Step module work flow.

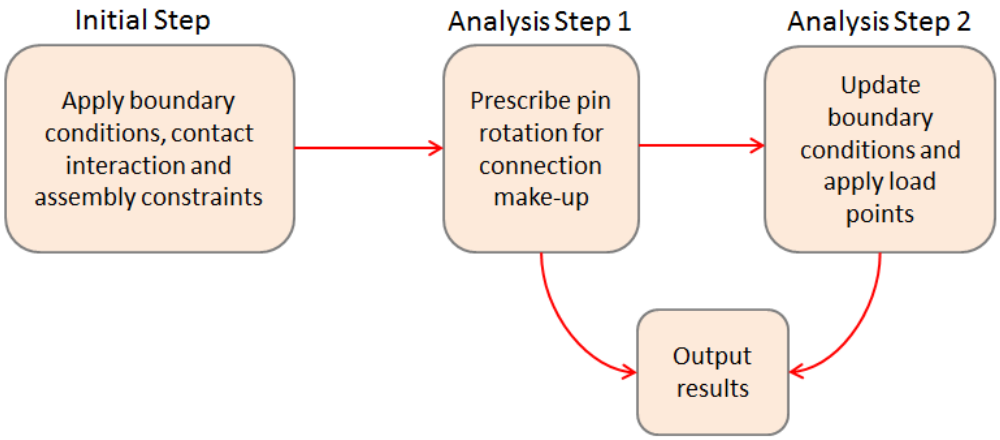

Figure 3.27: Abaqus CAE Step module work flow example.

Two analysis steps are created for the make-up test and a separate analysis step is created for each load point for applying the load sequence. The make-up test requires two analysis steps due to the fact that DIC test results deliver the surface strains and displacements after the torque is released from the power tongs. An additional analysis step is added into the FE model to remove the reaction torque from the connection developed from the pin rotation. The analysis step releasing the reaction torque is added to ensure that FE model replicates the make-up test as well as the DIC test procedure with a *virtual make-up test*; producing FE results as close as possible to the images developed from the DIC data.

3.6.1 Connection Make-Up

3.6.1.1 Physical Connection Make-up

For the make-up test, the pin is installed into the box manually for a hand-tight fit. Hydraulically actuated power tongs are used to hold the box fixed vertically as the pin is rotated into the box until the manufacturer specified torque value is reached called the "power-tight" make-up. The pin rotation and torque data is recorded into a torque-turn plot. Figure 3.28 shows an example of a torque-turn plot

generated during connection make-up. The power tongs grip the box and the pin on the pipe sections. It is necessary to record the total length of the connection pipe between the power tongs to apply boundary conditions at the same location in the FE model. Incorrect specimen length will misrepresent the torsional stiffness of the connection under test resulting in inaccurate reaction torque values. An image of the physical make-up test set up is illustrated in Figure 3.29.

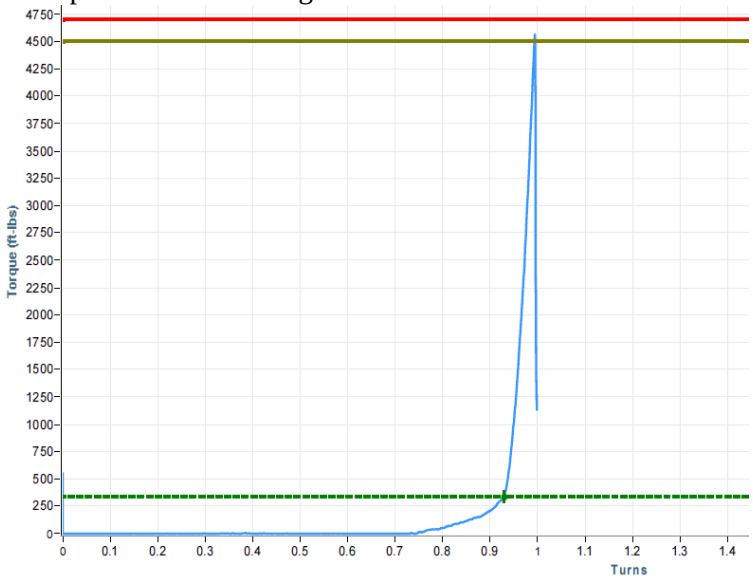

Figure 3.28: Torque-turn plot sample produced during connection make-up.

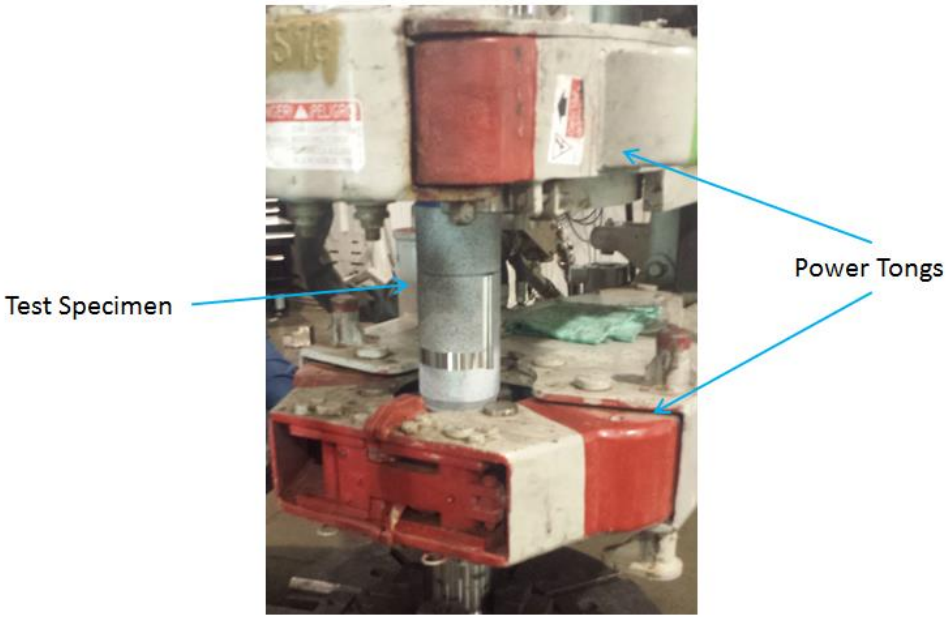

Figure 3.29: MIJ connection installed inside hydraulic power tongs during connection make-up.

3.6.1.2 FE Model Connection Make-up

Beam element pipe extensions length is updated on box and pin in the FE model to match the total length of the test specimen between the power tongs. Encastre boundary condition is applied on the end of the box pipe extension which makes all degrees of freedom zero for the nodes in the region. Pin rotation is prescribed in the cylindrical coordinate system z-axis (UR3) in radians at end of the pin pipe extension. Figure 3.30 displays an image of the 3D FE model showing these regions and Table 3.10 summarizes the applied make-up boundary conditions. Full 3D FE model is capable of replicating the actual make-up conditions. No other external loads or boundary conditions are required.

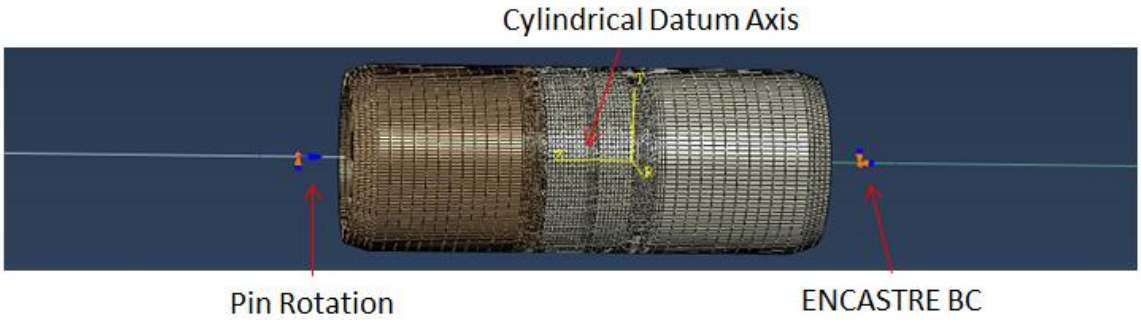

Figure 3.30: MIJ 3D FE model make-up boundary conditions.

Table 3.10: 3D FE model make-up boundary conditions applied at the box and pin matching the length of the pipe between the power tongs.

Make-UP Boundary Conditions	
Box	Encastre
Pin (cylindrical system)	UR1=UR2=0 UR3 = rotation (radians)

3.6.2 Load Frame Testing

3.6.2.1 Physical Load Frame Test

After the connection make-up, the test specimen is installed into a horizontal load frame for the ISO 13679 load series tests displayed in Figure 3.31. The load frame is capable of applying tensile, compressive, and bending loads to the connection along with internal and external pressure. For the correlation study on the MIJ premium connection, only tensile and compressive loads are applied with internal pressure. The load frame also incorporates horizontal buckling units (HBU) which act as anti-buckling devices. These devices prevent the connection test specimen movement in the radial direction. The end of the test specimens are sealed off with end caps used to hold internal pressure. The end caps also provide an additional tensile load from the internal pressure which must be accounted for in the total axial load. The overall length and locations of loading points, fixed points, and HBUs must be recorded at this time to use in the FE model.

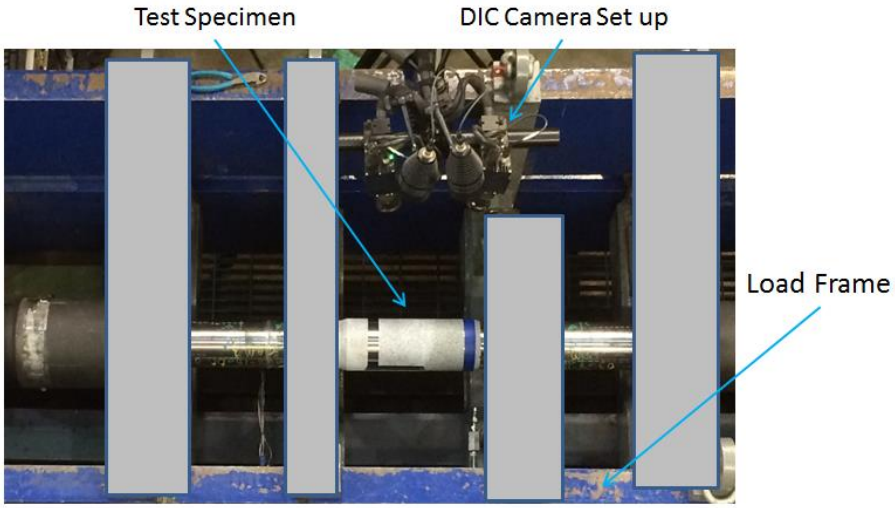

Figure 3.31: MIJ connection installed in load fame for ISO 13679 service loading tests.

Complete details and procedures of the load series tests can be found under ISO 13679 load series B [5]. Figure 3.32 illustrates a sample of the load points applied to a premium connection with respect to the 80% yield (blue) and 100% yield (red) von Mises Ellipse (VME).

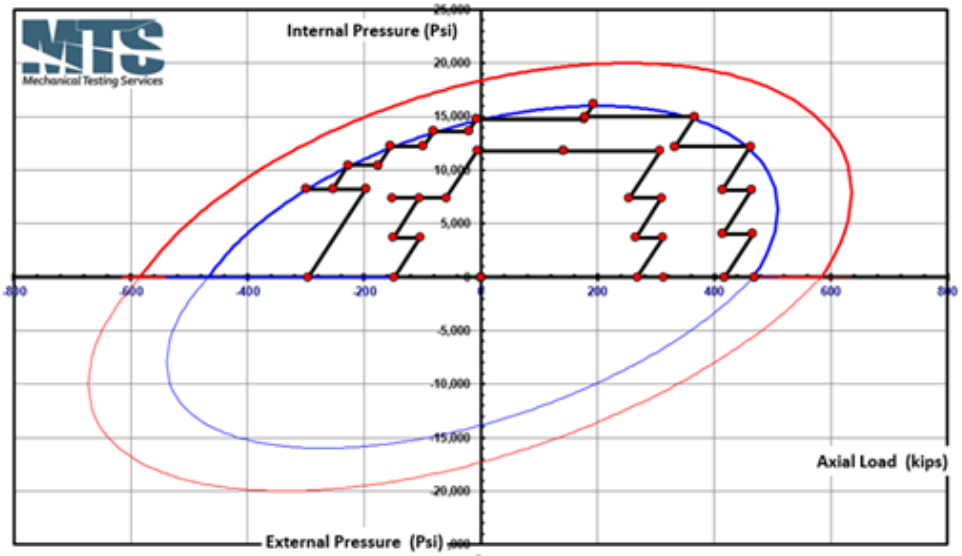

Figure 3.32: Sample of ISO 13679 Series B load points inside VME envelope. 80% yield strength (Blue) 100% yield strength (Red).

3.6.2.2 FE Model Load Frame Test

The FE model boundary conditions for the load sequence test are developed with the same approach to match the actual test with the 3D FE model simulation. The total length of the test connection is once again adjusted with the beam element extensions. The box end is held fixed while tensile and compressive loads are applied at the pin end similar to the actual tests. Internal pressure is applied over the complete internal surface of the made-up connection as a load without the pressure penetration interaction. The tensile load generated due to internal pressure is computed and included with the applied axial load during each load point. The end of the box pipe section is fixed with *Encastre* boundary conditions. Axial loads are applied on the end of the pin pipe section. HBU boundary conditions are applied at their respective locations. Figure 3.33 illustrates the 3D FE model loading and boundary conditions and Table 3.11 summarizes the boundary conditions. The values for applied axial load and internal pressure during each load point are listed in Table 3.12

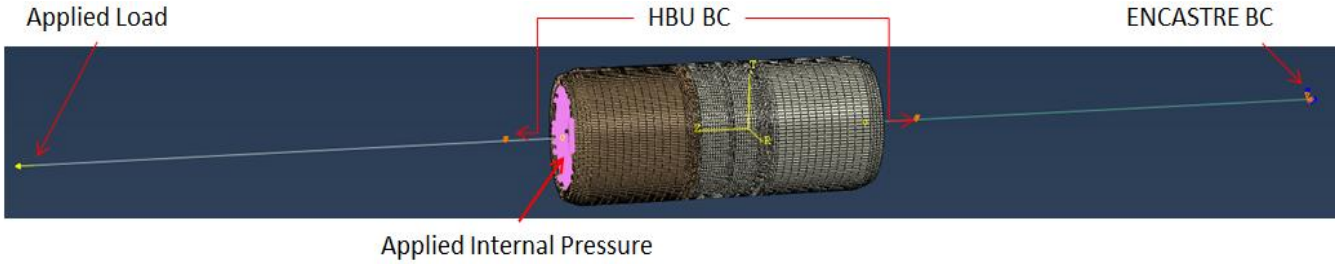

Figure 3.33: MIJ 3D FE model load series boundary conditions and load points.

Table 3.11: 3D FE Model load sequence boundary conditions.

Load Series Boundary Conditions	
Box end	Encastre
Box and Pin HBU (global system)	U1 = U3 = 0

Table 3.12: Applied loads on the MIJ connection FE model for load sequence testing.

Load Point	Machine Load (kips)	Internal Pressure (Psi)	Axial Pressure Load (kips)	FE Model Applied Tensile Load (kips)
1	314.1	2	0.0	314.1
2	268	3745	43.9	311.9
3	222.2	7448	87.4	309.6
4	166	11830	138.8	304.8
5	2.3	11865	139.2	141.5
6	-147	11868	139.2	-7.8
7	-239.9	7441	87.3	-152.6
8	-194	3697	43.4	-150.6
9	-148.1	1	0.0	-148.1
zero	-1.4	1	0.0	-1.4
10	468.1	2	0.0	468.1
11	418.1	4032	47.3	465.4
12	367	8200	96.2	463.2
13	316.1	12201	143.1	459.2
14	188.1	15019	176.2	364.3
15	1	16226	190.4	191.4
16	-184	14807	173.7	-10.3
17	-244	13671	160.4	-83.6
18	-300	12277	144.0	-156.0
19	-352	10455	122.7	-229.3
20	-398	8295	97.3	-300.7
21	-296	0	0.0	-296.0
22	-398	8239	96.7	-301.3
23	-352	10525	123.5	-228.5
24	-300	12268	143.9	-156.1
25	-244	13686	160.6	-83.4
26	-184	14779	173.4	-10.6

3.7 FE Model Data Extraction

The strain and displacement data is extracted from the surface of the box over the connection region to correlate the 3D FE model with DIC test results. FE model results are stored in an output database, .odb file, in the global x-y-z coordinate system. A node set named “extract_data” is defined on the box surface which is used by a Python script to extract the nodal displacement and strain results. Data variables names used in Abaqus are listed in Table 3.13. Figure 3.34 displays the defined data set on the box outer surface.

Table 3.13: Abaqus data variables for displacement, strain, and contact pressure.

Displacement	Strain	Contact Pressure
U1	E11	CPRESS
U2	E22	
U3	E33	

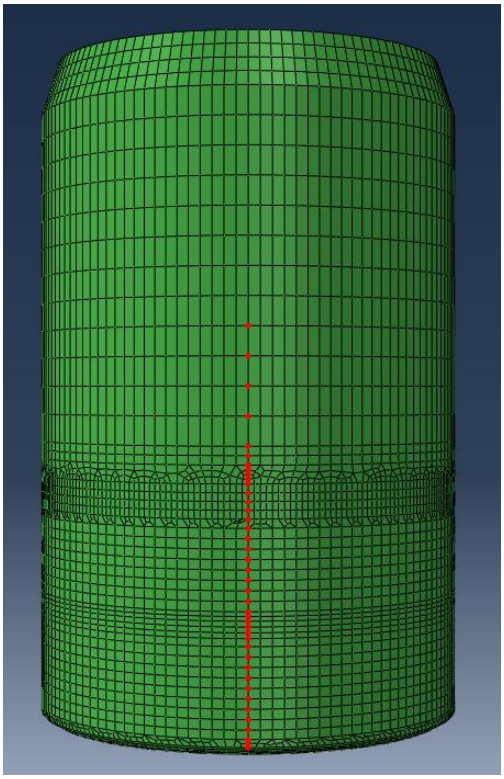

Figure 3.34: Node set defined on the box surface for strain and displacement data extraction.

A node set is also defined on the pin seal to extract contact pressure and seal length data. However, this data was extracted manually from the Abaqus result files. The Python scripts are currently under refinement for this process. Figure 3.35 displays the defined data set on the pin primary seal. DIC data acquisition from physical testing is presented in section 4.1.

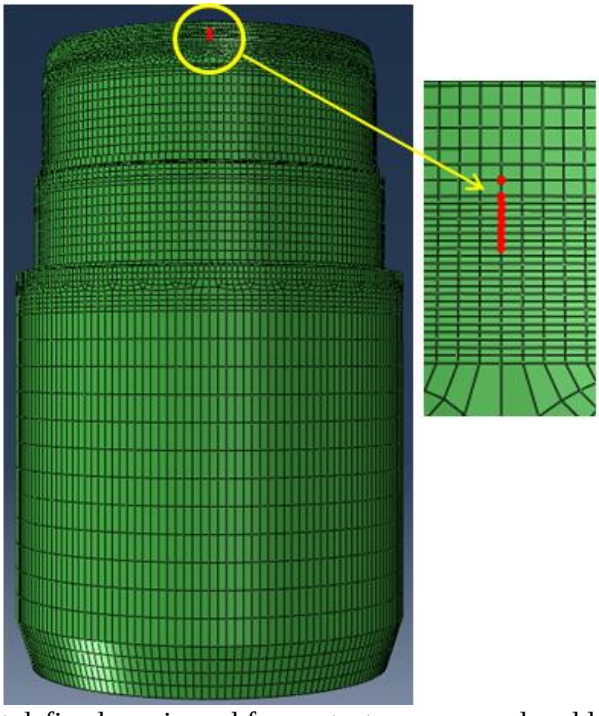

Figure 3.35: Node set defined on pin seal for contact pressure and seal length data extraction.

3.8 Modeling Decisions

The defeaturing of the helical thread geometry and replacing 3D elements with beams for the pipe extensions are two major aspects that benefit this approach of building a full 3D FE model. These decisions are made after thorough investigation to ensure that the results are not affected. Defeatured threads and beam elements reduce the element count by over 200,000 and model runtimes are reduced by hours with negligible effects on the analysis results.

3.8.1 Defeatured Threads

The helical threads are defeatured to reduce the element count by removing the radii on the thread flanks. Reducing elements in the threads lowers the contact solution time which provides a significant reduction in the overall model runtime. To compare the effects and results, a model is created including the radii in the thread form shown in Figure 3.36. Including the radii on the thread form is difficult to mesh coarsely while maintaining proper aspect ratio of the elements. Multiple elements through the thickness of the thread are required which considerably increases the element count in the contact regions. Figure 3.37 displays the difference in mesh scheme for defeatured and featured threads.

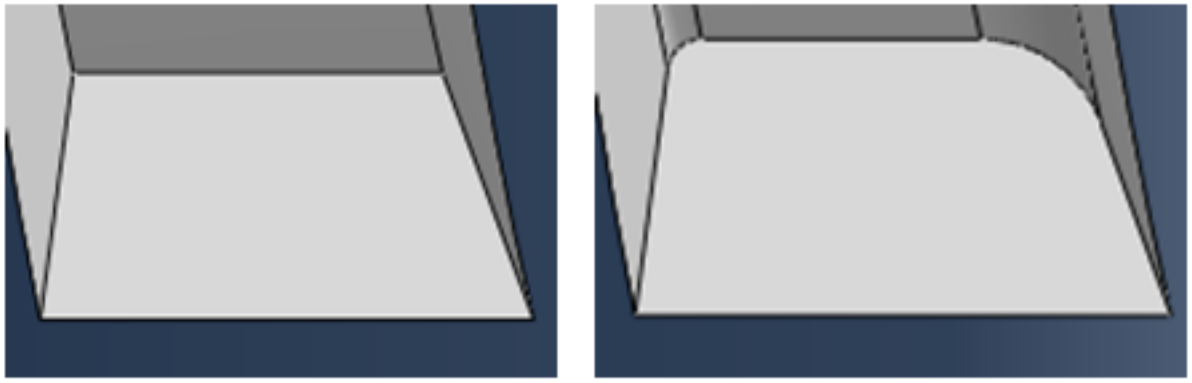

Figure 3.36: Defeatured thread geometry (left) and full featured thread geometry (right).

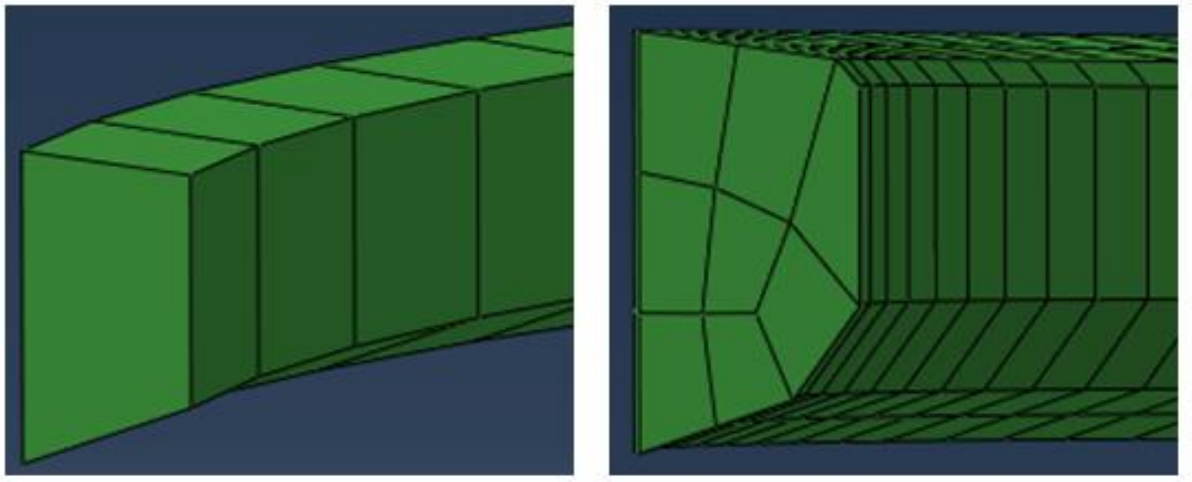

Figure 3.37: Defeatured thread mesh (left) and full featured thread mesh (right).

Figure 3.38 displays the longitudinal strain results for connection make-up tests performed with both types of thread geometry. The defeatured threads provide similar results as the featured threads while decreasing the required meshing and computing effort. The sum squared error (SSE) over the complete length of the data between the two models is $3.16e^{-8}\left(\frac{in}{in}\right)^2$ with difference in reaction torque below 0.3%. The defeatured threads reduce the model runtimes by approximately 70% with negligible effects on

the results. Table 3.14 lists the overall results between the two make-up models. The increase in number of elements and model runtime shows that this approach is effective in keeping the 3D models tractable. The reaction torque on the connection is slightly lower in the featured model. However, it was expected since there is a reduction in contact surfaces due to the radius on the thread flanks. The threads are free running and have no taper or interference fit in the MIJ connection considered for this study. Defeaturing of the threads must be investigated further for other thread forms used in premium connection designs before applying this approach.

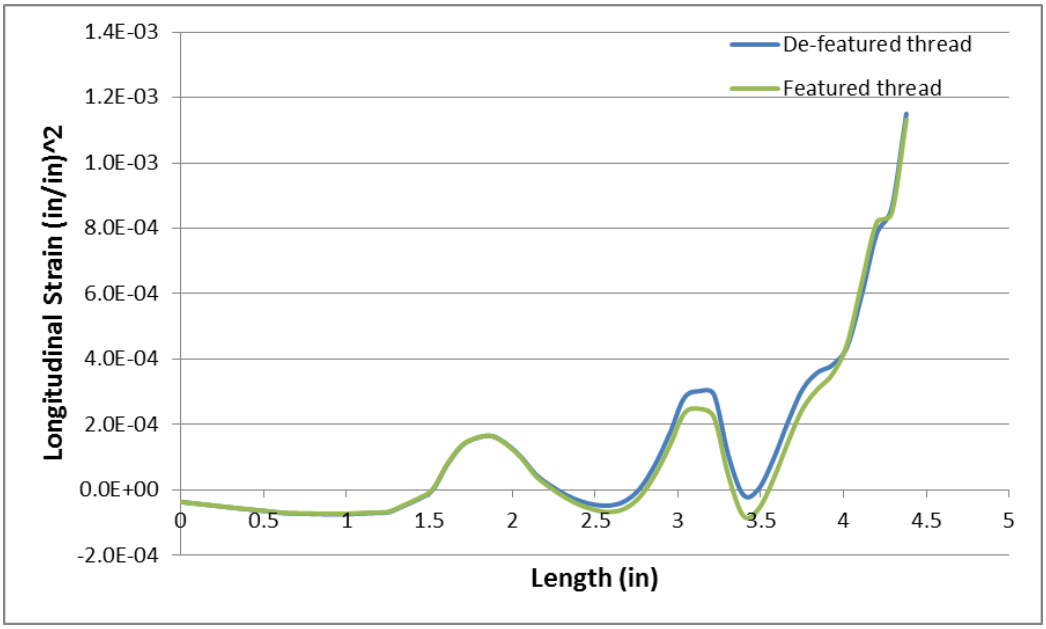

Figure 3.38: Longitudinal strain results for make-up test comparing defeatured and featured threads.

Table 3.14: Make-up test results with defeatured and featured thread geometry.

	Thread Geometry	
	Defeatured	**Featured**
Element count in the threads	3640	89040
Average aspect ratio	3.01	4.52
Make-up test run time (hr)	3.25	10.33
Reaction torque (ft-lbs)	4564	4513
Longitudinal Strain SSE (in/in)^2	3.16E-08	

3.8.2 3D Beams for Pipe Section

To confirm the use of beam elements, make-up tests are performed using 3D brick elements and beam elements as the pipe extensions. During make-up test boundary conditions, the pipe extension length is 1.25". Utilizing the beam elements save about 7700 3D elements. The model runtime is also shorter by about 8 minutes. Figure 3.39 displays the make-up model with 3D elements along with beam elements used to extend the connection pipe length. The results for both models are almost exactly the same with SSE of $6.62e^{-15}\left(\frac{in}{in}\right)^2$ for longitudinal strain shown in Figure 3.40. The reduction in element count, and runtime is not as significant as defeaturing the threads for the make-up model. However, full length of the test specimen is modeled for the load sequence testing which includes about 40" of pipe extension. In the mesh configuration matching the make-up model test, using beam elements for the pipe extensions saves over 122,000 elements justifying the modeling decision. Overall results for the two make-up models are listed in Table 3.15.

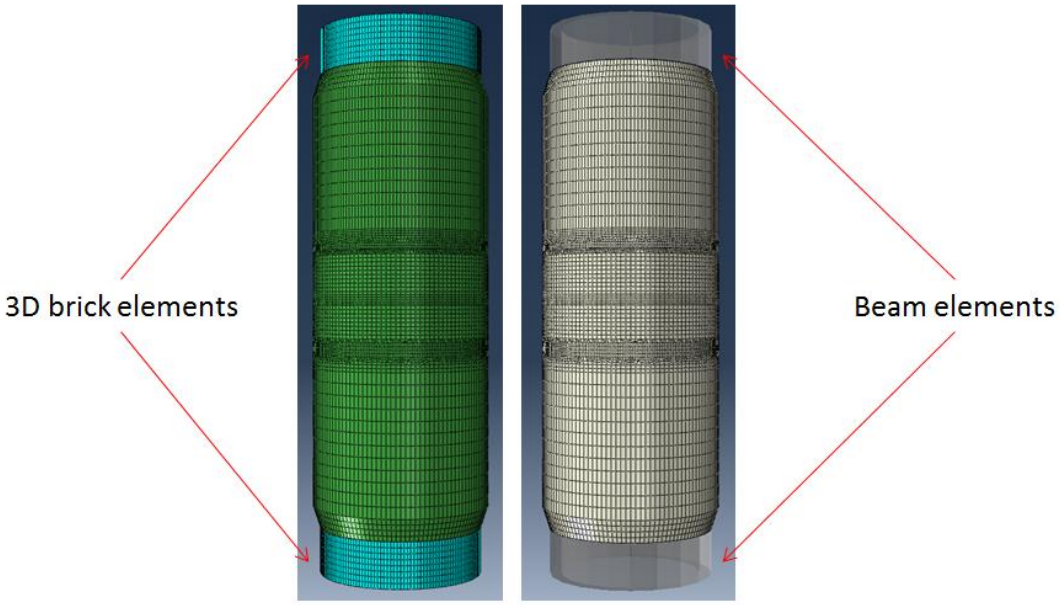

Figure 3.39: Make-up models developed with 3D elements and beam elements for extending connection pipe length.

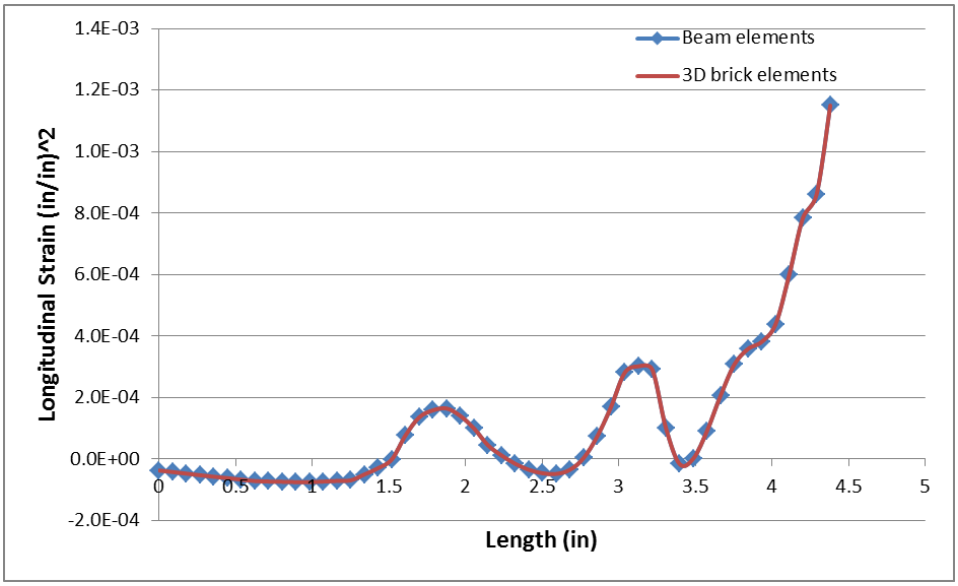

Figure 3.40: Longitudinal strain results for make-up test comparing beam elements and 3D brick elements.

Table 3.15: Make-up test results with beam elements and 3D elements for pipe extensions.

	Pipe Extension	
	Beam Element	**3D Elements**
Element count in the pipe	2	7700
Make-up test run time (hr)	3.25	3.38
Reaction torque (ft-lbs)	4564	4564
Longitudinal Strain SSE (in/in)^2	6.62E-15	

Chapter 4 Digital Image Correlation

The strain response on the outside surface of the box is dictated by the internal geometric features of the connection such as seals and the torque shoulder. Measured strain on the box surface is a resource for validation of the 3D FE model. Strain measurements during connection make-up and load sequence are typically performed using strain gages. However, strain-gage data is limited to only a few points over the connection surface and does not completely capture the behavior and mechanics of the connection features such as metal-to-metal seals and shoulder. Strain-gage results from a few points over the field do not provide a comprehensive representation of how the connection may be performing. Strain gage placement is also a critical step and small variations can provide large deviations in the strain results due to the complex strain field of the OCTG premium connections. Strain-gage data is usually acquired at locations that correspond to the connection features resulting in peaks on the connection surface. Figure 4.1 illustrates why it can be very difficult to estimate the proper strain gage location.

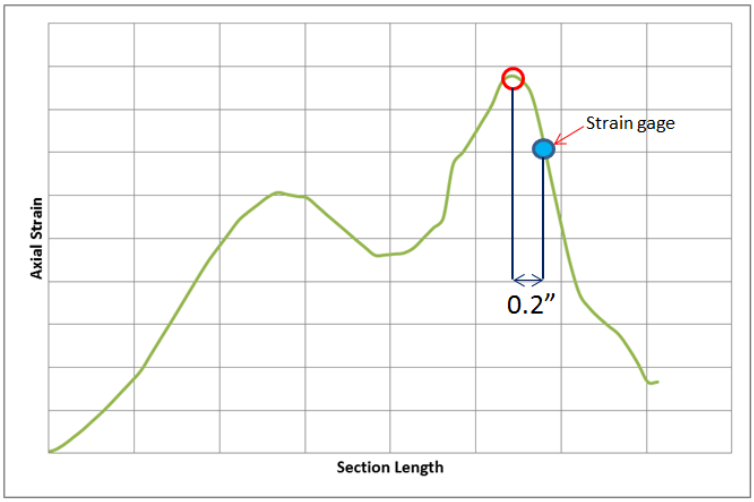

Figure 4.1: Sample of an OCTG premium connection axial strain representation. The plot does not refer to any specific connection.

Digital image correlation (DIC) technology is capable of providing high spatial density, full-field displacement and strain data on the measured surface of the connection. DIC is an optical 3D deformation measurement system. ARAMIS v6.3.0-3 software [22] produced by GOM Metrology Systems is used for measuring the displacement and strain response of the MIJ premium connection in this study. The ARAMIS DIC system estimates the displacement field produced by images of a deformed specimen compared with a reference image of the undeformed specimen. DIC system utilizes two high speed digital cameras to capture images of a test specimen typically prepared with a sputtered spray pattern. DIC testing can provide comprehensive results of connection features and response comparable to the strain gage technique. DIC measurements can be used to validate the 3D FE models with proper correlation methods for connection make-up. The validated 3D FE models can provide results for connection behavior and performance during make-up and service loads.

4.1 DIC Data Acquisition

DIC technology requires special consideration for calibration and experimental process to acquire accurate data. A few important aspects of DIC testing are required to ensure correct deformation results are:

1. Good camera calibration.
2. Good and consistent sputter pattern with good contrast and sharp sputter edges of nearly uniform size.
3. Proper camera and test setup with good lighting, clean and well-focused camera lenses with no glare.

Camera setup, sputter patterns, lighting, and system calibrations are all equally important to maximize the signal-to-noise ratio for the deformation results. The DIC testing for the MIJ connection was performed at Mechanical Testing Services (MTS) facility in Waller, Texas. DIC measurements are acquired through two test sessions:

1. Premium connection make-up.
2. ISO 13679 load series B tests.

Both tests are performed at the same location, but in different testing bays within the same facility. Make-up of the connection is performed using hydraulic power tongs. The made-up connection is installed in a load frame for service loading tests. Raw image data is transferred to Virginia Tech where it is processed using ARAMIS v6.3.0-3 software. The ARAMIS software refers to each pair of images from the cameras as a "stage". Conventionally, stage 0 is used as the strain-free reference image. Each subsequent stage compares the images associated with the current stage to the refernce image in stage 0. The difference between these stages corresponds to the displacement and strain values for one particular stage of specimen.

4.1.1 Specimen Preparation

Creating the random paint sputter pattern on the surface of the test specimen is a very critical step. The quality of sputter pattern will directly influence the strain measurement results. The basic principle for DIC is the tracking mechanism of the unique specimen pattern. The tracking mechanism is fulfilled by the algorithm assigning subsets throughout the area of interest with each subset containing a unique pattern. Thus randomness of the pattern is required. The density of the sputter pattern determines the spatial resolution of a measurement. If the pattern is too sparse, too dense, or the speckles are too large, spatial resolution of the measurement will suffer. Characteristics for a good specimen surface preparation are [22]:

1. The pattern on the surface should show good contrast.
2. The surface pattern must be dull. Specular reflections cause a bad contrast and brightness difference between the right and left camera which prevent the facet computation in the areas of the reflection.

Detailed guidelines for preparing DIC test specimens are found in ARAMIS user manual [22]. Figure 4.2 displays a DIC test image of the MIJ connection showing the prepared surface.

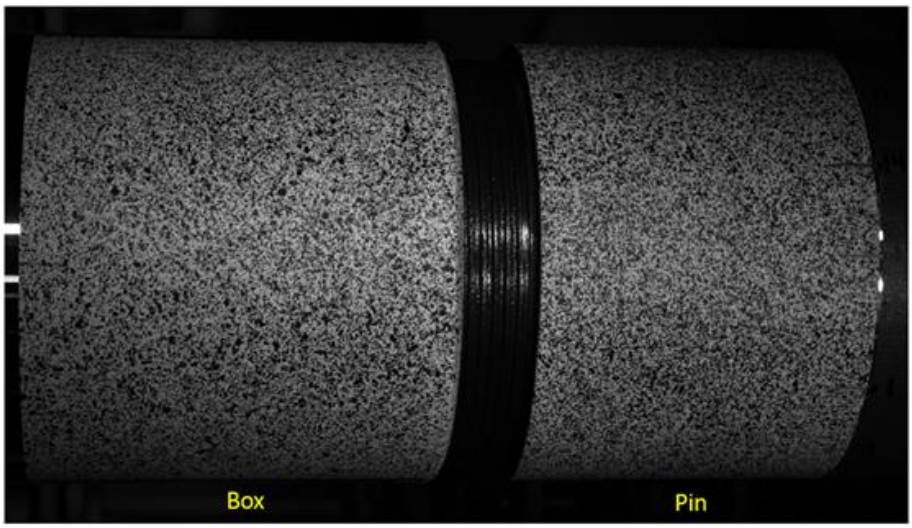

Figure 4.2: Sputter pattern painted on the surface of the MIJ connection prepared for DIC testing.

4.1.2 Camera Calibration

Good setup and calibration of the cameras is a critical step for collecting high quality DIC measurements. The calibration process is performed by placing a calibration panel in defined positions with respect to the cameras to establish a relation between a known 2D image coordinate frame with the 3D Euclidean global frame. The operator must choose an appropriate measurement volume prior to the camera calibration. The measurement volume depends on the size of the test specimen or the size of the area in the image. The measuring volume is selected for which the measuring area fills the entire image to utilize the full dynamic range of the measurement sensor. The measuring volume determines the distance between the left and right camera, distance between cameras and the test specimen, camera angle, and the size of the calibration panel. Lens focus and lighting adjustments are made during this phase to ensure a proper camera calibration. The camera calibration is performed with step by step instructions built into the ARAMIS software. The calibration results are displayed at the end of the calibration process in terms of a calibration deviation value. A "good" camera calibration yields a deviation value of between 0.1 to 0.4 pixels [22]. The calibration deviation values for all measurements made during MIJ connection tests are below 0.03 pixels.

4.1.3 DIC Make-up Test

The make-up test reference image of the box is taken prior to the pin installation in the hand-tight position. The final make-up stage image is taken after the power-tight make-up by the power tongs. DIC images are not the only test data recorded at this time. The hydraulic power tong actuator data acquisition system records the torque-turn data applied to the test speciemen. The operator must also record all the dimensions needed to apply the boundary conditions in the FE model when the power tongs are installed around the test specimen. Special care is necessary during the process to not damage the paint sputter pattern so it can be used for the load frame testing. Figure 4.3 displays the MIJ connection make-up test set up for DIC measurements.

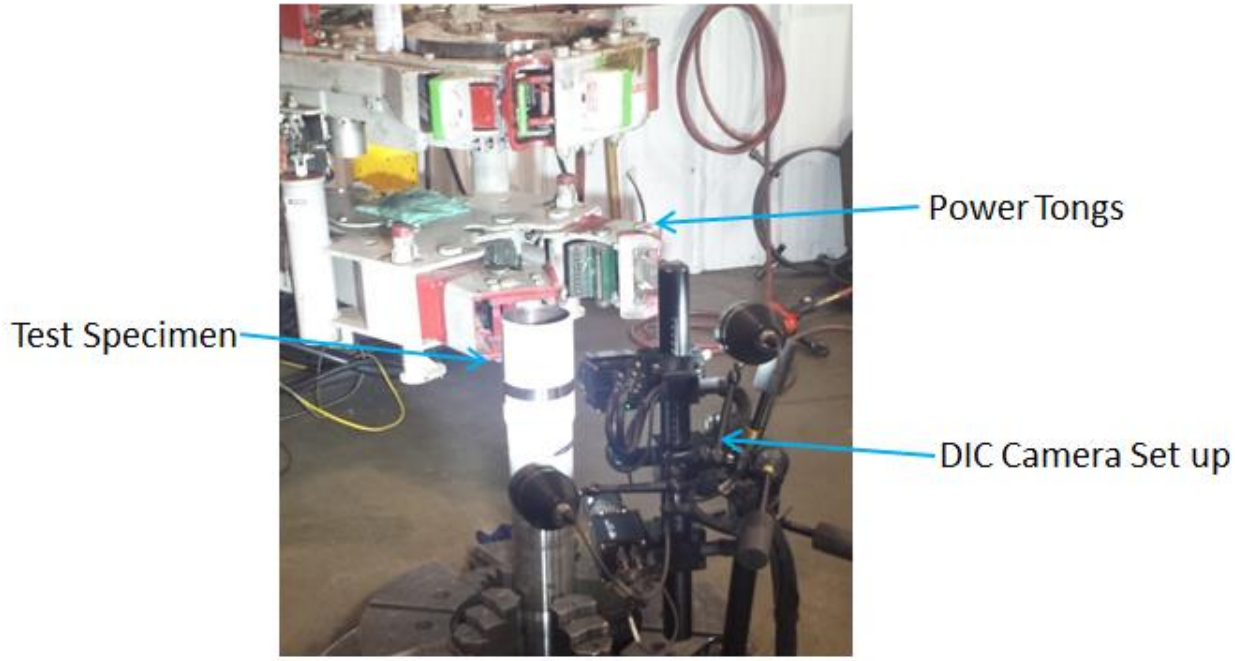

Figure 4.3: MIJ connection make-up test set up for DIC measurements.

4.1.4 DIC Load Frame Test

After the connection make-up is complete, the test specimen is removed from the fixture and prepared for load frame testing. End caps are mounted on both ends of the made-up test specimen. The end caps are

required for installing the specimen into the load frame. The DIC system is relocated to the load frame bunker where the cameras are setup and calibrated one more time. The paint pattern on the surface remains the same because undefromed reference images are acquired with that pattern. Similar to the make-up tests, boundary conditions and loading data must be recorded for use in the FE model along with the DIC images. Data required for boundary conditions includes:

1. Test specimen overall length.
2. Location of fixed point and loading points with respect to the connection.
3. Locations of the anti-buckling (HBU) devices.

The boundary conditions are not constant for every test specimen, therefore, the premium connection test specimen configuration must be recorded at the time of the test. Figure 4.4 shows the MIJ connection installed in the load frame for DIC measurments during load sequence tests.

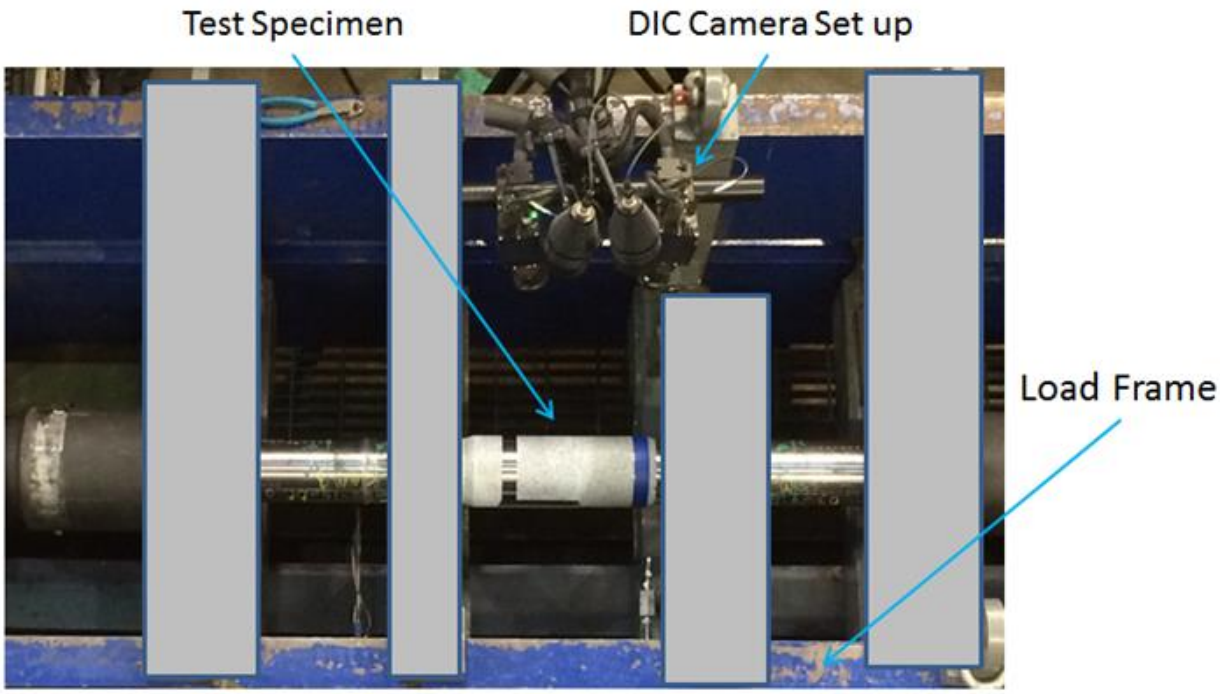

Figure 4.4:MIJ connection load frame test set up for DIC measurements.

4.2 DIC Data Processing

The strain and displacement fields over the surface of the box are extracted by post processing the DIC image data. The DIC images are post processed systematically over a defined area to a coordinate system consistent with the FE model results. The desired area of the image to be processed, the box surface in this case, is defined by masking off the image to only provide relevant data and save computing resources. Figure 4.5 displays the defined area on the box surface used to calculate the strain and displacement results.

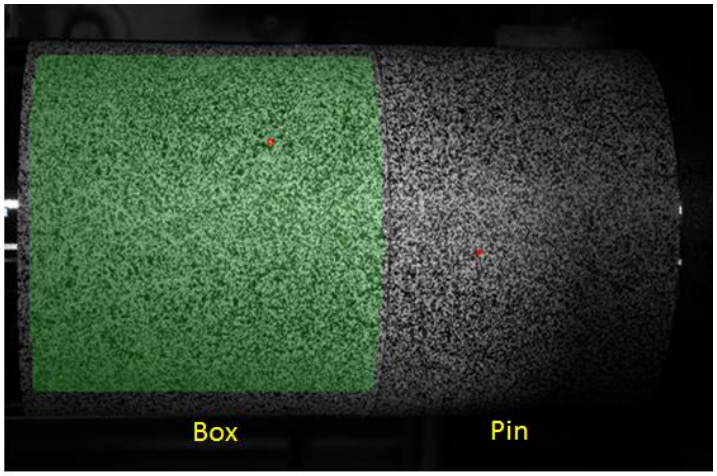

Figure 4.5: Strain and displacement data is only calculated over the defined highlighted area.

4.2.1 Coordinate System Relocation

The reconstructed 3D image from the DIC data is defined with respect to a global Cartesian coordinate system which has no physical relation to the test specimen coordinate system. The global coordinate system relocation is performed in the ARAMIS software on the MIJ connection image data by transforming the data from the default DIC global coordinate system to a user defined cylindrical coordinate system oriented to a cylinder fitted to the DIC image. The cylindrical coordinate system associated with the cylinder is consistent with the mechanics of the premium connection. The coordinate system is placed on the cylindrical axis of the box with the origin aligned with the secondary seal edge and y-axis aligned with the cylinder longitudinal axis illustrated in Figure 4.6. This location provides a distinct edge between the box and the pin in the image and ensures the accuracy of the placement of the origin point. The location differs from the origin set in the FE model; however, the DIC data and FE model results are transformed to align with a correlation coordinate system prior to correlation. The coordinate transformation associated with the data alignment process between the DIC results and the FE model is discussed later in section 5.1.1.

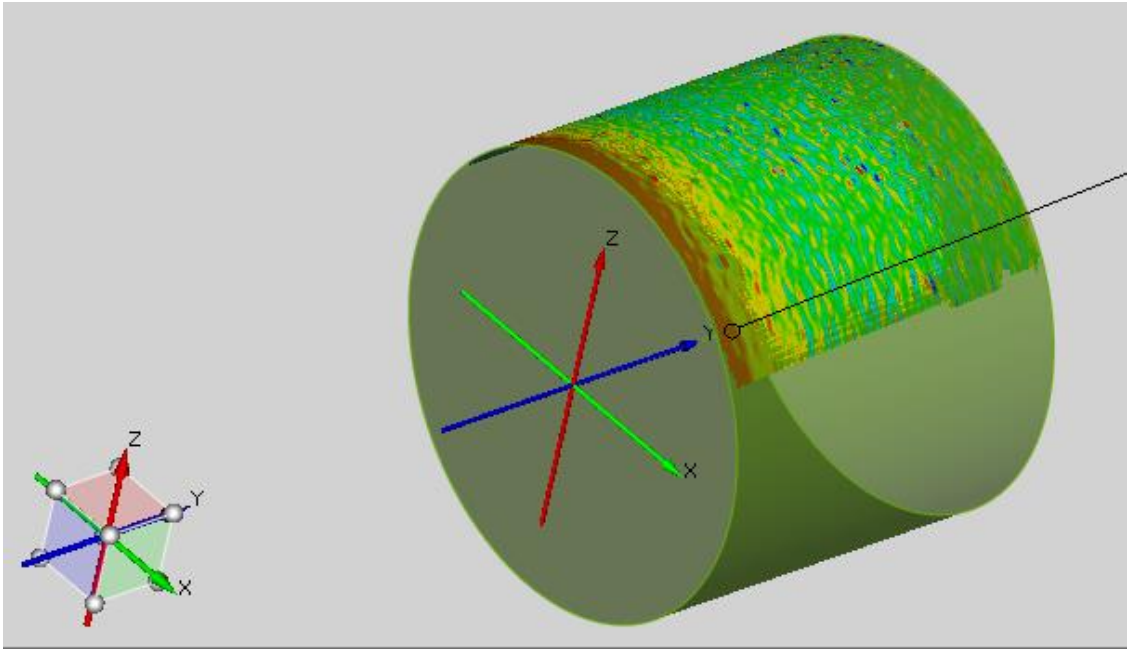

Figure 4.6: Transformed global coordinate system to cylindrical system with longitudinal axis aligned with the cylindrical axis of the DIC image.

Additional consideration for re-positioning the coordinate axis is that the global coordinate system (x-y-z) dictates the local coordinate system (x'-y'-z') on each point of the cylindrical reconstructed 3D surface. The significance of the local coordinate system is that all strain components are reported with respect to the x'-y'-z' coordinate system in ARAMIS. The rules for ARAMIS to determine x'-y'-z' through x-y-z are

1. the local direction x' is tangent to the surface of the local point and parallel to the x-z plane
2. the local direction y' is tangent to the surface of the local point and perpendicular to the local x'
3. the local direction z' is determined by right-hand rule

The benefit of defining the y-axis along the longitudinal direction of the fitted cylinder is that the local x' and y' axes represent the tangential direction and longitudinal direction respectively. Subsequently, the strain and displacement components are in the hoop and longitudinal directions illustrated in Figure 4.7.

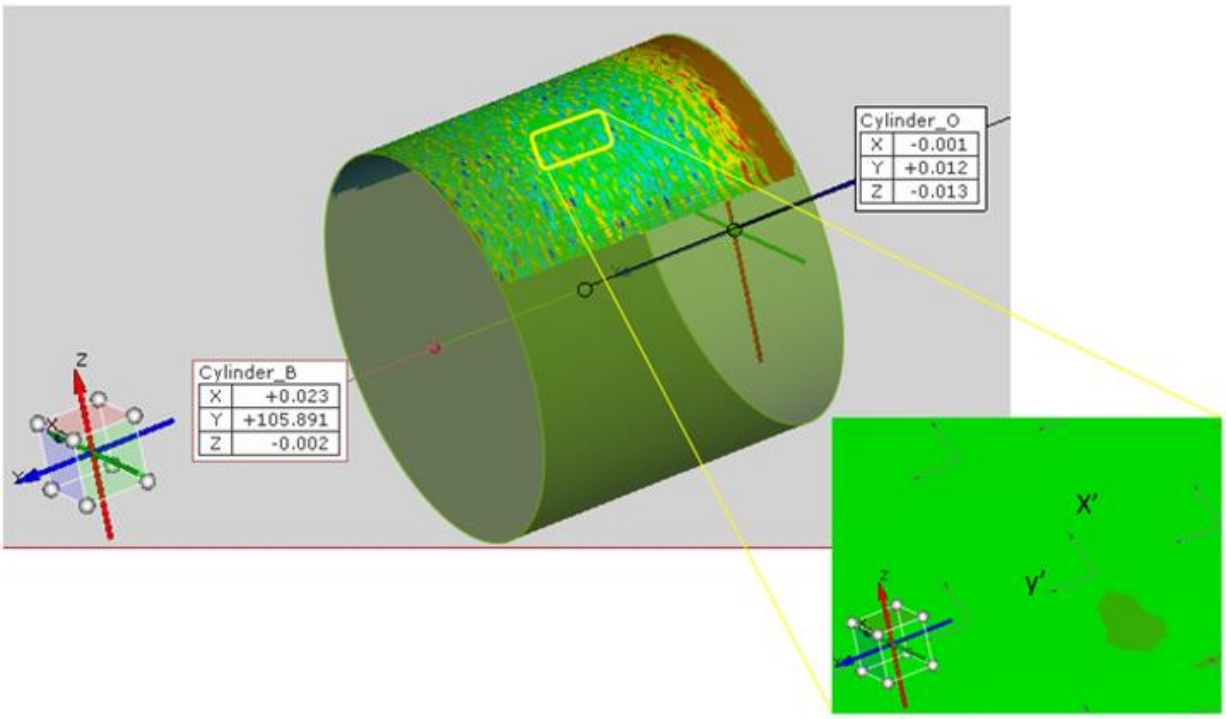

Figure 4.7: Local coordinates on the 3D surface, x'-y', defined by the global coordinates x-y.

4.2.2 DIC Data Export

The extraction of strain and displacement data from the DIC images is performed with five section lines (virtual extensometers) placed on the 3D image surface equal distance apart. Five section lines are selected to account for variations in the results over the surface due to the curvature of the cylinder. The number of section lines should be adjusted according to the size of the masked off image. Larger images may require more section lines for increased reliability of the results. The median values of the data from the section lines are used to estimate the displacement and strain components for correlation with the FE model results. Figure 4.8 displays the five section lines over the 3D DIC image surface.

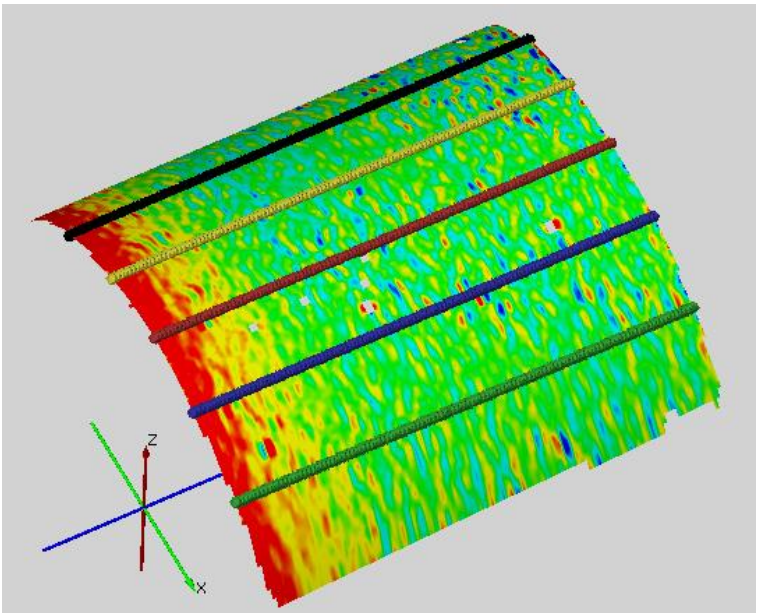

Figure 4.8: DIC image with 5 section lines over the surface for extracting displacement and strain data.

As mentioned in section 4.1, the strain-free reference image is set as "stage 0". Subsequently, the make-up is "stage 1", load point 1 is "stage 2" and so on until the last load point in the service loading test. Field data for each section line is written into one single ASCII file per stage. Consequently, a total of five data files are exported for every stage. The data files contain data fields for the undeformed and deformed coordinates of each section point along with the computed displacement and strain components. The data file structure includes header information followed by the data block illustrated in Figure 4.9.

```
# this is a export configuration file for ##### project. The export format is defined by YI LI
#
# Stage :   0.000000  -  1.000000
# Length in units of [in]
# Strain is displayed without a unit. It is converted into value between 0 and 1 in order to match the default output of strain from ABAQUS
#
# Index_x, Index_y, Coordinate-undef (x,y,z), Coord-def (x,y,z), Displ(x,y,z), Strain (x,y,xy, Major, Minor, Thicknessreduction)
#
#Datalines follow
   0       0.708661 4.174063 2.361916    0.708800 4.174147 2.361714    0.000139 0.000085 -0.000202    0.000628 0.001775 -0.001001 0.002695 -0.000292 0.002396
   1       0.708661 4.141345 2.361851    0.708831 4.141386 2.361644    0.000170 0.000041 -0.000207    0.000414 0.001138 0.000445 0.001356 0.000196 0.001550
   2       0.708661 4.108626 2.361601    0.708802 4.108621 2.361624    0.000141 -0.000005 0.000023    0.000334 0.000002 0.000069 0.000668 -0.000331 0.000336
```

Figure 4.9: Content structure of exported ARAMIS ASCII data file.

The data block contains the data fields for each point on a section line; each column represents one field following the convention defined in order:

- Column 1: `SectionPoint_ID`
- Columns 2-4: `Undeformed Coordinate (X,Y,Z)`
- Columns 5-7: `Deformed Coordinate (X,Y,Z)`
- Columns 8-10: `Displacement(x,y,z)`
- Columns 11-16: `Strain(x,y,xy, Major,Minor, Thicknessreduction)`

The exported ARAMIS data file contains a total of 16 fields. Each row represents one section point along the section line. The section points are data points computed along the reconstructed 3D surface. Therefore, the total number of section points varies slightly for each section line. The data near each end of the section line can be inaccurate due to edge effects. The edge data is trimmed to align with the FE model results for the correlation and error analysis. The user must make sure that the units are consistent between the DIC and the FE model results.

4.2.3 Noise Floor

Noise associated with DIC measurement originates from various sources, the instrument itself, system calibration, and the numerical algorithms of post-processing. To quantify the level of noise, the concept of a "noise floor" , for the DIC data is defined as the standard deviation of the fluctuation of the field variable signal. Figure 4.10 displays the longitudinal strain results for the strain-free reference image. Ideally, the strain-free image components should be zero and the strian field contour should be uniformly green. However, the histogram and data from the section lines provides a visual representaion of the noise in the results. The fluctuation around mean-zero signal for the section line curves represents the noise. The noise floor is quantified for the longitudinal strain at 0.015% or 150 micro-strain, and similarly for the hoop strain at 0.035% or 350 micro-strain.

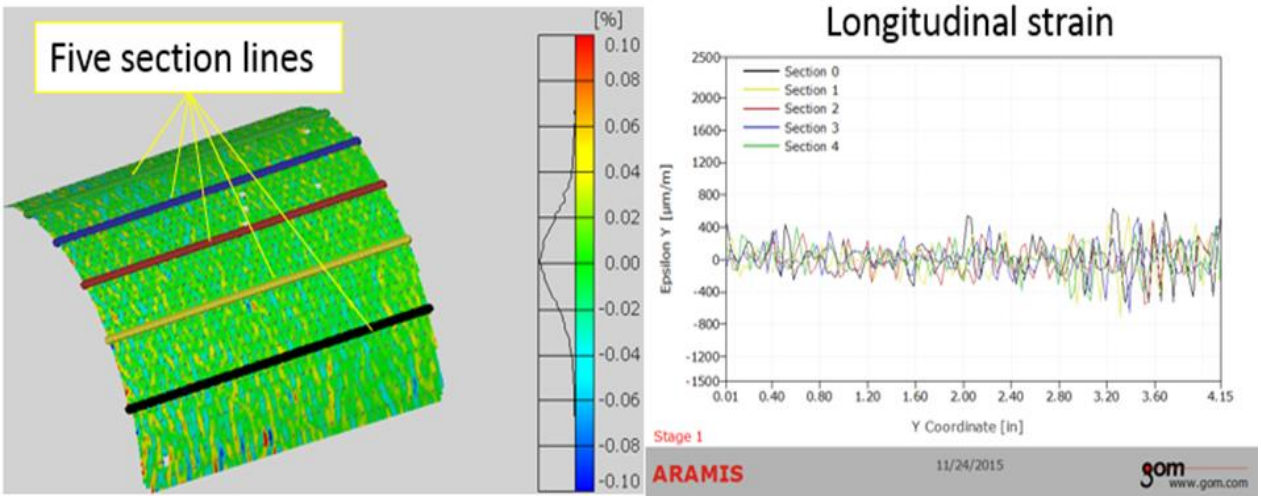

Figure 4.10: Longitudinal strain contour plot and results extracted from section lines for strain free reference image.

The test specimen and DIC set up is relocated after the make-up test for the load sequence tests. An "initial state" image results are used to quantify the noise floor at the second location. The noise floor for longitudinal strain is 0.016%, and 0.027% for the tangential strain. From the comparable values of noise floor between the two sessions, it can be established that the quality and consistency of the measurements are credible.

A significant implication of the noise floor is that actual strain developed in the connection below the level of the noise floor will not be captured by the current measurement. The noise floor can be reduced through careful experimental procedures and proper system calibration. The quality of the sputter pattern along with proper lighting and camera calibration are the critical aspects for minimizing the noise in the DIC measurements.

4.3 Pressure Cylinder Experiment

To improve confidence in the DIC data processing procedure, a simple experiment was performed on the Virginia Tech campus in Blacksburg Virginia. A polycarbonate cylinder is fabricated using commercially available materials. The cylinder surface was prepared with a sputtered paint pattern and internal pressure is applied to initiate longitudinal and tangential stress and strains for DIC imaging. Figure 4.11 displays the experiment set up with the prepared cylinder and the Aramis DIC camera system.

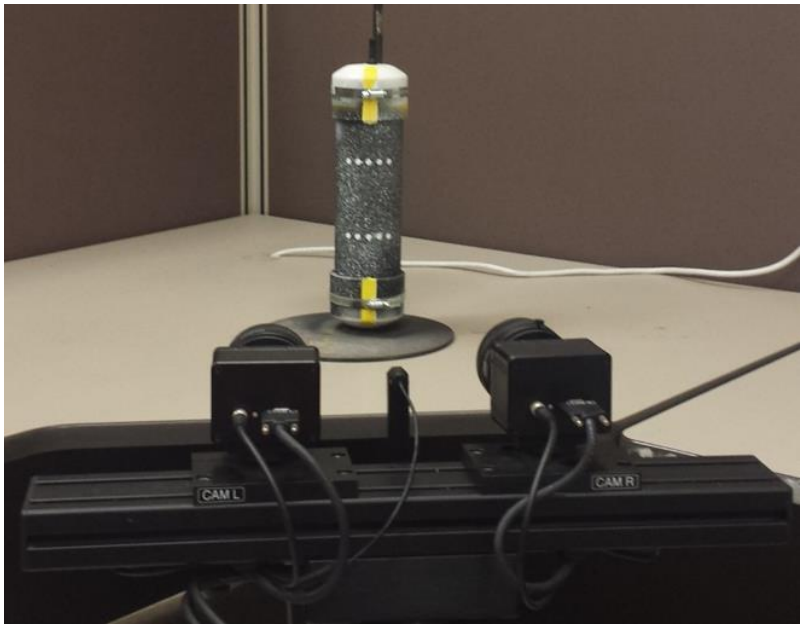

Figure 4.11: Pressure cylinder DIC experiment set up.

The main objectives for this experiment are to verify the DIC process and acquire experience with:

1. Fitting a cylinder to the DIC image and checking the results with the known dimensions
2. Relocating global coordinate system to user defined cylindrical coordinate system oriented to the fitted cylinder.
3. Exporting section line data from the ARAMIS software.

A finite element model of the cylinder is generated in Abaqus CAE. Estimated material properties are used in the FE model due to limited resources and time for obtaining exact material properties. The longitudinal and tangential stress values are calculated using a force balance which eliminates the material property influence. These hand calculation results are used to validate the FE model. The longitudinal stress, σ_Z, and tangential stress, σ_θ, are calculated using thin-wall cylinder theory in equation 4.1 and 4.2, where p is the internal pressure, R_i and R_o are inner and outer radius respectively.

$$\sigma_Z = \frac{pR_i^2}{R_o^2 - R_i^2} \tag{4.1}$$

$$\sigma_\theta = \frac{pR_i}{R_o - R_i} \tag{4.2}$$

The inner and outer diameters are measured from the fabricated cylinder and inner and outer radii are calculated at 1.62 inches and 1.75 inches. Internal pressure of 80 psi was applied. The finite element model is generated with the measured dimensions of the cylinder. The internal pressure is applied on the inside surface of the cylinder and the end caps to replicate the experiment. The results were transformed into a cylindrical coordinate system from the global Cartesian system. Figure 4.12 illustrates the tangential and longitudinal stress direction in the FE model. The results in Table 4.1 show the validation of the FE model with error of 3.34% for axial stress and 5.72% for hoop stress from the calculated values.

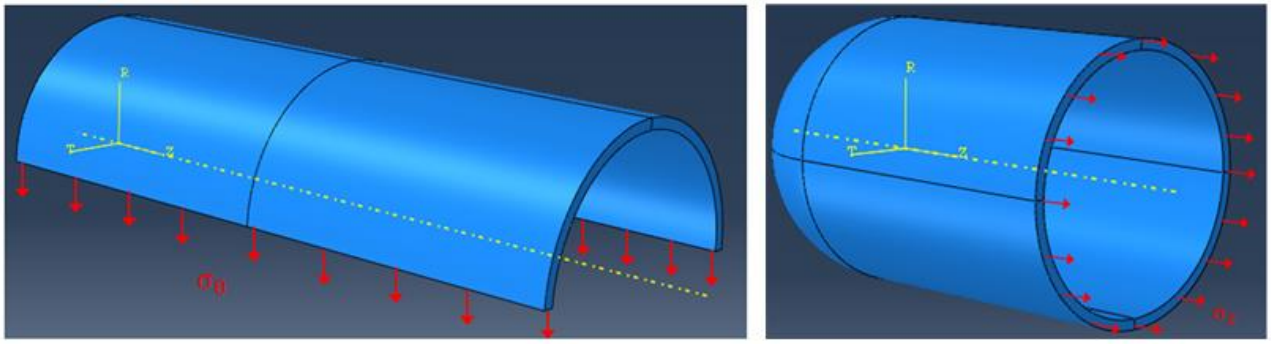

Figure 4.12: Tangential and longitudinal stress in the cylinder FE model.

Table 4.1: Calculated vs FE model longitudinal and tangential stress.

	σZ (psi)	σθ (psi)
Calculated	479	997
FE Model	463	940
% Error	3.34	5.72

Longitudinal strain, ε_Z and tangential strain, ε_θ results were extracted and compared in the cylindrical coordinate system between the FE model and the DIC test. The results were extracted from the middle of the cylinder to eliminate the edge effects from the end caps as shown in Figure 4.13. Only one section line was created in each direction on the DIC image. The average value from each section line is used to compare with the FE model results. The results in Table 4.2 indicate a valid correlation between the FE model and DIC.

Table 4.2: FE model vs DIC test longitudinal and tangential strain results.

	εZ (%)	εθ (%)
FE Model	0.0362	0.231
DIC Test	0.0396	0.212
% Error	9.39	8.23

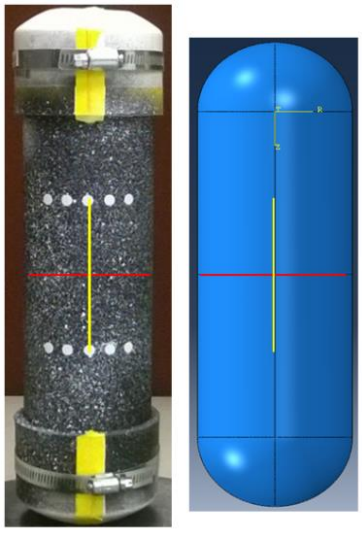

Figure 4.13: Longitudinal (yellow) and tangential (red) strain data extracted from DIC test and FE model from the middle of the cylinder.

The main contribution of error in the results is from the variations in cylinder surface geometry which were not accounted for in the FE model. The pressure cylinder specimen was fabricated with machined grooves before the sputter pattern was applied. The cylinder surface was machined for another DIC experiment not relevant to this thesis. Figure 4.14 illustrates the discrepancies in the cylinder surface visible in the DIC image as well. However, the results here are sufficient to ensure the dependability of the DIC data post processing procedures. The main objectives of the experiment were achieved by gaining experience with the ARAMIS software steps involved to export proper DIC data sets.

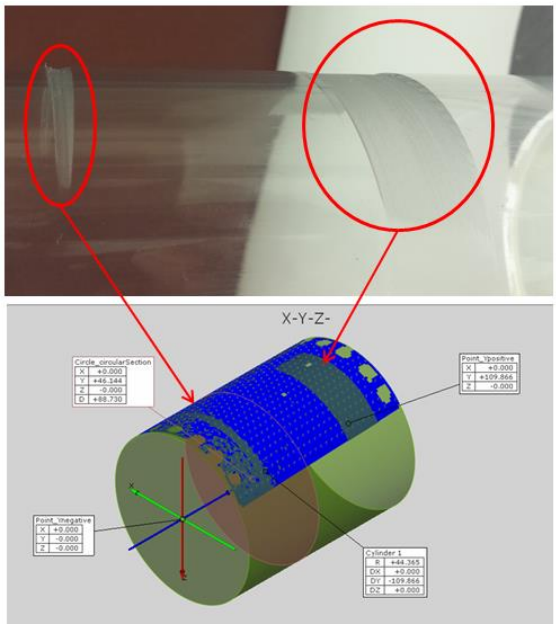

Figure 4.14: Machined grooves in the fabricated cylinder contribute to error in the DIC results compared with the FE model.

Chapter 5 3D Finite Element Model Validation

Once the 3D FE models are developed and DIC results are post processed, the next step is to compare the two sets of results. The make-up conditions for the FE model are calibrated against the DIC test results. After the FE models are calibrated for the make-up test, the service loading sequence is applied to the verified make-up FE model. The results from the FE model load sequence are compared with DIC test results from the load frame to validate the 3D FE model. Several FE models are created to produce the best make-up model correlation with the DIC results. The correlation and error analysis is performed using MATLAB and Python scripts.

5.1 Correlation Analysis

MATLAB and Python scripts are developed to extract DIC and FE results from the data files. The MATLAB script transforms both FE and DIC data to the correlation (cylindrical) coordinate system, and trims the data sets to user defined bounds. The DIC data is filtered and the correlation analysis is performed with spatial sum-squared error (SSE) of DIC and FE model results. The correlation error presented is the FE model results relative to the experimental DIC strain and displacement field. Figure 5.1 illustrates the work flow of the error analysis process by the MATLAB script.

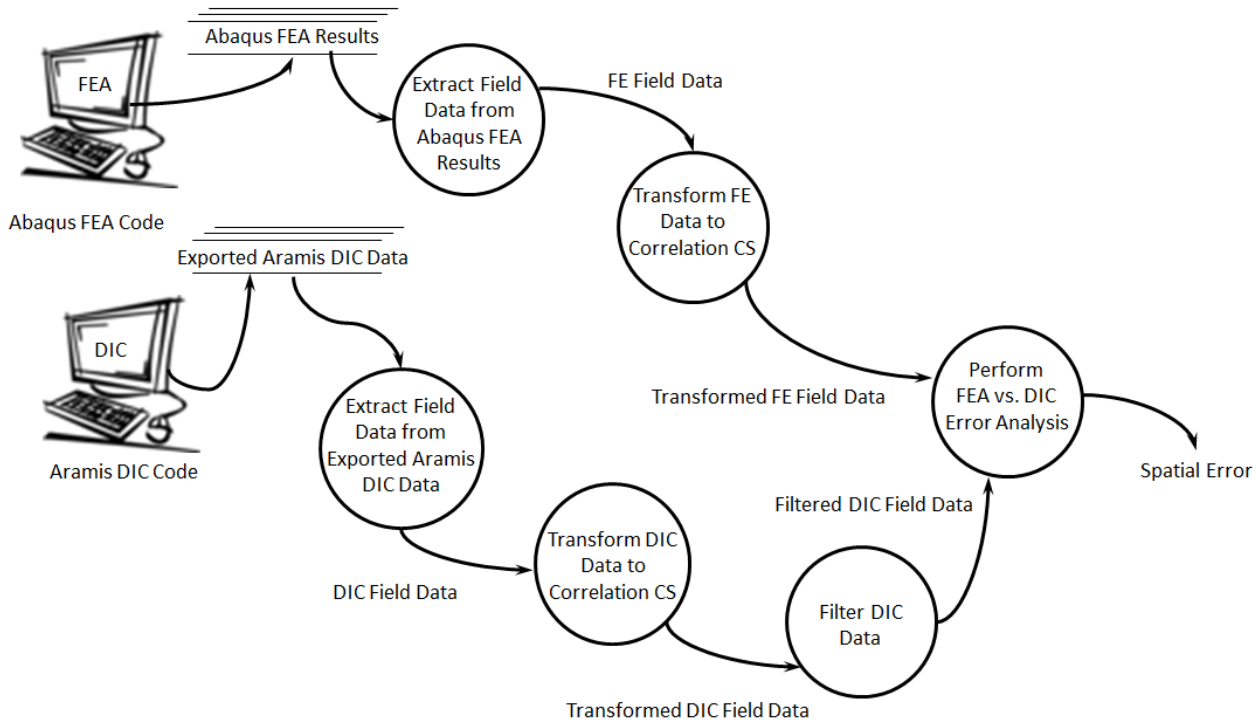

Figure 5.1: FEA and DIC results error analysis data flow diagram.

5.1.1 Data Alignment

The FE model results are stored in an output database file as mentioned in section 3.7. A Python script was developed to extract the displacement and strain field data from the pre-defined node set on the surface of the box. The FE data and the DIC results are imported into MATLAB in their individual Cartesian coordinates. It is critical that the physical locations of both data sets match for accurate correlation and error analysis. User defined translation and rotation vectors are specified in the MATLAB script to transform the data to a consistent *Correlation Coordinate System.* The data sets are transformed to a cylindrical coordinate system with the z-axis as the longitudinal axis, which is conventional for the mechanics of the connection illustrated in Figure 5.2.

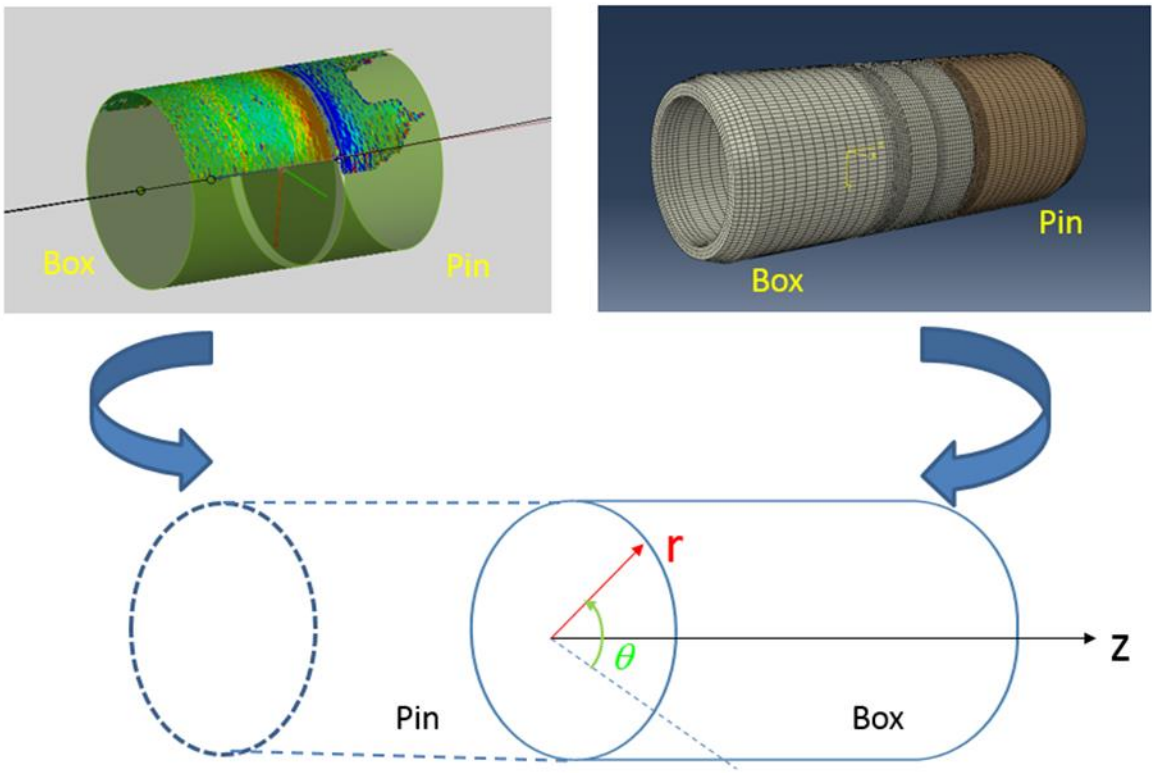

Figure 5.2: DIC and FEA results transformed to a consistent cylindrical coordinate system for correlation.

Special attention is required for a known reference point in the DIC images to align the correlation coordinate system at the same zero point as in the FE model. In this case, there is a distinct edge visible between the box and the pin in the DIC image where the coordinate system is relocated to as explained previously in section 4.2. The data set defined in the FE model is aligned with that edge to ensure the starting point on both sets is physically identical. It is possible to have a case where it is difficult to define a specific point to align the coordinate system. The user defined translation vector specified in the MATLAB script can be used to eliminate any discrepancy between the data sets alignment. The section lines created in the DIC image may not be the same exact length as the node set defined in the FE model. The image data along the ends of the section lines may not be credible as well. Therefore, the MATLAB scripts require user input for total length of the data over the surface of the box. The excess data is trimmed and not used during error calculations. The user must ensure that the total length defined for the data set includes all the internal features of the connection.

5.1.2 DIC data filter

The DIC data is exported for five section lines as described in section 4.2. The median values of the five section lines are computed into a set after the data has been aligned and trimmed to desired bounds. Image processing filters included in the ARAMIS software are not applied to the DIC data. The drawback of using the tools in the ARAMIS software is that the filtering is basically performed by smoothing operations reducing the available data. The median data from the section lines is filtered systematically using the minimum spatial wavelength determined from the mechanics of the connection with the MATLAB script. The spatial wavelength values are distinguished by the user by examining the raw unfiltered data. Figure 5.3 displays the filtered DIC data for tangential and longitudinal strain and displacement fields over the desired length of the box surface.

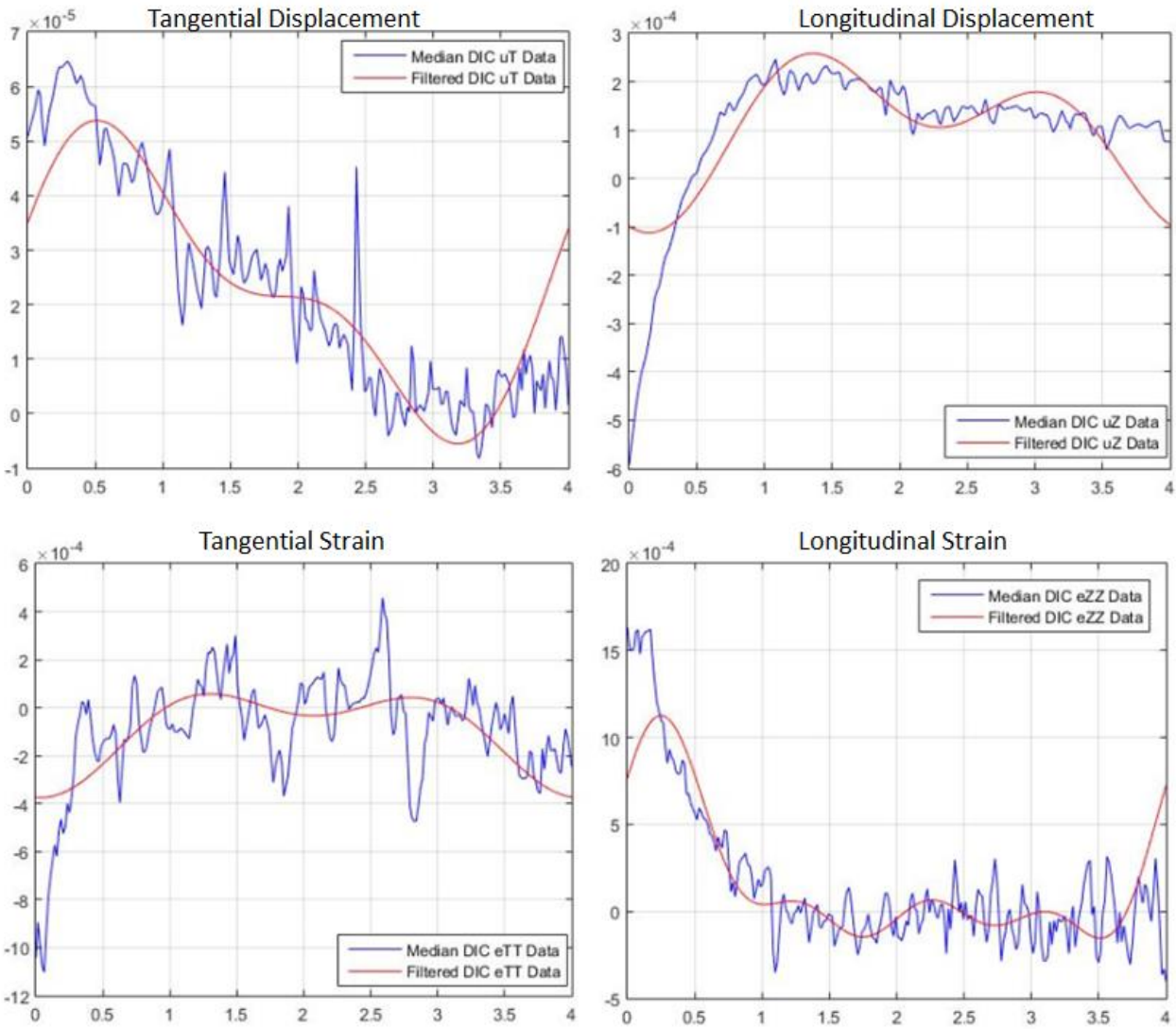

Figure 5.3: Filtered DIC data using minimum spatial wavelength compared with median DIC data from five section lines.

5.1.3 Sum Squared Error

To perform correlation error analysis, the number of data points in both, the DIC and FE model data sets must be equal. However, the number of data points from the FE model represents the node density in the region of the defined set, while the number of data points in the DIC data set represents the total number of section points of the virtual extensometer. Additional data points are computed within each data set to match the totals through interpolation functions. The correlation between the FE model results and DIC results is performed with the Sum Squared Error (SSE) method shown in equation 5.1.

$$SSE = \sum_{i=1}^{n} (FE_i - DIC_i)^2 \tag{5.1}$$

The SSE is the sum of the squared spatial difference between the FE model results and DIC data at each point. The make-up conditions for the FE model are calibrated to the DIC data by minimizing the SSE.

5.2 Make-Up Model Calibration

The principal advantage of the full 3D FE model is that the boundary conditions can be represented as close as practical to the BCs in the physical tests. The pin is rotated into the box to a hand-tight position

before the power tongs are actuated for the power-tight make-up. Therefore, it is difficult to determine the exact location of the hand-tight position which is considered the start of the power-tight make-up. The unknown starting point for the FE model connection make-up requires a calibration of the prescribed rotation value on the pin.

5.2.1 Pin Rotation Variable

The pin is initially assembled into the box at an estimated hand-tight location in the FE model. Several make-up steps are generated varying the prescribed pin rotation over a wide range of turns. The SSE is computed for the longitudinal strain to develop a response function for error with respect to the pin rotation. After bounding the error response, the FE models are generated for a narrow range of prescribed rotations to determine the best make-up state which provides the lowest error. The best correlation between the FE model and DIC make-up test is found at a pin rotation of 46 degrees with SSE of $1.37e^{-5}$ in/in. The plots showing the calculated error with respect to the pin rotation are displayed in Figure 5.4.

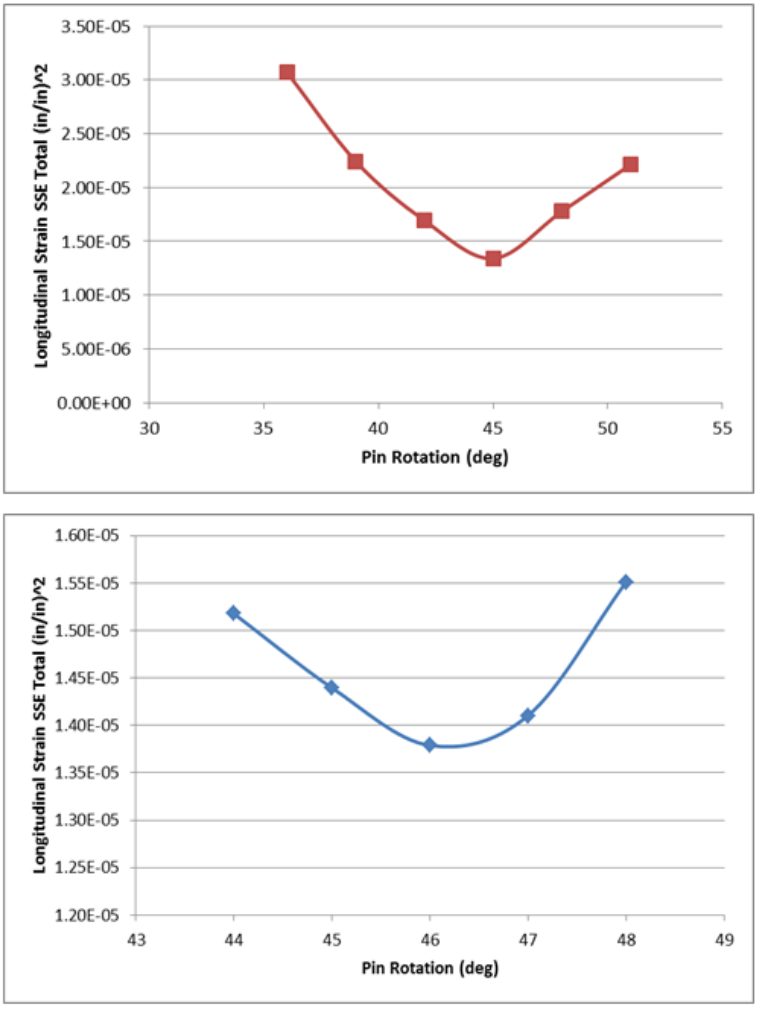

Figure 5.4: Pin rotation vs longitudinal strain SSE results for minimum error make-up model. Response function for error over wide range of pin rotation (top) and narrow range (bottom).

5.2.2 Make-Up Model Results

The make-up model is generated with the prescribed pin rotation of 46 degrees. Reaction torque is removed from the connection to simulate the release of the power tongs. The FE model results are then correlated with DIC results for displacement and strain fields. Table 5.1 lists the numerical results for the SSE between FE model and DIC results for tangential and longitudinal displacement and strain fields.

The connection section view plots for strain and displacement fields in Figure 5.5 and Figure 5.6 deliver a visual validation of the 3D FE model's capability to represent the dominant features in the mechanics of the connection. The full filed DIC results show that the test specimen does not make contact at the shoulder as shown by the results of the FE model. It would be difficult to capture such details with typical strain gage measurements. The shoulder contact presented by the FE model suggests a dimensional discrepancy between the test specimen and possibly due to geometric tolerances.

Table 5.1: Minimum error make-up model SSE results.

SSE Total Error			
uT	uZ	eTT	eZZ
1.40E-06	7.91E-06	1.16E-05	1.37E-05

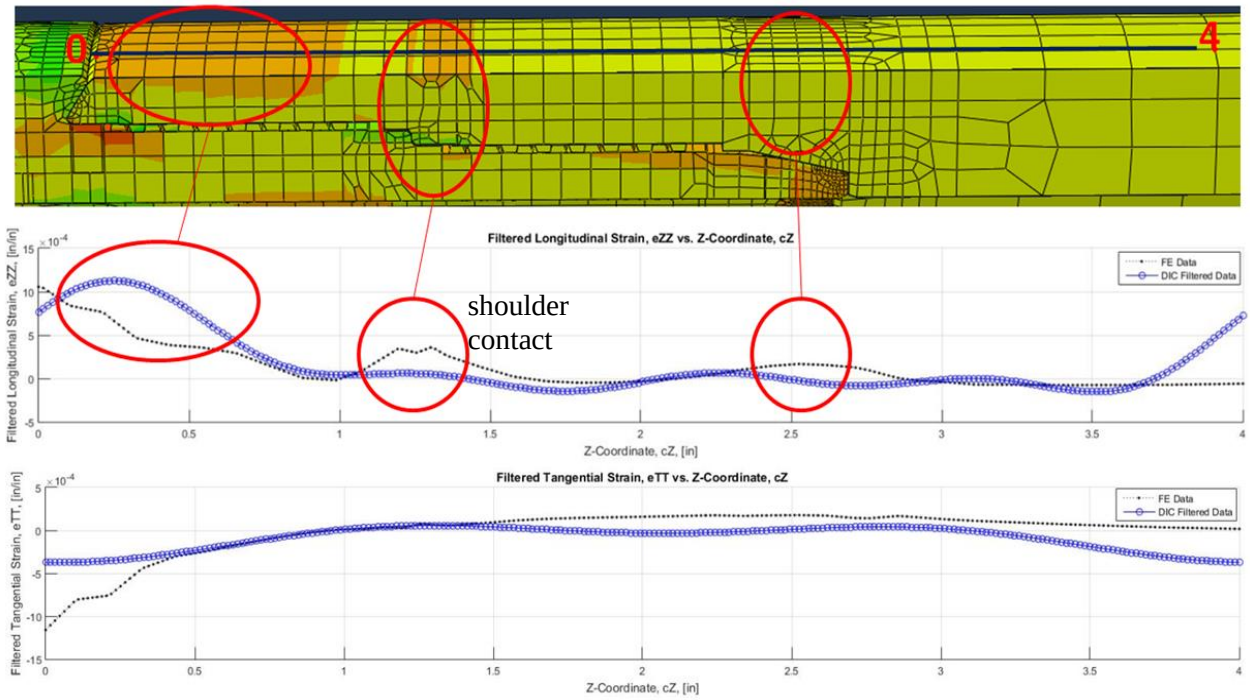

Figure 5.5: Longitudinal and tangential strain plots comparing FEA and DIC results.

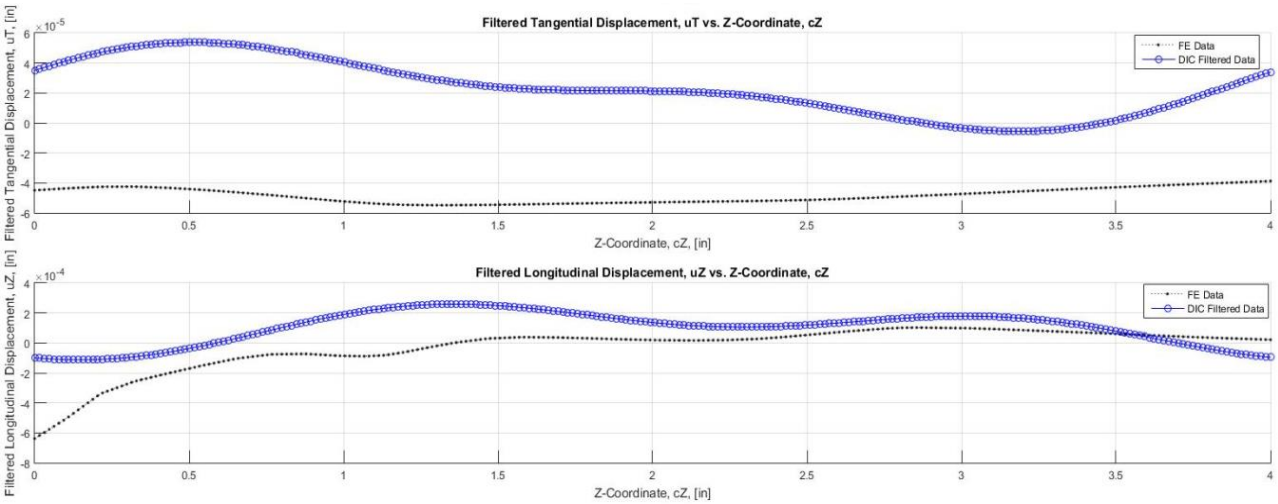

Figure 5.6: Longitudinal and tangential displacement plots comparing FEA and DIC results.

5.3 Make-Up Torque

Representing the connection make-up with a full 3D FE model provides the ability to capture the torque-turn relationship. The make-up torque on the connection due to the pin rotation can be directly measured on the 3D FE model. The make-up torque value is linearly related to the coefficient of friction, μ, prescribed in the contact regions. An estimated value 0.08 was used for μ initially for the make-up models. After the make-up model is calibrated, the torque value from the physical test is used to estimate the friction coefficient and develop a torque-turn plot. The μ value of 0.063 matches the make-up torque from the FE model to actual test almost perfectly. The calculated μ also falls within the range of typical tubing and casing thread compounds [20]. Table 5.2 lists the results of the make-up torque and μ with corresponding error and Figure 5.7 illustrates the developed response function. Torque-turn plot generated from the 3D FE model is displayed in Figure 5.8.

Table 5.2: Reconciliation of reaction torque with friction coefficient

Model	Make-up Torque (ft-lbs)	% Error
Actual	4563	
μ 0.08	5728	25.53
μ 0.063	4564	0.02
μ 0.06	4386	3.88

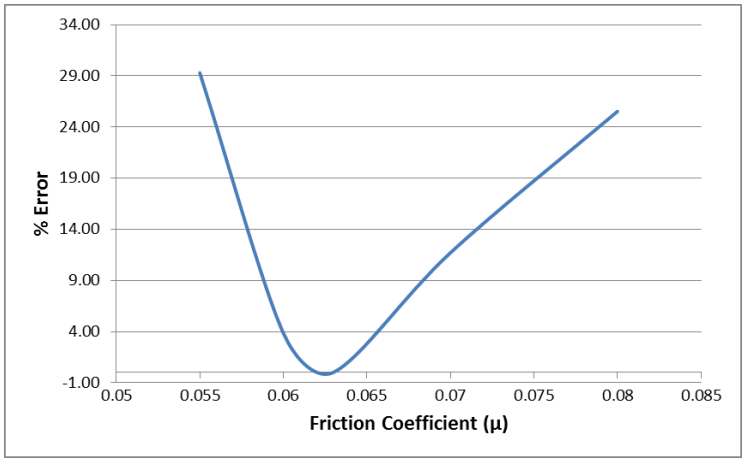

Figure 5.7: Response function for calculated and experimental make-up torque error from varying friction coefficient values.

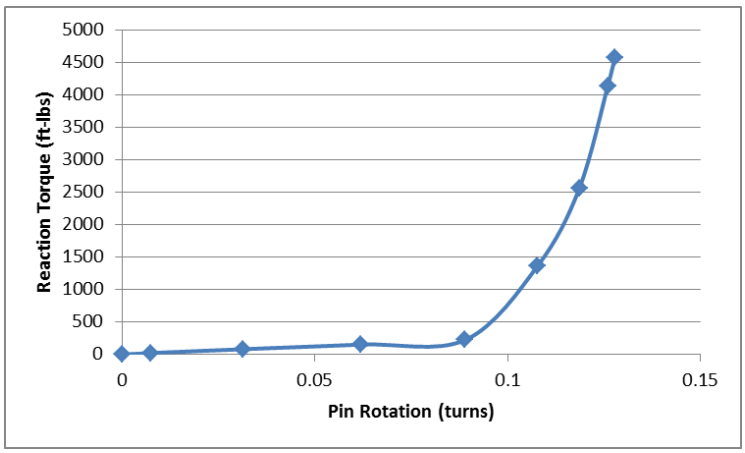

Figure 5.8: Torque-turn plot matches connection behavior with steep increase in the torque values after shoulder contact.

5.4 ISO 13679 Load Series B Application

ISO 13679 service loading tests are used for premium connection qualifications. The physical tests only provide a "leak" or "no leak" result for the connection seal performance. A common seal metric used to evaluate seal performance with FE models is to consider the length of the contact of the metal-to-metal seal and the total area under the contact pressure curve [1]. The MIJ connection considered in this research developed a leak after load point 26 out of 34 during the ISO 13679 series B loading tests. The 3D FE model validation is performed by observing the SSE against DIC results from the completed part of the Series B test. The seal contact pressure and length data is extracted from the FE model and briefly examined. The load sequence applied to the connection test specimen up to load point 26 is listed in Table 5.3. The SSE values start to increase at load point 16 and keep increasing until the leak occurred at load point 26. The longitudinal strain plots also provide a visual representation of the increase in correlation error presented in the next section.

Table 5.3: Applied loads on the MIJ connection FE model for load sequence testing.

Load Point	Machine Load (kips)	Internal Pressure (Psi)	Axial Pressure Load (kips)	FE Model Applied Tensile Load (kips)
1	314.1	2	0.0	314.1
2	268	3745	43.9	311.9
3	222.2	7448	87.4	309.6
4	166	11830	138.8	304.8
5	2.3	11865	139.2	141.5
6	-147	11868	139.2	-7.8
7	-239.9	7441	87.3	-152.6
8	-194	3697	43.4	-150.6
9	-148.1	1	0.0	-148.1
zero	-1.4	1	0.0	-1.4
10	468.1	2	0.0	468.1
11	418.1	4032	47.3	465.4
12	367	8200	96.2	463.2
13	316.1	12201	143.1	459.2
14	188.1	15019	176.2	364.3
15	1	16226	190.4	191.4
16	-184	14807	173.7	-10.3
17	-244	13671	160.4	-83.6
18	-300	12277	144.0	-156.0
19	-352	10455	122.7	-229.3
20	-398	8295	97.3	-300.7
21	-296	0	0.0	-296.0
22	-398	8239	96.7	-301.3
23	-352	10525	123.5	-228.5
24	-300	12268	143.9	-156.1
25	-244	13686	160.6	-83.4
26	-184	14779	173.4	-10.6

5.4.1 Load Series B results

The strain and displacement fields from the 3D FE model and DIC tests for load sequence are compared by observing the SSE similar to the make-up model. Figure 5.9 displays the longitudinal strain SSE with respect to each load point. The results show an increase in the SSE values after load point 15. Figure 5.10 provides a visual confirmation of the discrepancies between FE and DIC longitudinal strain results starting at load point 16. The discrepancies remain in the results until the connection experienced a leak after load point 26. Plots of longitudinal strain for all 26 load points are included in Appendix B. Numerical results for displacement and strain fields SSE are listed in Table 5.4.

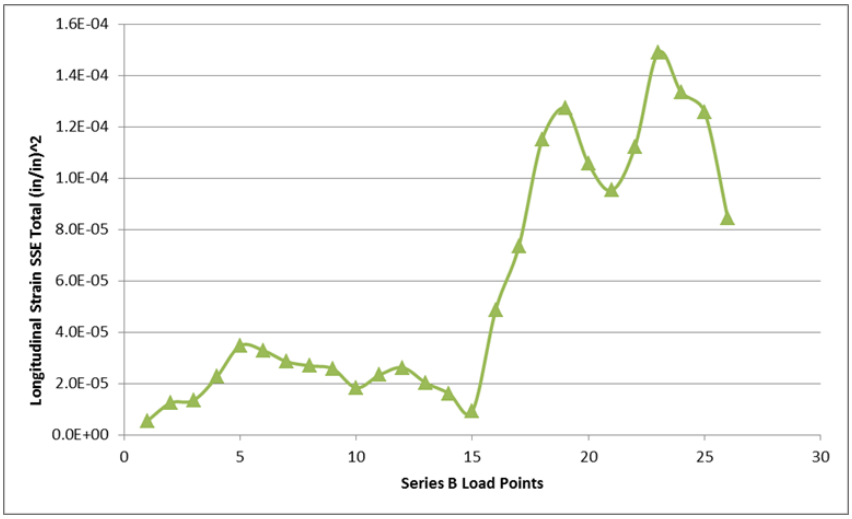

Figure 5.9: Longitudinal strain SSE at each Series B load point. The SSE values start to increase after load point 15.

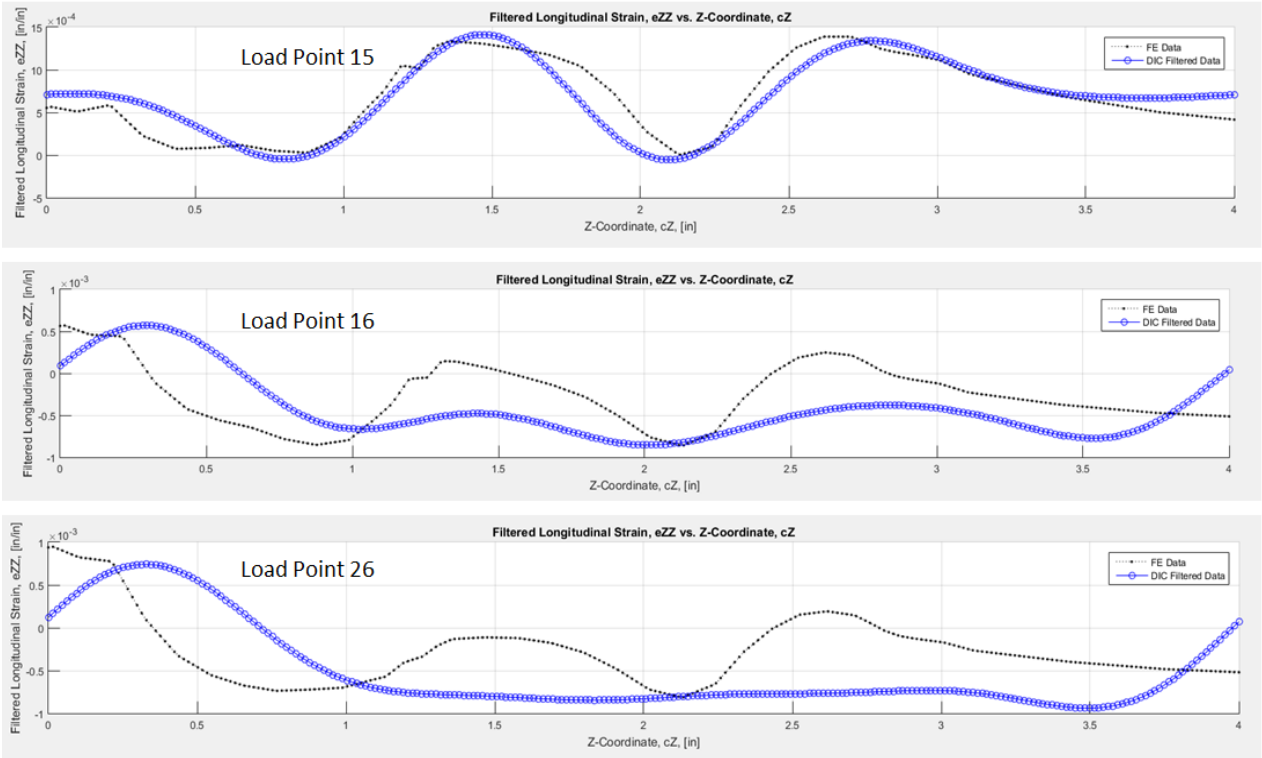

Figure 5.10: Visual confirmation of deviation between FE model and DIC results after load point 15.

Table 5.4: ISO 13679 load series B correlation error results.

SSE Total Error				
Load Point	uT	uZ	eTT	eZZ
1	1.36E-05	7.62E-01	3.06E-05	5.44E-06
2	1.75E-05	7.32E-01	3.64E-05	1.24E-05
3	3.37E-05	7.18E-01	3.88E-05	1.35E-05
4	4.23E-05	6.66E-01	3.76E-05	2.27E-05
5	3.98E-05	1.30E-01	2.66E-05	3.47E-05
6	4.30E-05	2.35E-03	3.88E-05	3.29E-05
7	3.02E-05	1.90E-01	4.12E-05	2.85E-05
8	2.11E-05	1.77E-01	5.36E-05	2.69E-05
9	1.42E-05	1.63E-01	4.69E-05	2.57E-05
10	1.36E-05	1.69E+00	3.53E-05	1.84E-05
11	1.44E-05	1.64E+00	3.82E-05	2.33E-05
12	1.90E-05	1.60E+00	4.29E-05	2.62E-05
13	2.75E-05	1.56E+00	2.97E-04	2.02E-05
14	3.88E-05	9.57E-01	3.91E-04	1.61E-05
15	5.04E-05	2.43E-01	3.81E-04	9.26E-06
16	4.98E-05	3.18E-03	4.57E-04	4.85E-05
17	4.67E-05	6.50E-02	4.34E-04	7.34E-05
18	3.66E-05	2.02E-01	4.89E-04	1.15E-04
19	2.27E-05	4.17E-01	5.52E-04	1.27E-04
20	1.62E-05	7.05E-01	5.48E-04	1.06E-04
21	5.77E-06	6.52E-01	4.12E-04	9.53E-05
22	1.82E-05	7.10E-01	5.13E-04	1.12E-04
23	1.65E-05	4.16E-01	5.41E-04	1.49E-04
24	2.47E-05	2.02E-01	5.00E-04	1.33E-04
25	2.57E-05	6.38E-02	5.69E-04	1.26E-04
26	3.84E-05	2.84E-03	7.19E-04	8.43E-05

Note that the longitudinal displacement, u_Z, error is significantly higher than the error associated with the other field variables. The test specimen experiences a rigid body translation when axial loads are applied in the load frame due to tolerances in the test fixtures. A rigid body movement correction factor is applied to the DIC image in the ARAMIS software to remove the rigid body translation effects. The longitudinal displacement reported by the DIC measurements is due to the strain developed only over the length of the image. The FE model results report the displacement due to strain for the full length of the test specimen which is over 14 times longer the length of the DIC image. Figure 5.11 displays the longitudinal displacement results for load point 1 and the difference in magnitude for DIC and FE values. As a result the SSE values are larger for longitudinal displacement. Estimate of the error due to test specimen rigid body translation is recommended for future work.

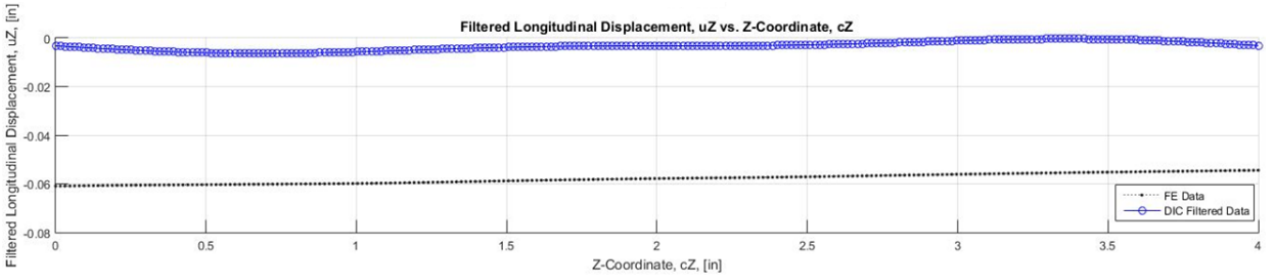

Figure 5.11: Longitudinal displacement results from load point 1 show the difference in magnitude between DIC and FE model values.

5.4.2 Seal Metrics

The 3D FE model can be used for design studies once it is verified and validated. Seal performance is the critical design element for premium connections. Seal metrics for seal contact pressure and seal length are easily extracted and examined. During the 3D FE model development, several upgrades are made on the mesh scheme in the seal region to acquire the best seal performance results. The controlled parametric meshing scheme permits generation of updated FE models effectively. The mesh updates correspond to model versions presented in section 3.3. In model version 1, the seal contact region aligned with the mesh transition region where the mesh is not uniform as shown in Figure 5.12. The mesh transition in the seal region is shifted over in version 2 to better capture the seal contact region displayed in Figure 5.13. Mesh density is increased in the seal region of the box and pin for smoother contact in version 3 and version 4 illustrated in Figure 5.14. The mesh of the rest of the model is not affected with modifications in the seal region. It is possible to update the mesh in the regions of interest only with the controlled meshing scheme which keeps the full 3D models manageable for the user.

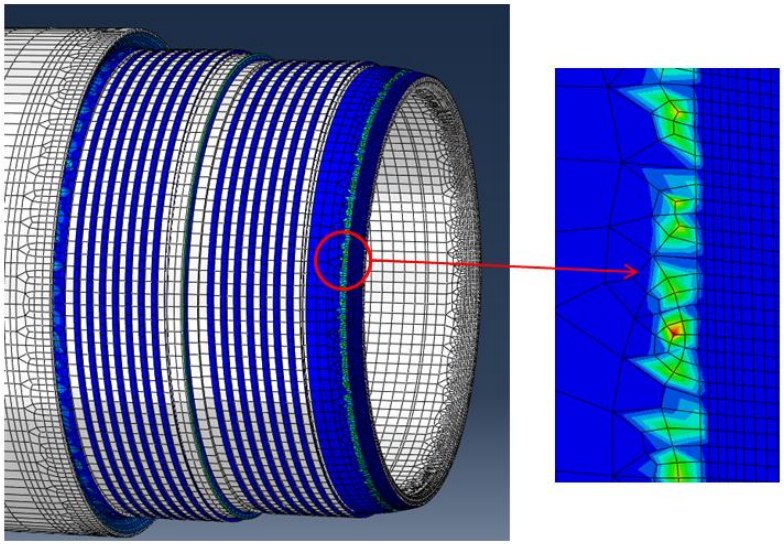

Figure 5.12: Primary Seal contact area placed mesh transition region in model version 1 required mesh scheme updates in the pin nose region.

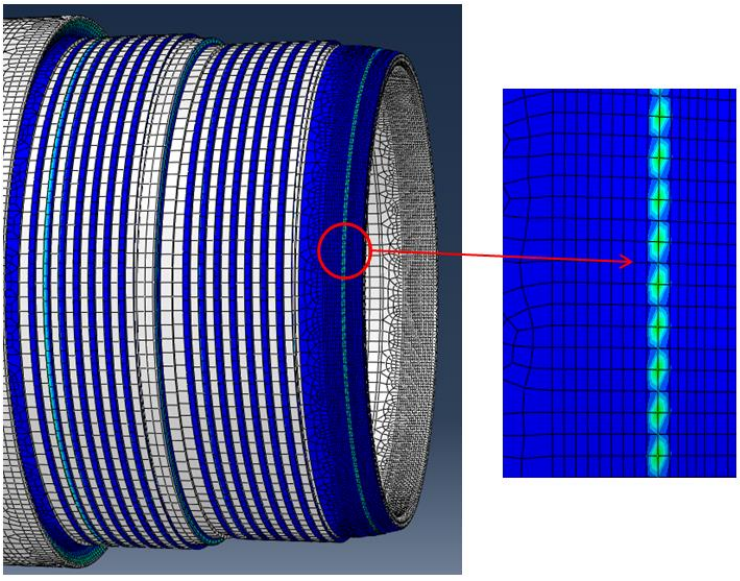

Figure 5.13: Primary Seal contact area in model version 2 with denser mesh region in the contact area.

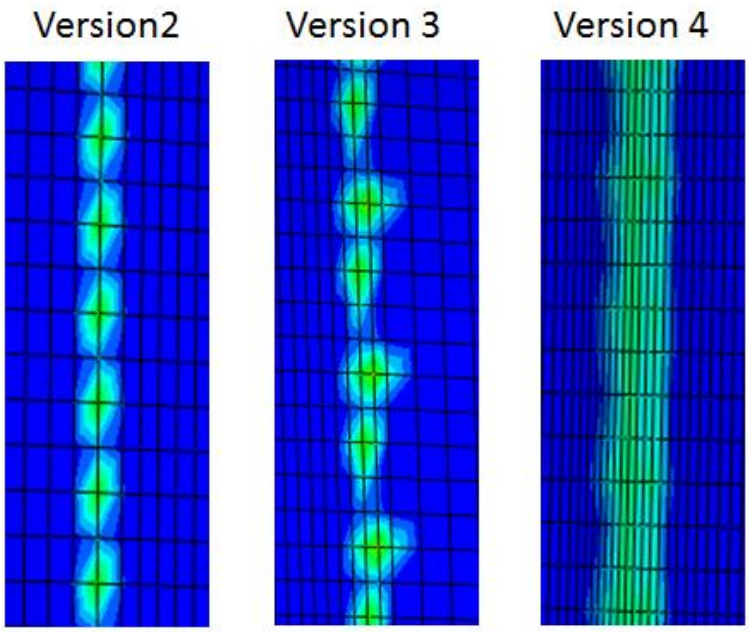

Figure 5.14: Contact pressure smoothing with mesh density increase.

The seal length and contact pressure and any other desired seal metrics results can be extracted to analyze seal performance under loading scenarios. Figure 5.15 displays the results of seal contact pressure over length for connection make-up and the first two load points. The seal contact pressure and the length increases as internal pressure is applied to the connection. The seal metrics show the capabilities of the 3D FE model providing insight inside the connection. Parametric studies can be executed to compare the seal performance by varying critical dimensions and load cases. Whereas the scope of the current research is on development of the 3D FE model, further investigation and optimization of connection seal metrics is recommended for future work.

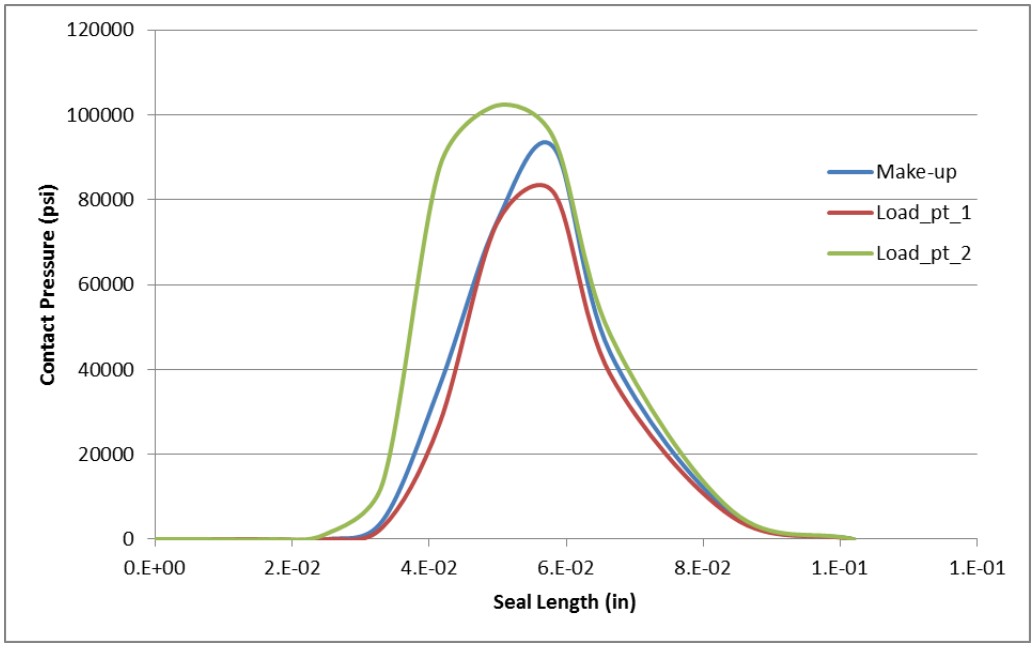

Figure 5.15: Seal contact pressure over length for make-up and first two load points.

5.5 Connection Performance

The 3D FE model delivers valuable insights for the connection performance. A brief study was performed to investigate possible cause of the MIJ connection test specimen failure after load point 26 with the 3D FE model load series simulation. The scope of this research is to create a methodology to develop at full 3D FE model, further exploration of the connection performance and leak diagnosis is recommended for future work.

5.5.1 Connection Leak Investigation

The application of ISO 13679 load series B sequence reaches the maximum compressive load starting with load point 19 as listed in Table 5.5.

Table 5.5: Maximum compressive load applied during ISO 13679 load series B.

Load Point	Machine Load (kips)	Internal Pressure (Psi)	Axial Pressure Load (kips)	FE Model Applied Tensile Load (kips)
19	-352	10455	122.7	-229.3
20	-398	8295	97.3	-300.7
21	-296	0	0.0	-296.0

While observing the primary seal behavior throughout the load sequence, it was discovered that the pin nose bottoms out into the box during load point 21. The pin nose contact with the box was not expected to occur by design. The MIJ premium connection used in this study employs design features to prevent this behavior under loading. Further observations revealed that the primary seal contact area significantly deteriorates due to the pin nose contacting the box after load point 21. Figure 5.16 illustrates the contour plots displaying nose contact with the box and contact area of the primary seal.

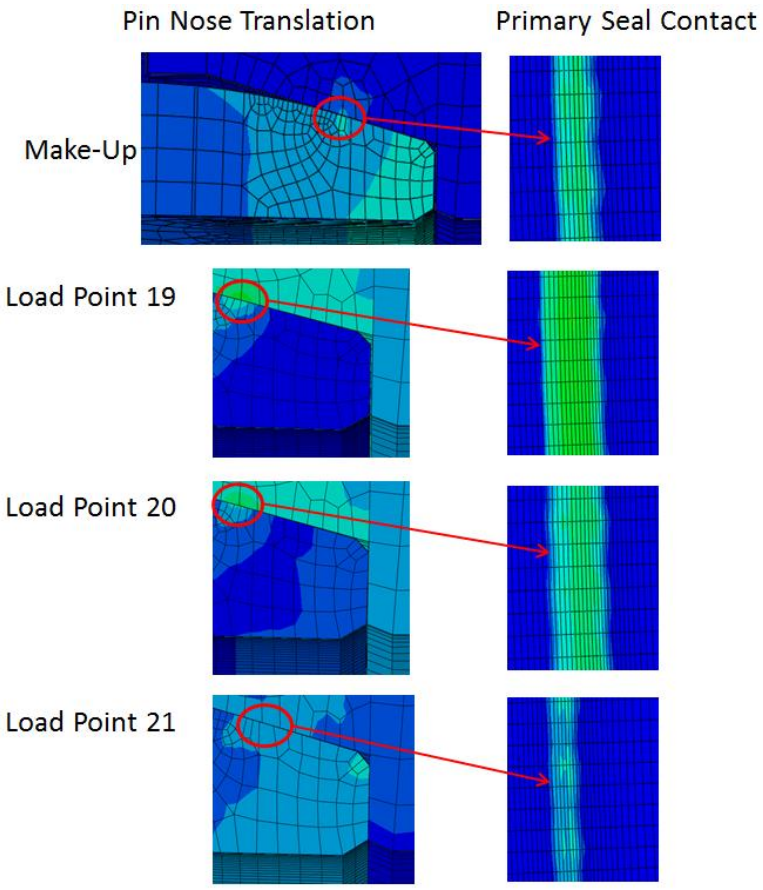

Figure 5.16: Pin nose behavior during max compression load points with corresponding contact area.

Additional investigation into the pin nose axial translation exposed bending behavior in the connection and plastic yield in the pin shoulder region after load point 19. One of the unique capabilities of the 3D FE model is demonstrated here as an axisymmetric model cannot simulate bending behavior. Figure 5.17 illustrates the von Mises contour plot of the connection load point 19 compared with load point 20/21 showing the bending behavior in the connection. Figure 5.18 shows the significant increase in plastic strain in the pin shoulder region after load point 19.

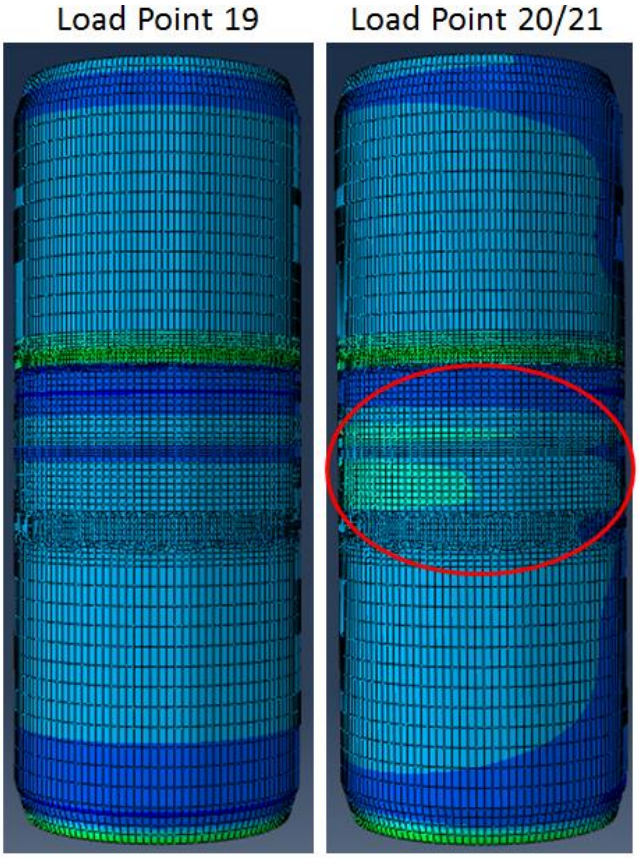

Figure 5.17: Bending behavior observed in the connection 3D FE model after load point 19.

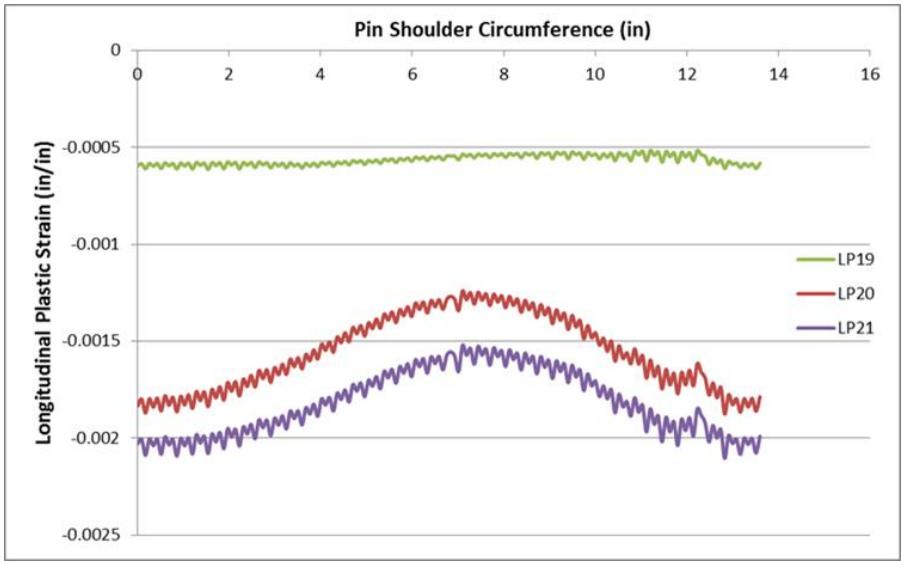

Figure 5.18: Plastic strain increase in the pin shoulder region after load point 19.

The MIJ connection test specimen was not available for observation from the manufacturer after the testing was performed. However, the DIC images in Figure 5.19 show a distinct edge at the connection secondary seal region when the leak was reported and the test was stopped endorsing the observations presented in this section.

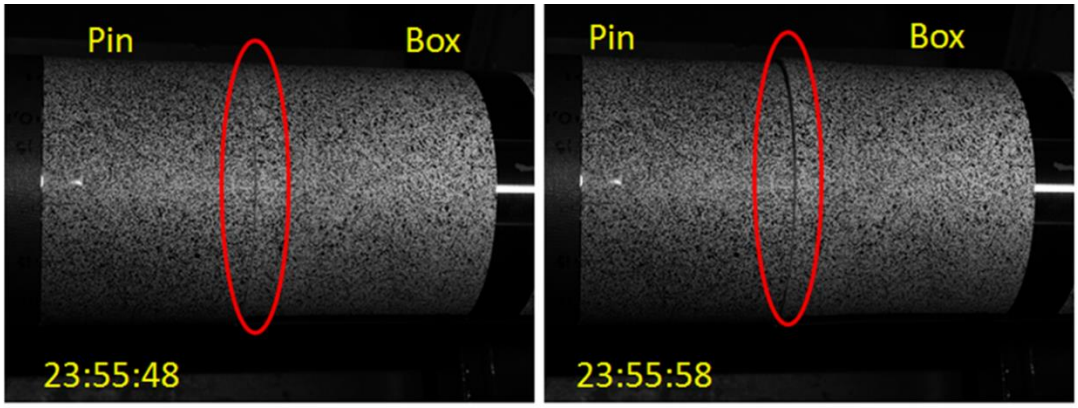

Figure 5.19: DIC images of the test specimen before (left) and after the leak is reported (right).

5.5.2 Axisymmetric Modeling Assumptions

Axisymmetric analysis assumes symmetry of the deformation field about the axis of rotation, this symmetry results in the displacement field independent of the circumferential direction. However, the connection make-up displacement results from the full 3D FE model shows variation over the box circumference possibly due to the helical threads and pin rotation. Variations in the circumferential displacement were observed after connection make-up on the box surface over the outer thread (OT), shoulder (SH), inner thread (IT), seal, and box region closer to the end of the connection. The defined data set regions are illustrated in Figure 5.20. The plots for the displacement field variables are illustrated in Figure 5.21. A rigorous study of premium connection axisymmetric models compared with full 3D models is strongly suggested for future work.

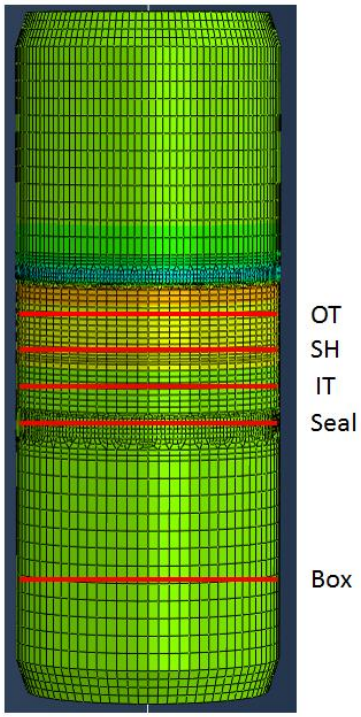

Figure 5.20: Location of the defined sets used to extract data over the box circumference.

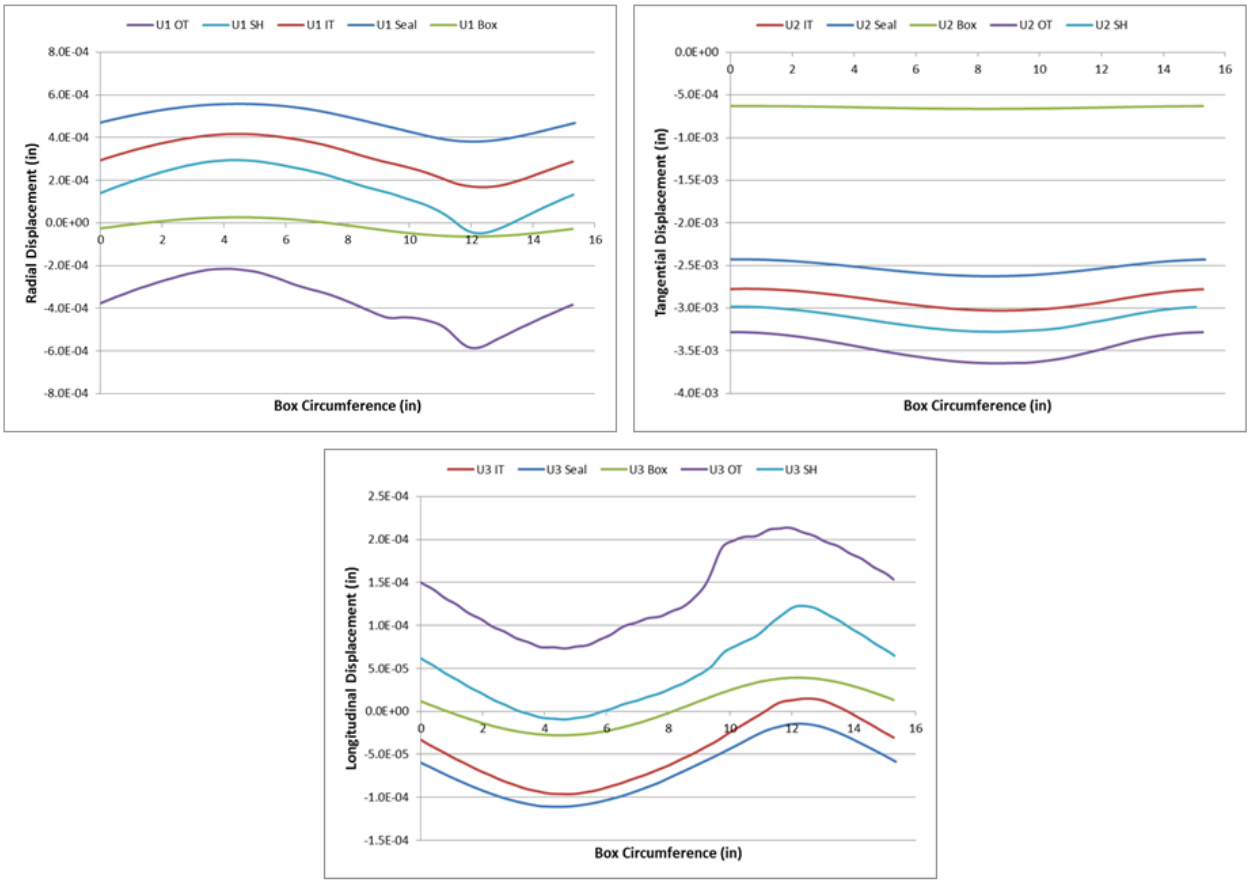

Figure 5.21: Displacement field plots from connection make-up over the box circumference.

5.6 Results Summary

A methodology to develop full 3D FE models for premium connections was successfully demonstrated with the MIJ premium connection. The parametric and scripted modeling approach accomplishes the research goals of:

1. The full 3D FE model must be parametric for user defined geometry and mesh updates.
2. The full 3D FE model should provide an efficient way to update the parameters.
3. The full 3D FE model must be manageable for the user and tractable for available computing resources.

Parametric decomposition of the connection and scripting of manual tasks keep the 3D FE models manageable for the user creating a productive design and analysis process which can be incorporated into current industry practice. The scripted approach successfully generates 3D FE models for the MIJ premium connection in seconds. It is possible to study effects of geometric and manufacturing tolerances and various geometric configurations. The parametric approach also allows scaling of the FE models to several sizes within the connection family. Complete mesh control provides an effective mesh scheme while keeping the models tractable for available computing resources. The parametric capabilities of this modeling approach permits exploration into design and evaluation of premium connections with full 3D models. The results from this study establish the feasibility of further development of full 3D FE models to reduce time and costs of physical testing.

The research objectives and hypothesis are supported with the verification of the 3D FE model with DIC experimental results for the make-up conditions. The full 3D FE model is capable of providing the best technical estimate of the make-up boundary conditions. The 3D FE model effectively represents the

torque-turn behavior of the connection and provides the designer a comprehensive look of the interactions between the seals and shoulder during connection make-up. Specifically for the MIJ connection used in this study; the effects of dimensional tolerance on the shoulder contact during make-up; and the pin nose contact with the box occurring during loading conditions delivered valuable insights about connection performance for the connection designer. The 3D FE model can simulate the bending behavior of the connection under compressive loads which would not be possible with the axisymmetric model. The 3D FE model provides meaningful seal metrics and best technical estimate of frictional properties. The 3D FE model validation with ISO 13769 load series B provides valuable information for connection performance to investigate failure of the test specimen and predict seal performance.

The 3D FE model make-up test verification with DIC measurements SSE results are listed in Table 5.1. Table 5.2 provides a friction coefficient estimate and make-up torque values after reconciling of the FE results with the DIC data. The SSE results for ISO 13679 are presented in Table 5.4.

Chapter 6 Summary, Conclusions, and Recommendations

6.1 Summary

Qualification of Oil Country Tubular Goods (OCTG) premium connections is a lengthy and expensive process. Validated FE models can enhance the development of the connection design process and significantly reduce physical testing time and costs with properly conducted virtual tests combined with a product-line evaluation approach. A review of the literature recognizes that finite element models combined with physical tests provide an effective tool for evaluating OCTG premium connections. The literature review confirms the necessity for further developing FE models to simulate connection performance under make-up and service conditions. A full 360 degree with helical thread representation of the connection is the most complete model with no associated assumptions. Development of a manageable full 3D FE model in this research effort is a leap forward from the current industry practice of axisymmetric FE models and a step towards proper virtual connection testing. Confidence in FE results is highly dependent on correlation with experimental data. The DIC displacement and strain measurements provide the required high spatial density data for accurate FE model verification and validation.

Full 3D FE models allow application of boundary conditions and loadings exactly as implemented in the physical test without any inherent assumptions. The industry conventional practice for developing 3D FE models is performed by importing 3D solid parts from CAD software into FE software. This method results in a model that is fixed with the geometric dimensions that it was imported in with. The full 3D FE models for premium threaded connections imported from CAD software are often intractable due to meshing of the complex geometric features and helical threads as one solid part. A parametric approach to building the full 3D model in Abaqus CAE was investigated and a methodology was developed to generate full 3D FE models manageable by the user. The FE models are developed for use as an effective design tool that allows the user to explore various dimensional configurations and design variables efficiently. The methodology permits the use of a single FE model to represent the virtual testing of a family of connections to meet specific performance needs for a given well design reducing overall testing time and costs.

Construction of a Metal-to-metal seal Integrated Joint (MIJ) type premium connection is presented in Chapter 3. Decomposition of the connection parts into smaller geometric components is a major contributor to the success of this approach. The components are parameterized utilizing dimensions provided in the technical part drawings. Python scripts are developed to update geometry parameters and assemble components into full 360˚ 3D solid parts. Helical threads are defeatured and generated with the same parametric scripting approach. Beam elements are implemented to represent overall pipe length of the test specimen. Defeatured helical threads and use of beam elements significantly reduce total element count and model runtimes with minimal impact on the connection make-up results explained in Section 3.8.

The parametric meshing scheme provides the user with complete mesh control to minimize total element count by controlling mesh density throughout the model. Systematic partitioning of the parts and assigning mesh seed parameters requires great care and effort for an accurate mesh between merging edges of the components as demonstrated in Section 3.3.1. Generating seed parameters and mesh transition regions necessitate user attention for maintaining proper aspect ratio in the elements. Minimizing element count is critical to keep the 3D models tractable for computing resources. The controlled meshing scheme maintains higher mesh density in the contact regions of seals and mid shoulder to properly resolve contact mechanics. Section 3.3.4 illustrates the development of the mesh and element distribution in the components over several model updates. Python scripts are developed to update mesh parameters and assemble parts similar to geometric updates for the FE model to be an efficient design tool.

An isotropic elasto-plasticity material model is calculated from manufacturer provided tensile test results of the MIJ connection material coupons. A classical metal plasticity model with isotropic hardening is

used to develop the plastic material response. The material model must account for plasticity since the seals and shoulder develop plastic zones in the contact regions during make-up and loading. The best possible material model is developed from the limited test data available.

Section 3.5 describes the contact properties and defined surfaces. Contact regions on the pin are assigned as the slave surfaces with higher mesh density and box regions as the master surfaces. There are no associated assumptions applying the boundary conditions with the 3D FE models. Make-up and load series testing boundary conditions applied to the FE model are identical to the physical tests.

Surface strain measurements made during connection make-up and load sequence are typically performed using strain gages. Strain-gage measurements are typically limited to a few points over the connection surface and do not fully capture the behavior and mechanics of the connection. Digital Image Correlation (DIC) technology is capable of providing high spatial density, full-field displacement and strain validation data for connection make-up and loading. However, proper correlation methods, experimental set up and system calibrations require special considerations for accurate results. The quality of the sputter pattern applied to the connection surface, lighting conditions, and camera calibrations are important to obtain the highest signal-to-noise ratio measurement data.

The 3D FE model validation with reference to DIC data is presented in Chapter 5. Coordinate system transformation and data alignment are critical factors in accurate correlation results. Special care is required when filtering the DIC results to avoid losing useful data. The sum squared error metrics quantitatively present the correlation between the 3D FE model and the DIC data. Pin rotation is used as a variable to calibrate the make-up FE model with the DIC data. The friction coefficient was estimated to develop a torque-turn plot with the lowest error make-up model. The calibrated FE model is subjected to the load sequence which is compared with DIC measurements. The validated 3D FE model provides valuable results and insights into the internal features of the connection.

6.2 Conclusions

Full 360 degree 3D finite element models are the most complete representation of OCTG premium threaded connections. A methodology to develop full 3D FE models for premium connections was successfully demonstrated with the MIJ premium connection. Parametric decomposition of the connection and scripting of manual tasks keep the 3D FE models manageable for the user creating a productive design and analysis process which can be incorporated into current industry practice. The scripted approach successfully generates 3D FE models for the MIJ premium connection in seconds. It is possible to study various geometric configurations, the effects of design and manufacturing tolerances, and scale the FE models to several sizes within the connection family. Complete mesh control provides an effective mesh scheme while keeping the models tractable for available computing resources. The parametric capabilities of this modeling approach permits exploration into design and evaluation of premium connections with full 3D models.

The MIJ connection 3D FE model developed in this study successfully demonstrates torque-turn behavior of the connection make-up boundary conditions. The virtual make-up model reconciled with DIC measurements reproduces the torque-turn response of the test specimen with a representative estimate of the friction coefficient of 0.063 that matches the applied torque value within 0.02% error. The 3D FE model validated with the load series results couples the experimental data with virtual analysis. The MIJ connection model successfully provides evidence of damage in the test specimen 10 load points prior to the physical “leak”. These insights are extremely valuable for design and analysis of the premium connections for failure modes. Validated 3D FE model provides meaningful seal metrics which are difficult to estimate experimentally and enables modeling of extreme loading scenarios. It is feasible for the methodology presented in this research effort to advance design and analysis process of premium threaded connections and minimize physical testing.

6.3 Recommendations

The virtual model is capable of representing make-up conditions and service loading accurately. The parametric capabilities of the 3D modeling approach permit exploration into design and evaluation of premium connections. Parametric studies can be developed to assess connection performance and reduce physical testing time and costs. Numerous aspects of the 3D FE model and DIC testing should be further explored to advance this research to minimize physical testing of the connections.

6.3.1 3D FE Model

The full 3D FE model is still in the early stages of development and shows promising results. Several features of the modeling process require additional exploration to create robust FE models to enhance the capabilities of virtual tests.

- Explore modeling techniques and connection features with more complex geometries of premium connections such as tapered and interference fit threads.
- Advance scripting process towards more automated model generation and data extraction.
- Improve meshing schemes and mesh transition regions.
- Investigate more effective material models for the plastic zone; this requires better coordination with material testing.
- Explore results of the 3D FE model compared with the axisymmetric model. Quantify the difference between the results of 3D and axisymmetric FE models.
- Advance axisymmetric models with results acquired from 3D models.
- Examine strategies and solvers to reduce model runtimes.
- Apply additional service loading such as bending, elevated temperature testing, and pressure penetration interactions in the seal regions.
- Advance correlation methods with improving DIC data alignment and filtering.
- Study seal metrics to enhance seal performance prediction capabilities.
- Investigate effects of geometric and manufacturing tolerances on connection performance.

6.3.2 Premium Connection Parametric Design and Evaluation

The main objective for this research was to develop the 3D FE models as an effective design and analysis tool. The goal is to implement a validated FE model to predict performance for a family of connections via virtual tests to reduce physical testing costs and time for design and qualifications of the connections. The methodology developed allows the 3D connection geometry to be updated and meshed so the user can study the effects of the various design variables on the connection. Table 6.1 lists some of the main design variables for OCTG premium connections. The service load variables for connection testing are listed in Table 6.2.

Table 6.1: Premium connection design variables for parametric study

Design Variables
Connection Type
Connecton Size
Connecton Gage Dimensions
Wall Thickness
Material Model
Seal Interference
Thread Interference
Pin and Box Taper
Make-up Torque
Friction Coefficient

Table 6.2: Premium connection service load variables

Load Variables
Tensile Load
Compressive Load
Bending Moment
Internal Pressure
External Pressure
Internal Temperature
External Temperature

Once the make-up model is calibrated against the DIC test results, the designer can quickly generate new FE models to explore effects of the design variables and geometric and manufacturing tolerances on connection performance during make-up and service loading. Various configurations may be tested with virtual tests resulting in only select final design configurations to be used in a physical test. The proposed approach can significantly reduce time and costs for physical testing. Similar arguments can be applied for a connection qualification process with product-line evaluation. Fewer connections can be qualified with physical tests. Results from the physical qualifications combined with FE models can create connection performance envelopes.

Bibliography

[1] Hilbert Jr. L. B., and Kalil I. A., 1992, "Evaluation of Premium Threaded Connections Using Finite-Element Analysis and Full-Scale Testing," IADC/SPE Drilling Conference, New Orleans, Louisiana, pp. 563–580.

[2] API Technical Report 17TR8, 2015, High-pressure High-temperature Design Guidelines

[3] Bradley A., Nagasaku S., and Verger E., 2005, "Premium Connection Design, Testing, and Installation for HPHT Sour Wells," SPE HPHT Sour Well Design Applied Technology Workshop; 17-19 May, 2005 The Woodlands Texas, USA.

[4] Powers J., Baker D., and Chelf M., 2008, "Application of Connection Productline Evaluation," IADC/SPE Drilling Conference; 4-6 March, 2008 Orlando Florida, USA.

[5] ISO 13679-2002 Petroleum and natural gas industries - Procedures for testing casing and tubing connections, International Organization for Standardization, Geneva, Switzerland.

[6] Ceyhan I., Khemakhem A. S. D., Coe D., Myers J. H., and Powers J., 2001, ExxonMobil Connection Evaluation Program, First Edition, ExxonMobil Upstream Research, Houston, Texas.

[7] Assaneli A., and Dvorkin E., 1993, "Finite element models of OCTG threaded connections," Computers & Structures, 47, pp. 725-734.

[8] Weiner P.D.,1968, "Analysis of Tapered Threaded Thick Walled Tubing Connections," Texas A&M University.

[9] Heijnsbroek E. P. L., 1995, "Sealing Mechanism of Dry Metal-to-Metal Seals," Delft University of Technology.

[10] Dvorkin E., and Toscano R. G., 2003, "Finite Element Models in the Steel Industry Part II: Analyses of tubular products performance," Computers & Structures, **81**(8-11), pp. 575–594.

[11] Galle T., Waele W., Wittenberghe J., and Baets P., 2014, "Optimal Make-up Torque for Trapezoidal Threaded Connections Subjected to Combined Axial Tension and Internal Pressure Loading," ASME Pressure Vessels & Piping Conference; 20-24 July, 2014, Anaheim, California

[12] Sugino M., Ugai S., Nakamura K., Yamaguchi S., and Hamamoto T., 2015, "VAM®21, an Innovative High-performance Premium Threaded Connection for OCTG," Nippon Steel & Sumitomo Metal Technical Report No. 107.

[13] Ostergaard, E. B., 2013, "A Refined Methodology for Calibrating Premium Threaded Connection Make-ups", M.S. Thesis, Virginia Polytechnic Institute and State University, Blacksburg, VA.

[14] Khemakhem A. S. D., Biegler M. W., Baker D. A., Burdetter J. A., Dale B. A., Mohr J. W., Ceyhan I., Powers J., Myers J. H., and Asman M., 2009, "Method and System for Evaluating Groups of Threaded Connections. U.S. Patent Application Publications No.: US 2009/0250926A1."

[15] Fan J., Yang Z., Wang J., Ding S., Liu C., and Shi Z., 2009, "Parametric Finite Element Modeling and Nonlinear Analysis of Vehicle Brake," IEEE International Conference on Mechatronics and Automation; 9-12 August, 2009, Changchun, China.

[16] Jiapeng T., Ping X., Baoyuan Z., Bifu H., 2013, "A Finite Element Parametric Modeling Technique of Aircraft Wing Structures," CSAA Journal of Aeronautics, **26**(5), pp. 1202-1210

[17] Galle T., Pauw J., Waele W., Wittenberghe J., and Baets P., 2014, "Validating Numerically Predicted Make-Up of Threaded Connections Using Digital Image Correlation and Infrared Monitoring," JSA, 49, pp. 492-500.

[18] Vespa M., 2015 "Introduction to Oil Country Tubular Goods (OCTG)," EdX. Web. March, 2015.

[19] Dassault Systèmes Simulia Corp., 2014, "Abaqus/CAE 6.14-EF1 Build ID: 2014_14_18-11.27.55 44621."

[20] ISO 13678-2010 Petroleum and natural gas industries – Evaluation and testing of thread compounds for use with casing, tubing, line pipe and drill stem elements, International Organization of Standardizations, Geneva, Switzerland.

[21] Advanced Research Computing at Virginia Tech, http://www.arc.vt.edu.

[22] Optical Measuring Techniques, ARAMIS User Manual- Software v6.3 rev-c.

Appendix A

Fully constrained sketch operation

When a sketch is fully constrained in Abaqus CAE sketch module, it is noted by the sketch turning green. If a sketch parameter is updated in a fully constrained sketch, the whole sketch updates to keep the geometry of the part intact. Figure A.1 illustrates an example of an unconstrained sketch compared to a fully constrained sketch. When the height of the rectangle is updated, the unconstrained sketch skews the shape of the rectangle while the fully constrained sketch retains the proper shape.

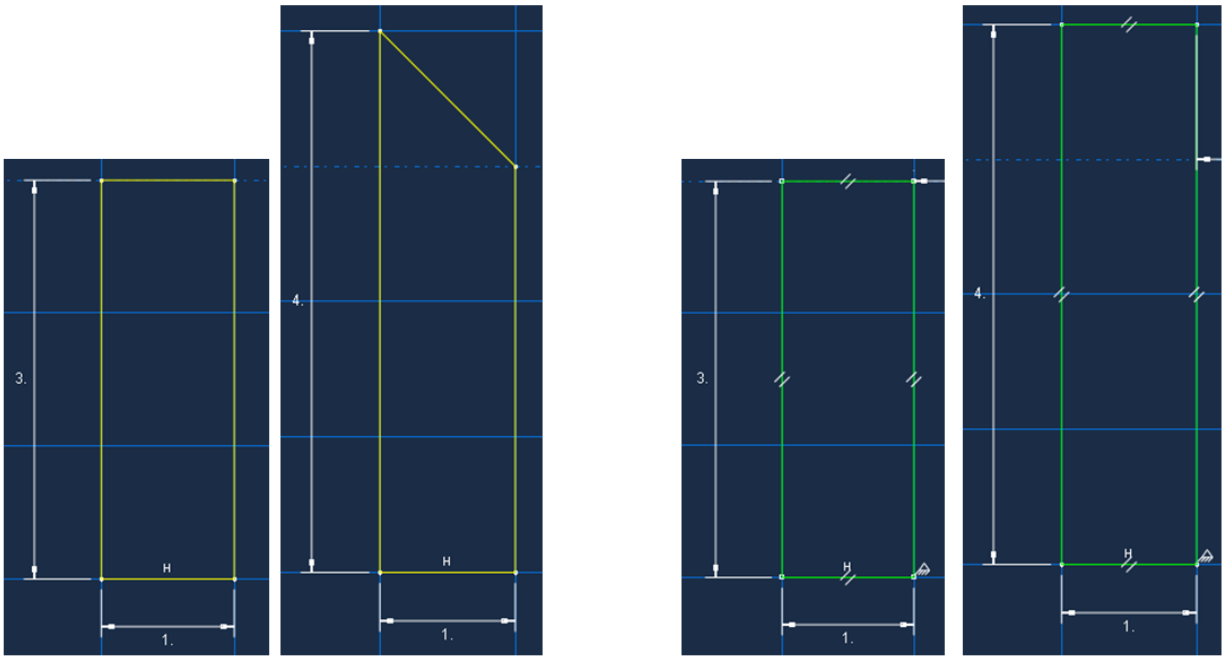

Figure A. 1: Unconstrained sketch with updated parameter (left) and a fully constrained sketch with updated parameter (right).

Appendix B

Load Series B Longitudinal Strain Plots

Load point 1-15 FE results and DIC experimental results match the connection mechanics. The DIC results do not match the FE results starting from load point 16. The physical leak happens at load point 26, but the results show that connection failure start a lot earlier.

Load Point 1

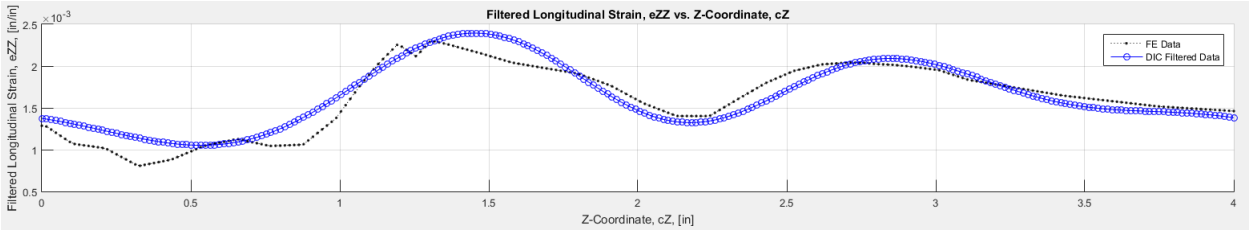

Load Point 2

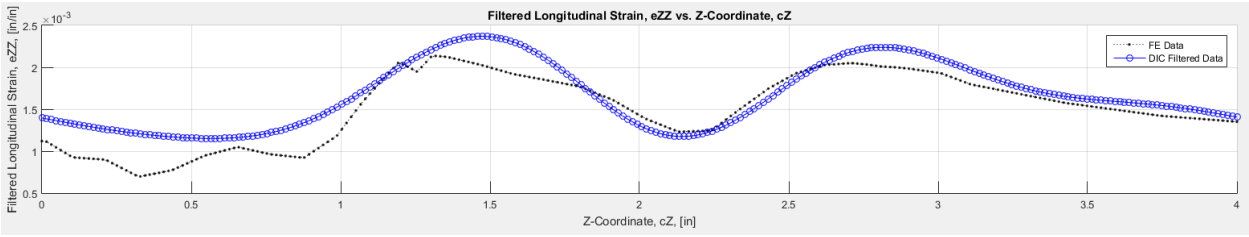

Load Point 3

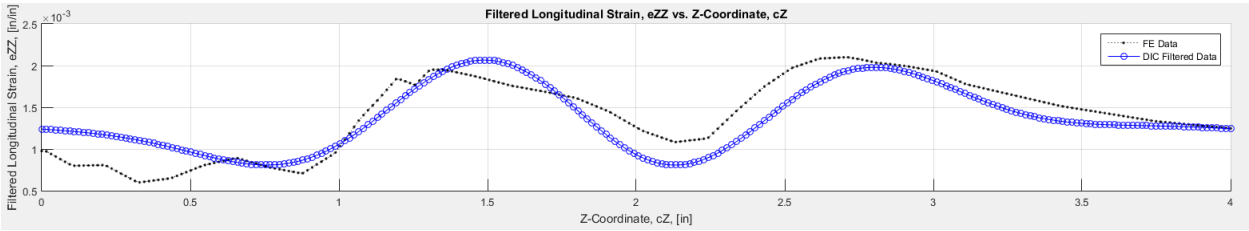

Load Point 4

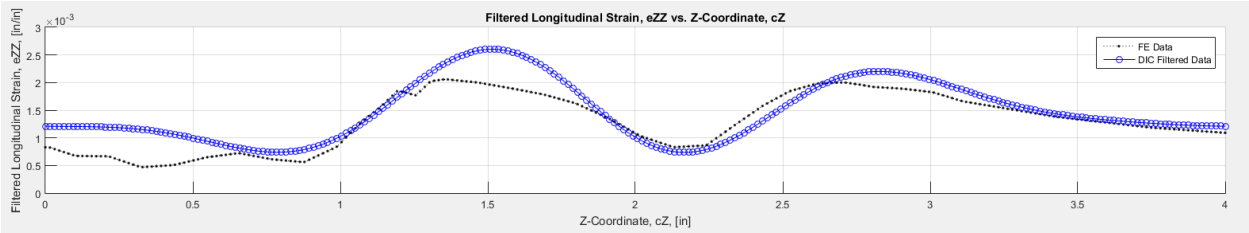

Load Point 5

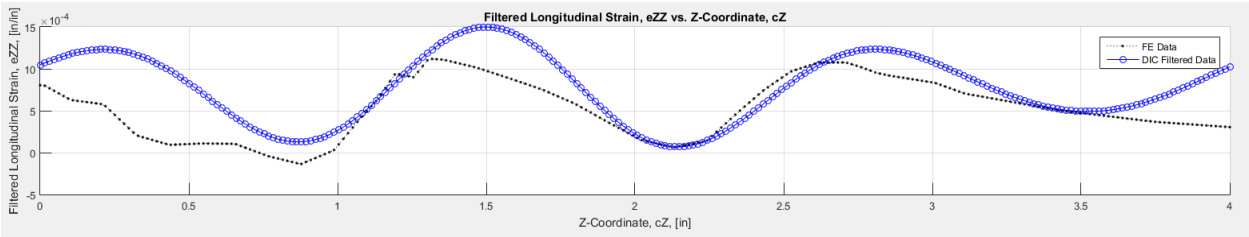

Load Point 6

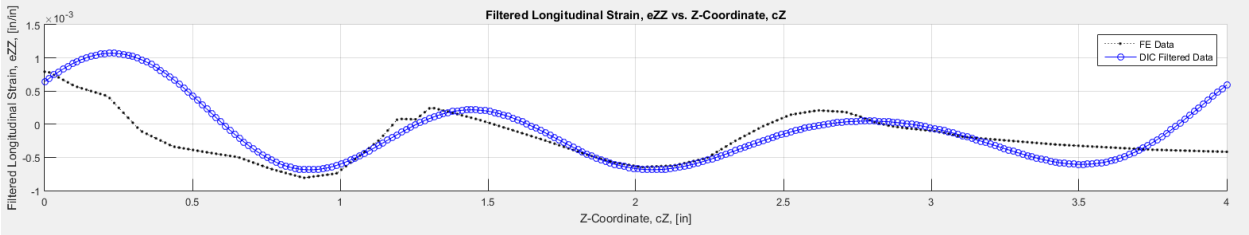

Load Point 7

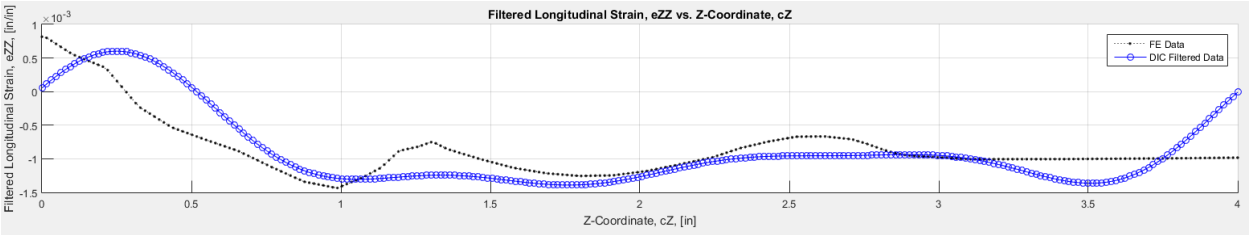

Load Point 8

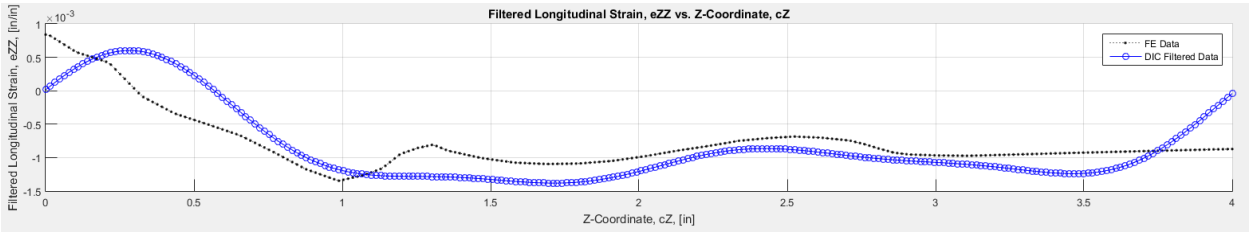

Load Point 9

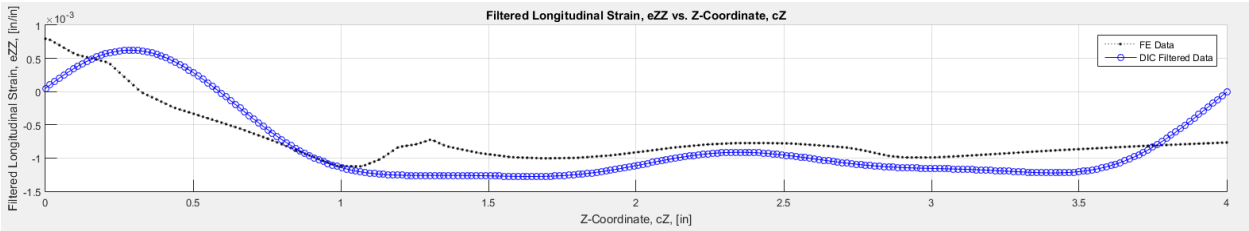

Load Point 10

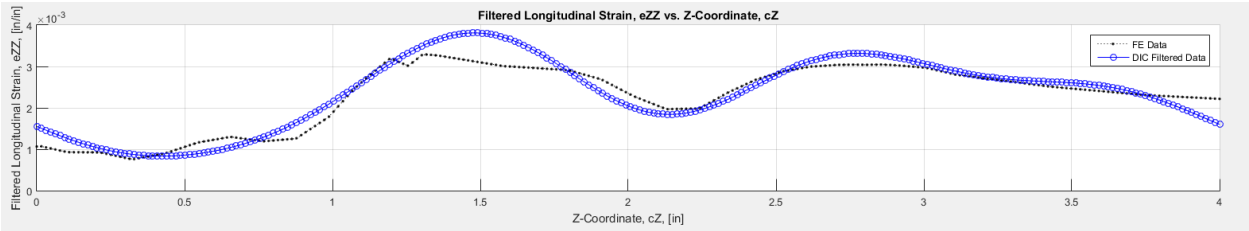

Load Point 11

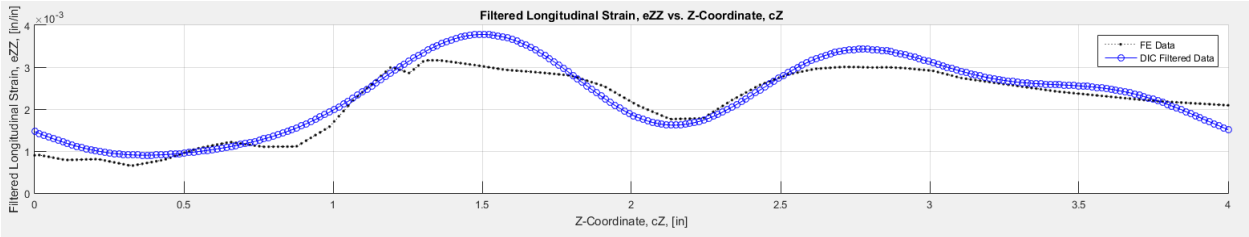

Load Point 12

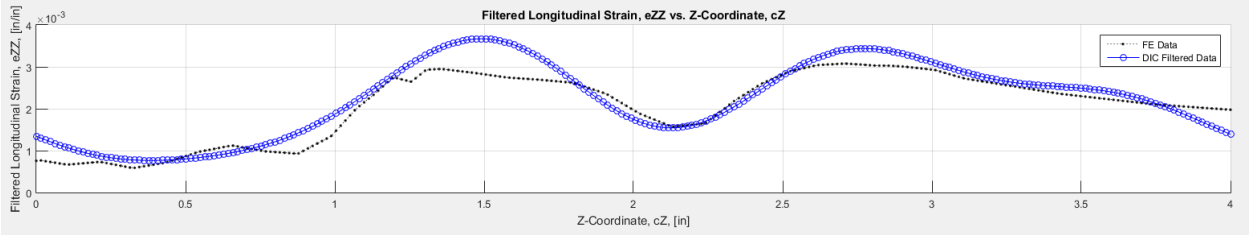

Load Point 13

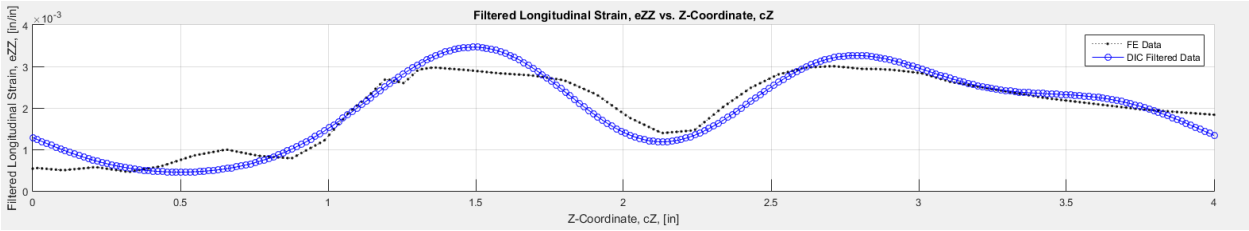

Load Point 14

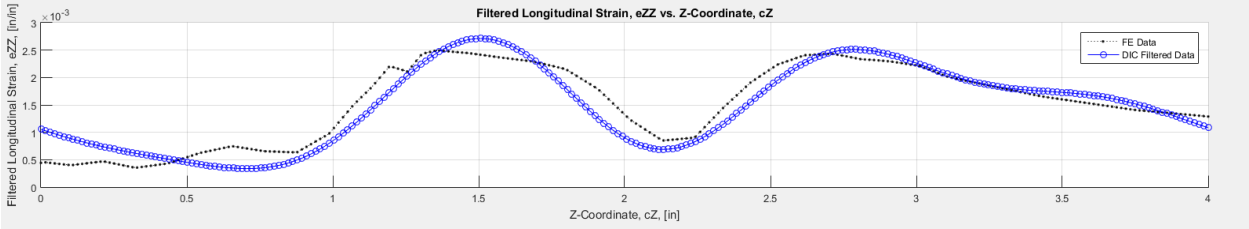

Load Point 15

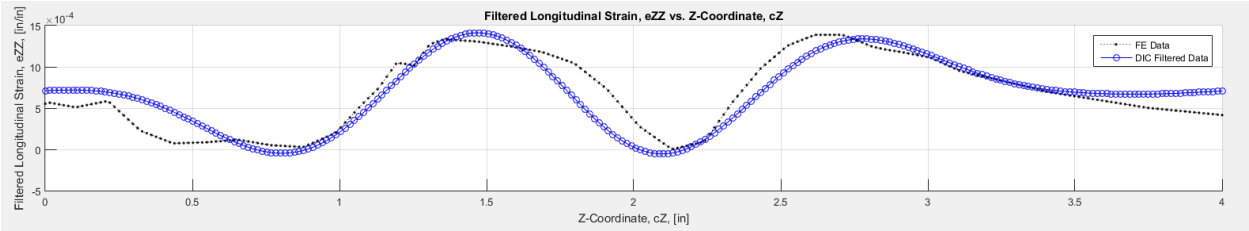

Load Point 16

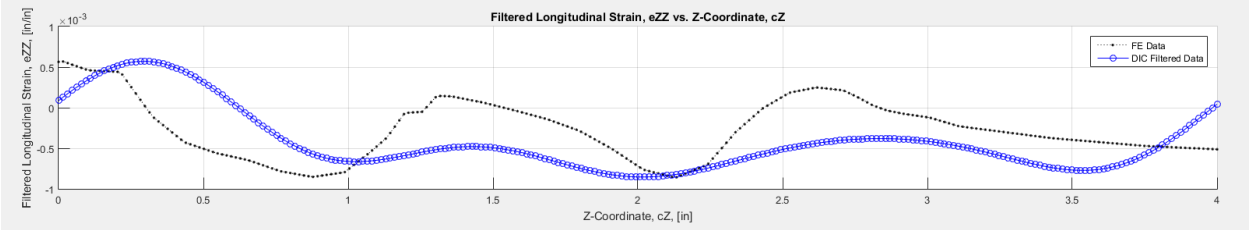

Load Point 17

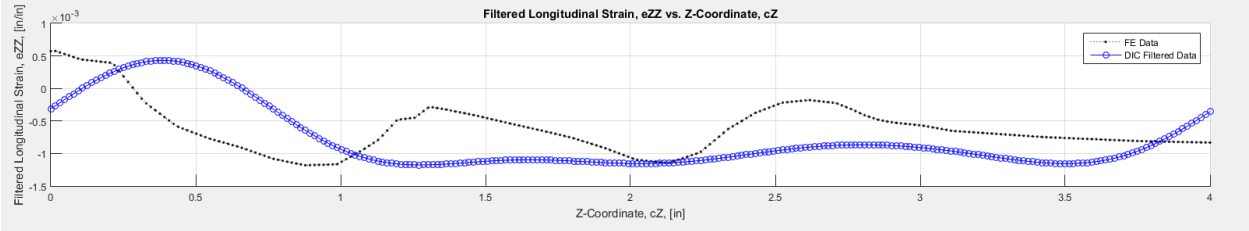

Load Point 18

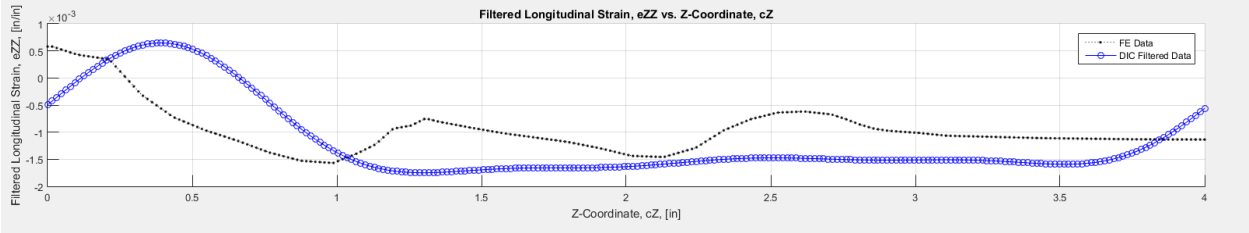

Load Point 19

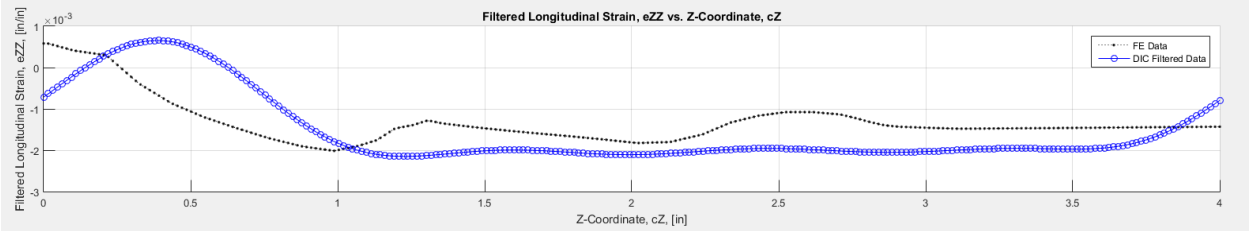

Load Point 20

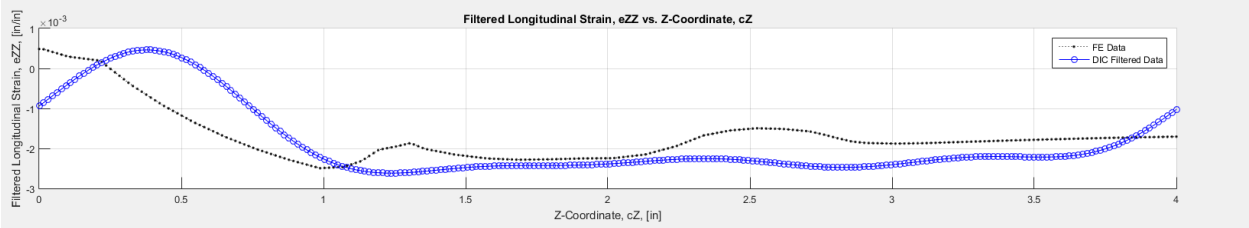

Load Point 21

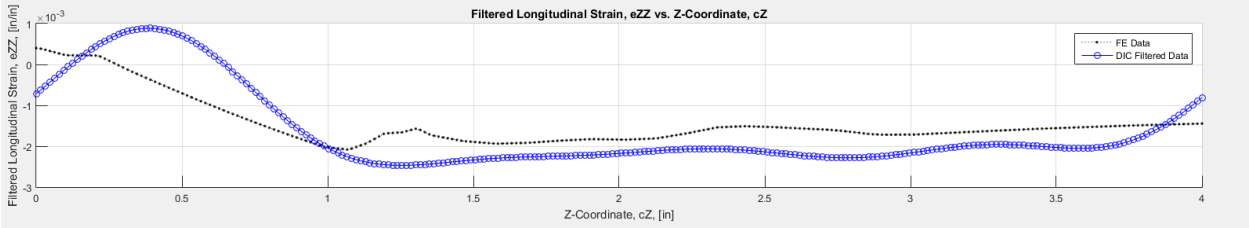

Load Point 22

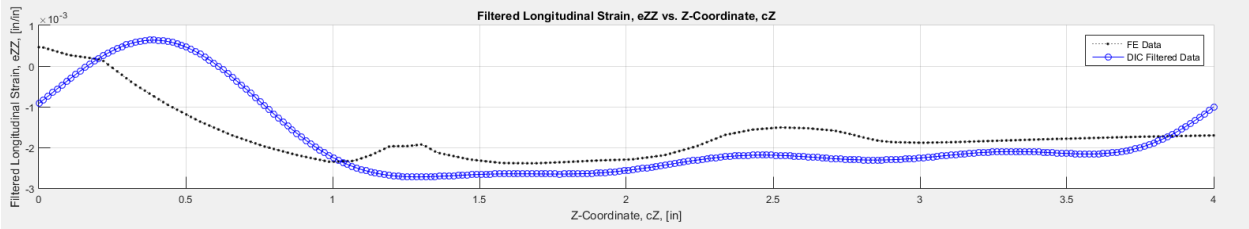

Load Point 23

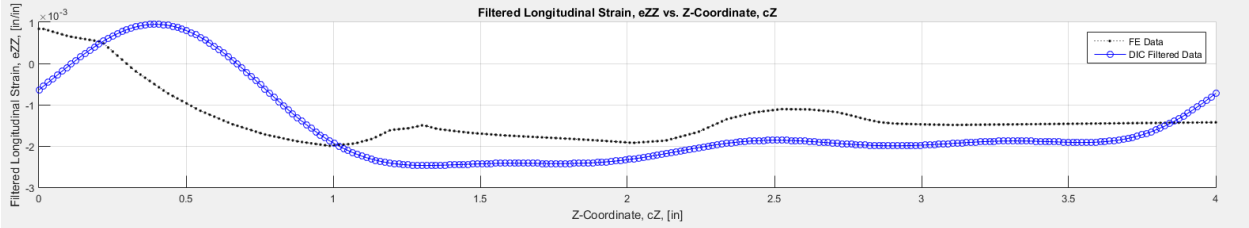

Load Point 24

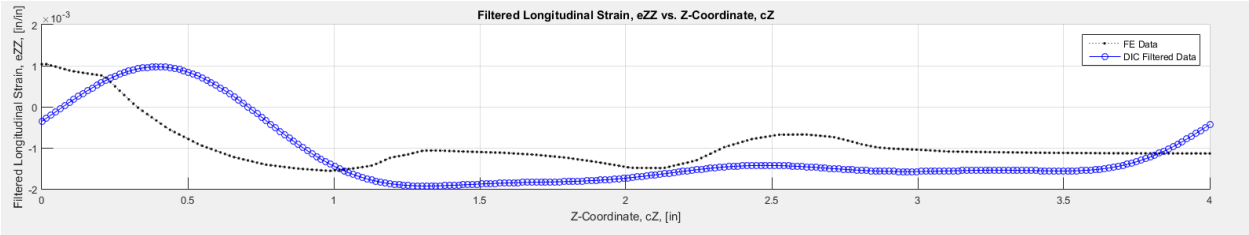

Load Point 25

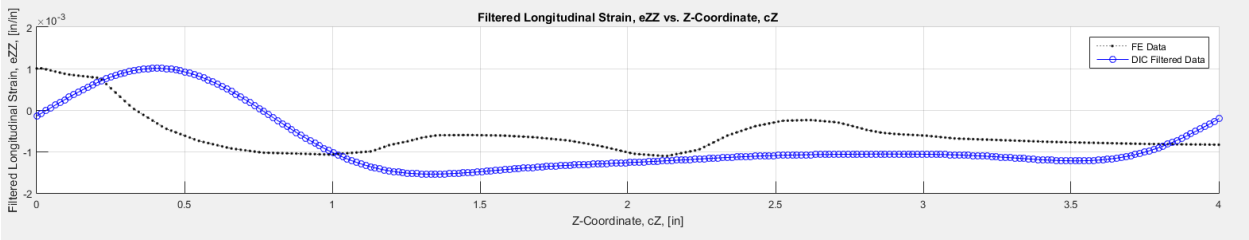

Load Point 26